ABSTRACT

Title of Dissertation: SUBTASK CONTROL IN HUMAN LOCOMOTION

David Michael Logan, Doctor of Philosophy, 2014

Dissertation Directed by: Professor John J. Jeka

Department of Kinesiology

Maintenance of upright posture during walking is one the most important tasks to ensure flexible and stable mobility, along with speed adjustment, wayfinding and obstacle avoidance. These underlying functions, or subtasks, are simultaneously coordinated by the nervous system, which relies heavily on sensory feedback to obtain continual estimates of self-motion. This dissertation reports the findings of four experiments which made use of visual and mechanical perturbations to probe the interplay of these subtasks during treadmill walking. To confront the inherent nonlinearity of human gait, novel frequency domain analyses and impulse response functions that take into account phase of the gait cycle were used to characterize perturbation-response relationships. In the first experiment, transient visual scene motion was used to probe how visual input simultaneously influenced multiple subtasks, but at different phases of the gait cycle. In the second experiment, kinematics and

muscle activity response variables showed an amplitude dependency on visual scene motion during walking that indicates vision is reweighted in a manner similar to standing posture. The third experiment used a metronome to constrain walking, revealing two time scales of locomotive control. The final experiment made use of both visual and mechanical perturbations simultaneously to probe the subtasks of postural orientation upright and positional maintenance on the treadmill. Doing so revealed that the nervous system prioritizes control of postural orientation over positional maintenance. In sum, this dissertation shows that sensory and mechanical perturbations provide insight as to how the nervous system controls coexisting, underlying functions during walking.

SUBTASK CONTROL IN HUMAN LOCOMOTION

By

David Michael Logan

Dissertation submitted to the Faculty of the Graduate School of The University of Maryland, College Park in partial fulfillment of the requirement for the degree of Doctor of Philosophy

2014

Professor John J. Jeka, Chair

Associate Professor Noah J. Cowan

Research Assistant Professor Tim Kiemel

Professor William S. Levine

Assistant Professor Ross H. Miller

Dedicated to Elizabeth and the boys,

forever a source of inspiration and joy

TABLE OF CONTENTS

LIST OF FIGURES

Chapter 1: Introduction and Organization

Walking is a form of locomotion that most of us successfully perform every day. Our proportionally massive trunks do not topple over our legs, we can produce the appropriate forces against the ground to get to where we need to go and we can even avoid obstacles in our path if they arise. This dissertation works towards understanding how all of these subtasks, or underlying functions of the overarching walking task, are performed simultaneously.

That successful locomotion includes, but is not limited to, control of equilibrium, propulsion, and fulfilling environmental demands is certainly not a new idea (Forssberg 1982). The term subtask and its first usage in the human walking literature can be credited to Winter (1989) and his proposal of a task-related theory of gait that dictated three subtasks as necessary elements underlying the task of safe walking. These subtasks include support maintenance by the stance limb, control of posture upright in sagittal and frontal planes, and proper foot trajectory control for clearance during swing and stable landing during heel strike (Winter 1989). In more dynamic environments, however, additional subtasks such as hazard accommodation/avoidance or positional maintenance on a treadmill must be successfully performed. Recently, there has been renewed support for the idea that subtasks of human locomotion are modular in nature, and are enacted by distinct combinations of muscle activations (McGowan et al. 2010; Neptune et al. 2009; Chvatal & Ting 2013).

In this work a simplified view of subtasks is used. The subtask of upright postural control during walking is observed through changes in trunk orientation

while the subtask of speed control is observed through a measure of whole body displacement and supporting changes in leg trajectories. When possible, changes in muscular activity with appropriate timing allow further insight into timing and prioritization of these subtasks.

When thinking about how the subtasks of walking are controlled by the nervous system, one must certainly take gait cycle phase into account. That is, the state of the musculoskeletal plant as each limb moves from heel strike to heel strike and the whole body moves in and out of phases of double support will alter how the nervous system enacts an ongoing subtask or the degree to which a new subtask can be incorporated into the ongoing walking behavior. This was made apparent by a previous study by Logan et al. (2010) which showed a significant covariance between the thigh and visual scene motion that did not occur during early to mid-stance phase, but varied in magnitude throughout the swing phase (Logan et al. 2010).

At first, this finding fit into an expected narrative that the input-output relationship of visual perturbations to leg segment motion could not be characterized with the standard linear time-invariant (LTI) techniques being used. As a phase-dependent covariance shows that the relationship between vision and the thigh segment did vary based on phase of the gait cycle, the relationship is not time-invariant. Thinking deeper about this covariance in the thigh response inspired thinking on how phase-dependence during human walking could emerge during perturbation experiments. A phase-dependence could be due to the actual phase of the gait cycle that subjects were in when the stimulus occurred and/or

the phase of the gait cycle when the response could occur. The former implying some neural and/or sensory process has taken place while the latter could be due to purely biomechanical constraints. The most extreme alternatives could be that the phase-dependence of thigh angle response is due to a gating of sensory input at a specific perturbation phase or that the nervous system continually initiates a response but the biomechanical state of the limb does not allow a response to occur. The potential for these two very different interpretations of the same data inspired the experiment reported in the third chapter of this dissertation and provided the impetus for reporting and interpreting input-output relationships with respect to both stimulus phase and response phase (normalized response time) in these studies of subtask control.

Here the subtasks of walking are investigated in a series of treadmill walking experiments that appropriately take into account gait cycle phase and make use of input-output mappings elicited by visual and mechanical perturbations. This dissertation is organized in chapter format beginning with a review of the relevant literature. The use of visual and mechanical perturbations as probes for the neural control of human walking are reviewed, the potential issues with applying these probes, and the use of metronomes as rhythmic auditory cueing to constrain locomotive control.

Following the review of the literature, a recently published manuscript which provides evidence for the use of vision for multiple subtasks during treadmill locomotion is presented in Chapter 3. This manuscript uses commonly used time domain measures to show the use of vision for changes of trunk

orientation for upright equilibrium and modulation of leg segments for both hazard accommodation/avoidance and positional maintenance on the treadmill. Chapter 4 marks a transition in analysis tools used in this dissertation. Harmonic transfer functions (HTFs) allowing input-output mappings between broadband, pseudorandom perturbations and response variables are computed in the frequency domain prior to transfer into the time domain as phase-dependent impulse response functions (PD-IRFs). The Appendix provides an introduction to these methods developed by Dr. Tim Kiemel. These tools were critical at this juncture as the experiment reported in Chapter 4 used frequency domain measures to show that the sensor fusion process of sensory reweighting is used for walking.

Chapter 5 marks a transition from using perturbations of visual scene motion to investigate the use of vision during walking to using visual scene motion as a probe to investigate subtask control. This chapter reports an experiment investigating the phase-resetting strategy used by the nervous system for the subtask of positional maintenance on the treadmill. In addition to the treadmill dictating a fixed speed, walking was further constrained in this study by dictating cadence on the treadmill with a metronome. By comparing non-metronome and metronome conditions, it was revealed that maintaining position on the treadmill was linked to phase resetting on a short time scale while being unlinked on a longer time scale, suggesting two timescales of control for walking. Finally, Chapter 6 reports an experiment which also used visual perturbations to probe subtask control in conjunction with adding a mechanical perturbation to

study the interaction of trunk orientation and positional maintenance subtasks. When active, neural driven responses to both perturbations were observed, the subtask of postural control upright was prioritized in terms of time over maintaining position on the treadmill.

Chapter 2: Background and Review of the Literature

The problem

During walking the nervous system is confronted with grand challenges to both control and sensation. The challenge of control comes from the need for the nervous system to control an abundance of elemental variables not yet clearly defined that could be muscle modules (e.g., Chvatal & Ting 2012), kinematic trajectories (e.g., Borghese et al. 1996), abstract representations (e.g., Dingwell & Cusumano 2000), or something else yet to be formulated. The abundance of degrees of freedom from which these elemental variables arise must be orchestrated appropriately for functional outcomes of walking such as maintenance of balance upright and moving from place to place.

Critical for neural control processes during walking; sensory inputs provide information about the environment and the body itself as it moves through the environment. In all motor behaviors, however, the nervous system must deal with sensory processing issues such as noisy sensors (Faisal et al. 2008) and multisensory integration (the so-called “binding problem”). In the rhythmic behavior of locomotion, additional complications arise such as transitory inputs of some sensory organs due to the phase of the locomotive cycle.

Studies which manipulate sensory information allow insight into neural control and studies focusing on neural control inform about how sensory information should be used to enact that control. This linkage can be formalized by control theoretic approaches to understanding human motor control, and specifically the joint input-output approach to system identification. This approach

relies on the use of both mechanical and sensory probes for the study of motor behavior. As visual sensory and mechanical perturbations will be used in the proposed research, human walking studies making use of these perturbations and the implications for neural control are reviewed. As entraining step period with auditory stimuli is of critical interest, its use in human locomotion will also be reviewed. Finally, the literature regarding the use of phase resetting in human locomotion is discussed.

Visual inputs: insight into function and control

To begin it will be helpful to review those studies (and schools of thought) which manipulate vision in some manner during locomotion in order to describe how visual inputs have some functional influence on walking.

First, moving in the correct direction (steering) and direction one faces (heading) are reliant on visual information. Evidence suggests that steering behaviors are actually specific to the type of optic flow. Steering behaviors were significantly different for type of optic flow (translation, rotation, combined) and focus of expansion (0°, ±20°, ±40°) finding that rotations of the body were not seen unless there was rotation of the visual scene. Additionally, medial-lateral shifts observed in the opposite direction of the focus of expansion (FOE) suggest that FOE may steer one's M/L components during locomotion (Sarre et al. 2008).

Previously, steering synergies identified in eyes open and closed conditions by Vallis and Patla during "burst of air" perturbations could explain movement of the trunk in response to steering via perturbation. As these authors

believe, the trunk may be part of a kinematic synergy whose direction is dictated by a reference frame defined by the head in the act of steering (Vallis & Patla 2004). Yet, this egocentric reference frame is also contextually dependent on optic flow and those head and eye movements leading to the change in direction of locomotion (Hollands et al. 2002).

Even in visuo-locomotor adaptation paradigms, it seems optic flow is the culprit for heading corrections rather than other sensory features such as target drift (Bruggeman et al. 2007). Conflicting evidence still exists, however, that suggests motion parallax may play a larger role than optic flow in the control of heading (Schubert et al. 2003). In sum, visual information is vital to moving the right direction and maintaining the correct heading direction.

Next, there are those studies that investigate how visual information is used to stabilize the head on the trunk during a walking trajectory. When making turns, it has been shown that the head turns approximately 250 ms prior to a shift of the COM in the medial/lateral plane. Hollands and colleagues suggest that these anticipatory head turns allow the body to reorient itself during turning and are not subservient to gaze (Hollands et al. 2004). Additionally, studies by Hicheur and colleagues found that this anticipatory turning of the head has similar orientation angles to both the left and right and could be considered a “global mechanism”. They also found that the geometry of the distorted path was reflected in the geometry of the head orientation and noted head rotation was slow in frequency content for stable transfer of body mass (Hicheur et al. 2005). This head and trunk coordination has also been investigated by suppressing the

vestibulo-ocular reflex (VOR) to show a reduced head and trunk coordination that leads to a more stable trunk and less stable head (Cromwell et al. 2004). Finally, having subjects perform tasks with higher gaze stability requirements (reading letters vs. focusing on a dot) increases head instability and did not change trunk stability during locomotion. Introducing the dimension of gaze stability requirements further complicates the stability of the head on the trunk during locomotion (Mulavara & Bloomberg 2002).

Finding its origins in Gibson's work, the notion that optic flow velocity and displacement may guide locomotion has evolved from sensory phenomena to clinical tool (Gibson 1958). Being influenced by the moving-room postural studies of Lishman and Lee, Konczak altered optic flow in an experiment where subjects walked in a moving hallway. He found a large portion (42%) of subjects to slow from their regular step velocity when the global optic flow was moving through subjects and a lower portion (25%) of subjects to have faster velocities when the optic flow was moving towards the front of subjects. Konczak proposed the idea that optic flow velocity does not necessarily destabilize the body; rather, it has a modulatory effect on gait velocity (Konczak 1994). Next, Zijlstra and colleagues suggested that visually-guided walking adjusted the ratio of the stride length (SL) over the stride frequency (SF) (Zijlstra et al. 1998). Prokop and colleagues went on to name SL, SF, and walking velocity (WV) the three main components of locomotion in their study of self-driven treadmill walking with tunnel-like virtual display. With their setup, they were able to increase and decrease WV via directional optic flow in a much more efficient manner than Konczak. They found

that the SL was changed while SF remained constant during optic flow conditions. Changes in SL, they argue, are the reason that optic flow is able to modulate changes in WV. Also of note, the use of long trial lengths (10 min/~800m) revealed less use of visual information over time as events in the stride cycle increased in variability (Prokop et al. 1997). Last, this guiding effect of optic flow has been shown to aid in the recovery of stroke patients by increasing gait speeds during virtual moving rooms (Lamontagne et al. 2007).

In addition to studies that investigate the effects of visual scenes on the velocity of movement, there are studies that investigate the structure of virtual displays and their influence on postural sway during locomotion. Warren, Kay, and Yilmaz performed a series of experiments with treadmill walking and virtual display that revealed the visual coupling of sway (via neck kinematic) to virtual environment is dependent on the geometry of the scene (Warren et al. 1996). In their first experiment, they changed the visual scene by direction (0°, ±30°, ±60°, 90°), type (rotation or translation), and frequency (.25 Hz and .4 Hz). They found similar responses to both rotation and translation, but much higher responses to the .25 Hz frequency. They also found that sway is directionally specific to driving visual scene. Yet, this directional specificity was anistropic to reveal that visual coupling is higher in the M/L plane than other planes of the body. In their next experiment, they eliminated motion parallax through using a traveling front wall to see if motion parallax was the cause of the anisotropy. They also tested the effect of using varying displacement amplitudes to investigate the “control” of the visual scene. They found that eliminating the traveling hall and using the traveling

wall led to a decrease in the anistropic effect while increasing the visual scene displacement caused higher amounts of sway during locomotion until saturation. These higher amounts of sway, however, were not proportional to the increases in visual scene amplitude. In their final experiment, they rotated the platform 90° to change body orientation and made subjects turn their head to the visual scene to test the hypothesis that the anisotropy was due to the constraints of biomechanics or somatosensory stimulation. They found that the anisotropy remained through higher responses in the A/P plane and that this reversal confirmed that the anisotropy was not due to biomechanics or somatosensory input; rather it was due to the distinction between motion parallax and optic flow (Warren et al. 1996). Not only did this series of experiments support the idea that visual coupling is based on scene geometry, they revealed how sensitive the nervous system is to the many possible changes in visual information.

In an investigation which was the precursor of many of the ideas contained in this dissertation, Logan et al. (2010) compared the use of visual stimuli in standing and walking behaviors. By recording kinematics from multiple segments of the body, this study was able to study many functions of vision during walking. In trunk orientation, frequency response functions (FRFs) from vision were similar between standing and walking at low frequencies. This finding shows how the nervous system uses vision for control of posture upright during locomotion. An additional, gait cycle phase-dependent response was observed in the thigh angle during walking conditions. This covariance peaked during the response phase of swing. This modulation could represent the use of vision for

speed control or obstacle avoidance/ accommodation, and has inspired further experimentation. In comparison to Warren et al.'s collection of a single marker at the neck (Warren et al. 1996), Logan et al.'s study of the multiple segments of the body showed how vision can influence multiple processes simultaneously during locomotion.

Indeed, manipulations of visual information have been shown to have an effect on heading, steering, head stability, head-trunk interactions and body sway during locomotion. These studies show that vision is clearly used for multiple subtasks during human locomotion. Next, we turn to some recent studies by Kuo and colleagues that are concerned with locomotive control on the whole. Rather than using visual manipulations to imply function of those visual inputs, these studies use vision as a perturbation to gain insight into the control process.

O'connor and Kuo first used visual perturbations to study differences in control of human walking in the frontal and sagittal planes (O'connor & Kuo, 2009). Subjects walked on a treadmill in front of virtual displays which translated in either the sagittal or frontal planes. These authors hypothesized that visual scene motion in the frontal plane will cause larger variability in step width when compared to the effect of sagittal plane scene motion on step length variability, reflecting the larger active control effort required by the nervous system in the frontal plane. These hypotheses stemmed from previous work (Bauby & Kuo 2000) in which a musculoskeletal model for walking was developed that emphasized the mechanical configuration of the human body was passively stable in the sagittal plane and was intrinsically unstable in frontal plane. The little

used somatosensory input of the legs, the authors argue, is used in sagittal plane control while intrinsic instability in the frontal plane requires more active control from the nervous system. Furthermore, these ideas have arisen with inspiration from passive dynamic walking machines that are passively stable in the sagittal plane as they can produce coordinated walking without control, and rely on the interaction of inertial and gravitational mechanics and oscillations produced by intermittent foot contact with a sloped ground (McGeer 1990; Collins et al. 2001). Returning to O'Connor & Kuo (2009), their hypothesis was confirmed when they observed variability in step measures to be approximately ten times more sensitive to frontal plane visual perturbations. These authors then concluded that control of balance in the sagittal plane during walking is a series of passively stabilized falls. More recently, this group has repeated this experiment with measures of metabolic rate, and found degree of variability in step parameters to be correlated with energy expenditure in all conditions (O'connor et al. 2012). In this case, visual perturbations were used to increase variability in step parameters in order to cause more control effort by the nervous system. As these authors conclude, energy expenditure is correlated with the increased control effort needed to correct for these visual perturbations.

Finally, these notions of passive versus active stability have been recently used in studies investigating the interaction of visual scene perturbations and speed. Like Kuo and colleagues, Wuehr and colleagues subscribe to the idea that passive stability mechanisms are at play more so in the sagittal plane compared to the frontal plane. At various treadmill speeds, these authors looked

at step width and length measures (coefficient of variation (CV), detrended fluctuation analyses (DFA)) with and without vision. Frontal plane gait parameters at all speeds suffered when vision was taken away while sagittal plane gait parameters suffered only at slow speeds when vision was taken away. Thus in addition to the planar aspect, there appears to be speed-dependent component to active control. These authors suggest that stability in the sagittal plane is more actively controlled at slower speeds while passive stability mechanisms and automated rhythm generators passively control the sagittal plane at faster speeds (Wuehr et al. 2013). In sum, the notion of plane-dependent degree of active control is catching on the human locomotion literature, and vision is being used to introduce variability in locomotive system to induce active control.

Insights into neural control using mechanical perturbations

To begin a review of mechanical perturbations during locomotion, one can start with those initial studies by Nashner and colleagues which were heavily influenced by previous studies in standing postural control. Nashner first probed human locomotive control during over-ground walking by moving a platform unexpectedly underneath subjects walking on a walkway. With a focus on sagittal and vertical plane kinematics and EMG of the leg segments, Nashner sought to "demonstrate the function of these EMG adjustments in maintaining the balance of the walking subject" (Nashner 1980). After applying translating (vertical and sagittal) and rotating (sagittal ankle rotation) perturbations at four time points of

the stance phase, it was found that EMG responses mimicked those observed during standing postural control and that postural adjustments were essentially overlaid onto locomotive adjustments. Additionally, he found that adjustments to these mechanical perturbations were proportionally much larger than expected as the perturbations were not large in comparison to regular motion of the body during walking. As the modulations in EMG were simply changes in amplitude of the same activations producing the gait cycle, Nashner proposed a conceptual model of locomotive control that makes use of an “adaptive element” which allows adjustments of the endogenous rhythm generator to accommodate external perturbations. This adaptive element receives both the anticipated motions of the legs and sensed motions of the legs and then transforms “discongruent features into the appropriate parametric commands” (Nashner, 1980). In sum, Nashner used mechanical perturbations to over-ground walking to theorize about an adaptive controller for stepping motions which is intertwined with a neural mechanism concerned with maintenance of posture upright during locomotive behavior.

In a related study, Nashner and Forssberg (1986) used mechanical perturbations of a different type to focus on postural control during treadmill walking. In this study, subjects were mechanically perturbed by their upper body by having to pull a handle in a self-paced fashion or in response to a tone. As this pulling is a threat to upright stability during the ongoing locomotive cycle on the treadmill, these authors were interested in understanding the kinematic features and muscle activations that would either prevent a loss of balance in a

feedforward (in the case of self-paced arm pulls) or feedback manner (in the case of arm pulls in response to the tone). During the self-paced pulls, subjects would pull the handle around heel-strike and adopt a muscular activation strategy (increased hamstring/ gastrocnemius activation during stance) of postural stabilization prior to activation of the biceps brachii for handle pulling. During trials dictated by a tone, this strategy was maintained when arm pulls were required in the majority of gait cycle phases. If the arm pull was required late in swing phase, however, this “posture-first” strategy was not enacted as it would be destabilizing to weight acceptance during heel-strike. According to the authors, a “redistribution of postural activations” occurred and the nervous system (via sensory inputs) operates in a feedforward manner to anticipate that the process of shifting weight support from one limb to the other will counteract the arm pull perturbation. In sum, Nashner & Forssberg showed that a similar stabilization strategy for maintenance of posture upright during treadmill walking (Nashner & Forssberg 1986) was observed during perturbations occurring during standing postural control (Cordo & Nashner 1982). Once again, using a mechanical perturbation to probe walking revealed the subtask of postural control overlaid on the locomotive cycle.

Following a tradition in the animal literature of seeking so-called “stumbling corrective responses”, there have been several more studies which probe specific phases of the gait cycle with a mechanical probe to learn about the nervous system’s strategy to deal with such perturbations. In one such study, Eng and colleagues presented subjects with a thin metal obstacle at random gait

cycles in either early or late swing while walking over-ground. They found that the phase of swing in which they presented the obstacle dictated the specific strategy used. When the obstacle was presented in early swing, subjects typically used an elevating strategy consisting of swing limb flexion associated with swing limb biceps femoris activation and stance limb extension. And when the obstacle was presented in late swing, subjects adopted a strategy where the swing limb was quickly extended to shorten the step length and this was associated with either a decreased vastus lateralis activation or increased activation of the biceps femoris in the swing limb. These authors observed that the obstacle avoidance response in humans is based upon the phase of the gait cycle that the response is initiated. During early swing, ample time for the appropriate clearing of the obstacle can occur while during late swing the strategy is to quickly step prior to the obstacle so the appropriate planning can take place and the other limb can clear the obstacle (Eng et al. 1994).

Expanding on the study of Eng et al. (1994), Forner-Cordero and colleagues used precisely timed pulling of the swing leg to also study stumbling corrective responses in humans (Forner Cordero et al. 2003). Some innovations were made in this study as an additional phase of perturbation was studied, many steps following the perturbation were studied, the duration of the perturbation was varied and a treadmill was used to regulate the speed of walking. Short duration perturbations in early swing elicited a mixture of an elevating strategy, delayed lowering strategy and lowering strategy across subjects while long duration perturbations in this phase elicited a delayed

lowering strategy. Delayed lowering strategies are those which shorten step period in the next or 2 steps after the perturbation to accommodate the perturbation. Short range perturbations of mid and late swing always caused a lowering strategy. From these various perturbations, the authors recast these responses of the swing leg to mechanical perturbations in terms of step after perturbation rather than strategy (elevating, lowering) of step during perturbation. To conclude, these authors classify responses to mechanical perturbations as those that can be fixed quickly within cycle or those which may destabilize gait and must be corrected slowly over time.

With these results in mind, these authors went on to create a mechanical model of stumbling recovery. With the model's goal of recovery reaction being control of the trunk during double support, it was found that large steps during an elevation strategy could alleviate trunk torques due to the perturbation in a single step while many steps would be needed to alleviate these trunk torques in the case of the lowering strategy (Cordero et al. 2004). In short, this modeling approach supports the idea that quick steps can alleviate unwanted trunk torques due to external mechanical perturbations (Cordero et al. 2004). More recently, this author has begun to use optimal control approaches to find the optimized trajectories to produce a biomechanical model of the stumbling response. This effort has yielded simulations of the stumble response and a potential recovery strategy used by muscles in the model including increases in stance leg extensors and swing leg flexors (Forner-Cordero et al. 2011).

More recently, several groups have used mechanical perturbations to further support or disprove ideas about organizational principles in the musculature of locomotion. That is, mechanical perturbations are being used to test locomotive control principles already developed rather than probing the system to develop such control principles. Recently, Oliveira and colleagues were interested in how various mechanical platform (sagittal and frontal surface translations) perturbations similar to those of Nashner's study (Nashner, 1980) would affect the basic motor modules for locomotion identified by Ivanenko and colleagues (Ivanenko et al. 2005). They hypothesized that new modules to counteract the mechanical perturbation would be created and these modules would then be superimposed on the previously identified basic modules (Oliveira et al. 2012). Using bilateral recordings of sixteen muscles, non-negative matrix factorization (NNMF) revealed four motor modules explaining greater than 90% of the variance in muscle activations in both perturbed and unperturbed conditions. For the most part, sagittal plane perturbations had preserved modules with activation signals of these modules altering based on changing kinematic needs. Frontal plane perturbations, however, caused the loss of a module and this was due to the subject's higher priority for balance preservation compared to propulsion during these frontal plane platform translations. Interestingly, Oliveira and colleagues reached a similar conclusion to Nashner (1980) in that new activations/modules were not required for the nervous system to respond to walkway perturbations. Once again, existing activations/modules are used to promote upright stability (Oliviera et al. 2012). In an extension of previous work in

standing postural control and stepping movements, Ting's group has also recently perturbed the modules made up of muscle activations (muscle synergies) through both anticipated and unexpected translations of the walkway (bi-directional frontal/sagittal) during over-ground walking. Using NNMF on sixteen muscles from one side of the body, they found six to eight muscle synergies dependent on such with several and the additional synergies being subject-specific modules for medial/lateral limb control. These authors found that the mechanical perturbation (in both unexpected and expected perturbations) simply shifted the timing in these spatially-conserved muscle synergies to accommodate biomechanical demands. Of note, these authors conclude that this flexible timing in the use of these muscle synergies allows for a "library" of subtasks to be recruited when needed (Chvatal &Ting, 2012). In all, both of these groups have concluded that the low-level muscular organization is preserved in the face of mechanical perturbations to the base of support to enact higher level goals such as maintenance of posture upright and moving along a walkway.

Recently, Ahn and Hogan have used the Anklebot as a mechanical perturbation to the gait cycle trajectory of the legs as an insight into the control process during locomotion (Ahn & Hogan 2012). Motivated by studies which posited control of foot trajectories to be supra-spinal, these authors used periodic torque inputs to plantar flexion at periods different from their preferred cadence to support the notion that control of foot trajectories is due to a nonlinear neuro-mechanical oscillator and not prescribed by supraspinal control. As hypothesized, entrainment of the gait cycle occurred in almost all subjects (18 of

19) marked by stride duration converging to the perturbation period dictated by the stride 34/80 total trials. This total number of trials was low because entrainment only occurred if perturbation occurred near subjects' preferred walking cadence (narrow basin of entrainment). Of note, the phase at which stimulus was initiated did not affect the rate or degree at which entrainment occurred. However, subjects typically enacted the phase locking with the phase of gait where additional plantar flexion caused by the Anklebot assisted propulsion (push-off). From these findings, the authors conclude that perturbing the limit cycle is all about perturbing the "low level", primitive forms of control during locomotion and shows how normal, locomotive kinematics of foot trajectory are not prescribed via higher centers. Thus, these authors have used a mechanical perturbation of the lower limb to observe entrainment of the neuro-mechanical oscillator for locomotion and provide support for the separation in control of low level propulsion and higher level "episodic supervisory control of a semi-autonomous periphery" when needed for cases such as irregular footholds or obstacle avoidance.

To conclude the review of mechanical perturbations and human locomotion, it is worth noting an investigation by Varraine and colleagues (2002) which studied the interaction of mechanical and visual information in treadmill walking. This group's main concern during walking was the intensity command(IC) which consists of those lower level central pattern generators (CPGs) that will decide the propulsive forces to power through the gait cycle. As a result, Varraine and colleagues believe maintenance of this IC is the goal of

controlling gait. In their first experiment, subjects walked on a self-driven treadmill with backward movement of a virtual hall with the task of maintaining same IC. There were three conditions during this task: FLOW (sinusoidal variations of the optic flow at .0083 Hz), FORC (sinusoidal variations in treadmill resistance at .05 Hz) and COMB (both starting in phase with each other). They found the stimulus frequency component of the power spectral density (PSD) at the optical perturbation to be greater in COMB condition than in FLOW condition. Also, they found less variation of stride frequency in the FLOW condition than the other two conditions. Finally, they bolstered Prokop's idea of attenuation by finding that the spectrum integral of walking velocity is much lower in the last cycle than the first cycle of gait (Varraine et al. 2002).

In a second experiment, Varraine and colleagues told the subjects their goal was to maintain a constant WV in either presence or absence of optic flow and presence or absence of external force perturbation. They found the walking velocity spectrum component in congruent condition lower than condition without optic flow while the force spectrum component is higher with congruent flow than without congruent flow. They reason that compensation for WV changes is in the form of increased force during locomotion. They also note that phase delay in the COMB condition compared to the FLOW represents a neural time delay for integration of force information (Varraine et al. 2002). In sum, this study shows that visual and mechanical perturbations interact, and emphasizes the need for independent sensory and mechanical stimuli.

In all, mechanical perturbations have been used to probe the control of locomotion in a variety of ways. It is clear that the goal of many of these studies with mechanical perturbations is to study some sub-function, or subtask, of locomotion such as postural control upright or obstacle avoidance. The entire locomotive behavior, however, may emerge as later studies employing modeling approaches may attempt to integrate subtask control into an entire hypothesized control scheme. An example of this is observed in Ahn and Hogan's (2012) entrainment work which led to development of a walking model that could reproduce such entrainment without a supraspinal influence or continuous sensory feedback occurring through a central pattern (CPG) network (Ahn & Hogan 2013).

Rhythmic auditory cueing and human locomotion

The use of a device such as a metronome for rhythmic auditory (RAC) to regulate step period has been used to regulate cadence in controlled experiments, and has more recently been used for insight into neural control strategy. Use of a metronome for RAC has also shown promise in clinical applications.

Studies of RAC are typically performed in a single session in the clinic in or in a pre-post test format following intervention studies. In a meta-analysis of visual, auditory and somatosensory cue studies in Parkinson's disease (PD) patients, only rhythmic auditory cues were found to be effective in improving

walking speed (Lim et al. 2005). Although the idea for use of RAC for PD patients has been around since 1942 (Von Wilzenben 1942), Lim and colleagues concluded that the only study of high methodological quality that showed a positive effect of RAC in PD patients was a study by Thaut and colleagues that showed an increased gait speed after 3 weeks of RAC training (Thaut et al. 1996). There was, however, additional limited evidence for the use of RAC for improving stride length and cadence of PD patients (Lim et al. 2005).

In addition to PD, RAC during walking has been studied to a more limited degree in Huntington's disease, stroke, and cerebral palsy. Use of RAC in stroke survivors has shown RAC to increase gait symmetry (Roerdink et al. 2007) and increased velocity and stride length due to a 6 week RAC training intervention (Thaut et al. 1997). In Huntington's Disease, conflicting reports have observed an increased walking velocity after RAC training in one study (Thaut et al. 1999) and no effect of RAC in various walking tasks (normal, carrying a tray) in another study (Delval et al. 2008). A recent study in ambulatory adults with cerebral palsy, however, has shown that RAS can improve gait deviation index (GDI) and sagittal plane pelvis tilt/hip flexion during over-ground walking trials with RAS (Kim et al. 2011). Interestingly, a follow-up three times a week, three week intervention study showed that RAS improved a host of gait parameters (increased cadence, increased walking velocity, increased stride length), sagittal pelvic tilt/ hip flexion, and GDI (Kim et al. 2012) in post-intervention testing. In sum, the use of RAC needs be more fully investigated in other patient populations while study in PD patients is more extensive with a longer history.

In healthy populations, however, RAC is typically used as a control condition or throughout an experiment to eliminate alterations in step period for insight into other processes during locomotion. The use of metronome conditions for this function is prevalent across the walking literature, and this brief review will only provide examples of this use of RAC. One flavor of these types of studies are those that constrain gait frequency across a range of conditions to interfere with gait cycle parameter relationships and then test if a hypothesized objective function can still account for the relationships across parameters. In one such study, RAC was used to alter speed-frequency curves of treadmill walking and the metabolic cost of transport was determined to be the underlying minimized objective function to produce the preferred gait (Bertram & Ruina 2001). Another type consists of those studies which use metronome in all conditions in order to regulate cadence across subjects to control for variability in step period between subjects. Often times these studies just simply note in the methods section that a metronome was used for this reason. An example of this can be seen in a study by Danion and colleagues in a study of increasing treadmill resistance to study kinematics and EMG in conditions when subjects either resisted or did not resist changes in treadmill resistance. The use of the metronome is simply mentioned in the abstract and methods, and was used so that stride frequency wouldn't vary between subjects when dealing with the mechanical perturbation (Danion et al. 1997). A final type of study using metronome to eliminate step period are those studies when metronome conditions are used to perturb seemingly unrelated response variables. One such study is a study by Latt and colleagues that used

metronome condition to test the effect of constraining cadence on head and pelvis accelerations. These authors believed that gait cycle parameters were intertwined with upright stability measures of head and pelvis measures. The study found that there is a certain range of cadences that are associated with measures (harmonic ratios) of head and pelvis accelerations in vertical and sagittal plane which were ideal for upright stability (Latt et al. 2007). Interestingly, Latt and colleagues viewed upright stability and moving from point to point as the only critical activities during walking, and they believe these two activities were intertwined. This was their “indirect” reason for looking at the effect of regulating cadence on trunk stability measures.

Recently, auditory entrainment via metronome has been used for insight into neural control as experimental evidence has supported step period as a control variable for treadmill walking. Dingwell and colleagues (2010) found that subjects sub-optimally overcorrect deviations in position on the treadmill through stride to stride alterations in a combination of stride length and stride period along a goal equivalent manifold (GEM). Using detrended fluctuation analysis (DFA) and optimal control approaches, these authors argue that anti-persistence in speed emerges due to sub-optimal over-corrections due to an increased central control (Dingwell et al. 2010). Put simply, this “anti-persistence” means that deviations in one direction are likely followed by deviations in the opposite direction. Furthermore, a control strategy of goal equivalent adjustments in stride period and stride length on a stride to stride basis was determined.

Terrier and Deriaz (2012) were interested in understanding how adding a metronome would constrain these stride to stride alterations. Also using DFA approaches, they hypothesized that stride speed (SS) and stride time (ST) would show an anti-persistent pattern as they would be tightly controlled in the metronome condition while stride length (SL) would not be and show a statistically persistent pattern. These results would follow a previous study in over-ground walking (Terrier et al. 2005) in which ST was anti-persistent while SL and SS was not (due to freedom to modulate SS over-ground). They confirmed anti-persistent dynamics in the time series of stride speed (SS) during treadmill walking without a metronome with stride time (ST) and stride length (SL) remaining persistent. Upon adding a metronome to treadmill walking, all time series (SS, ST, SL) were anti-persistent. These authors also observed (as expected) that adding a metronome would reduce stride to stride variability in ST to a greater degree when compared to SL and the effect of the metronome was greater at slower treadmill speeds. Contrary to their hypothesis, stride length was also tightly controlled during the metronome condition even though a constraint was not necessarily placed on that gait parameter. These authors argue that cross-regulation of SL and ST occurred which led to an absence of redundancy among the gait parameters. In accordance with Dingwell et al.'s proposal of the GEM of ST and SL, dictating both ST and SS will indirectly cause control of SL for subjects to accomplish the goal of staying on the treadmill (Terrier & Deriaz 2012).

In a related study, Terrier (2012) expanded upon these DFA measures to determine if measures of fluctuation magnitude and long term stationarity applied to SS, ST and SL were altered by metronome conditions. This study hypothesized that these measures would reveal similar effects as previous work (Terrier & Deriaz 2012) using DFA analyses to study stride to stride fluctuations. The measure of global fluctuation magnitude used was standard deviation across the entire trial and Non-stationarity Index (NSI) was used as a measure of consistency in local averages with consistency in local averages associated with low NSI. Global fluctuation magnitude was not altered by the use of a metronome on the treadmill, and attributed to the global fluctuation caused by treadmill walking. NSI of SS, SL and ST was found to be low during treadmill and metronome conditions, indicating that all three measures had local averages which were consistent. Correlations between newly calculated measures of NSI and the DFA analyses of previous work (Terrier & Deriaz 2012) were also computed. NSI and scaling exponents of the DFA analysis were positively correlated. Terrier concluded that the locally consistent means (low NSI) and statistical anti-persistence observed previously result from a “lost” degree of freedom; there is no longer redundancy between step length and step period for flexible control. With this result and previous literature in mind (Haussdorf et al. 2005; Dingwell et al. 2010) Terrier then proposes that gait control has two modes: a long-range, fractal-like mode for a “steady gait” across many strides and a more resulting conscious, tightly controlled mode observed the anti-persistent patterns in short-range stride to stride corrections (Terrier 2012).

In summary, RAC has been used to control cadence and some investigators have recently compared RAC to non-RAC conditions for insight into how regulation of cadence fits into neural control strategy for walking. Additionally, RAC with use of a device such as a metronome has shown clinical promise for PD patients. It appears that a likely future direction of this work is to use RAC conditions to theorize about deficits in locomotive control that arise as a result of PD.

Phase resetting in human walking?

Phase resetting and its implementation into the control scheme for human locomotion is of critical interest. The shortening or lengthening of cycle period is plausibly a strategy for the human locomotive control system to mediate the effects of sensory and mechanical perturbations to locomotive cycle. Surprisingly, there are few studies which explicitly focus on phase resetting during human walking.

The experimental protocol of Ahn and Hogan (2012) explained above could be adjusted slightly to test for phase resetting of the locomotive cycle using the Anklebot. In fact, a colleague of Ahn and Hogan attempted to cause phase resetting in subjects by applying plantar-flexions via Anklebot using 400 perturbations during 20 minutes of treadmill walking. These perturbations were spaced pseudorandomly so that ~ 40 perturbations occurred at each 10% bin of the entire gait cycle. After clear deviations from nominal trajectories with phase

response curves for all subjects that were not distinguishable from 0, it was concluded that some higher level neural controller must execute corrective actions to the deviations in the kinematic trajectories. Modulating the timing of the gait cycle is not the strategy as a zero phase shift was observed (Klenk 2011).

Also reporting a non-effect amidst other findings, Capaday's group attempted to observe phase resetting due to transscranial magnetic stimulation (TMS) of motor cortex. TMS at various phases of the gait cycle did not change the time (using phase resetting curve) a step was to initiate. From this result, Capaday concluded that motor cortex was not involved in the timing of those activations which promote the gait cycle (Capaday et al. 1999). Of note, the behavior during this TMS was self-paced treadmill walking, and subjects did not face a perturbation additional to the TMS which could have elicited phase resetting.

Feldman and colleagues, on the other hand, used a mechanical perturbation during treadmill walking to test the idea that phase resetting must occur for humans as it represents a shift in the referent body configuration (Feldman et al. 2011). These authors hypothesized that an irreversible "long-lasting phase resetting" will occur after restoration of constant speed gait on the treadmill following a mechanical perturbation. They argue that this must occur as the following gait cycles must enact a strategy to overcome an "overall loss" in body displacement that occurs. Subjects walked on self-paced treadmill and the mechanical perturbation consisted of a cuff around the leg that would unexpectedly "freeze" or block forward motion of the leg for 250 ms of the swing

phase. Phase resetting was calculated as phase difference between actual limb position and its projection from pre-perturbation trials. Responses to mechanical perturbations elicited a long-lasting phase advance of ~ 110º that was whole-body as the same phase advance was observed in the multiple limbs studied. These authors then note that bipedal stability requirements hinder the ability to apply the extensive study of phase-resetting in animal models to humans, and they note that long-lasting phase-resetting has been observed in one participant in one study (Kobayashi et al. 2000) prior to their study. Interestingly, these authors propose that this global phase-resetting is about preventing falls as the correct referent body condition is employed. Additionally, the referent body location is controlled and these authors believe it incorrect for one to think that there is a separation in control of posture and movement during walking.

Although there are few studies of human locomotion which explicitly study phase resetting in a systematic fashion, there are many studies (some even mentioned in other sections above) which report alterations in step period, stride period, etc. in the step/stride of a sensory or mechanical perturbation (and following step/stride, perhaps) without formally mentioning that there is an investigation of transient phase-resetting. The results of these studies are not mentioned here as this survey of the literature attempted to find systematic studies of phase-resetting in human locomotion. Attention is now turned to those modelers and robotics designers who hypothesize about a phase resetting mechanism in human locomotion

Several models have implemented phase resetting by modulating features of preformed kinematic joint trajectories with real time sensors of joint motions. In one such study, Yamaski and colleagues used first a double pendulum model and then a model of human locomotion to gain insight into the actual functions of phase-resetting (Yamaski et al. 2003). These authors use the support of these two different models to show that phase resetting could be critical for aiding the system's state point back into the basin of attraction and also to reduce the time that this state point takes to get back to the limit cycle (convergence time). Unfortunately, Yamaski and colleagues could not lower the convergence time (via phase-resetting implementation) in their bipedal locomotion model. More recently, Nomura and colleagues used prescribed gait trajectories of limb segments to constrain plant models of biped human gait and biped humanoid robots (Nomura et al. 2009). Essentially, these authors show that dictating kinematic trajectories of these models will force stable nonlinear dynamical systems to emerge. Upon addition of phase-resetting to these systems, stability improved to external mechanical perturbations at specific phases that were previously susceptible to instabilities (Nomura et al. 2009). Phase-resetting could be a critical strategy at specific phases (such as single limb support) where the body may not be as intrinsically stable against mechanical perturbations.

Those seeking to model the neural control of bipedal locomotion may also choose to implement phase resetting processes into their models via sensory information. In order to modulate timing of the gait cycle, sensors are integrated into bipedal walking models to play a major role in dictating a time-advanced or

time-delayed state of the system. Recently, Aoi and colleagues implemented phase-retting in a human walking model which contained both a model of the musculoskeletal system and the neural control system. The nervous system model consisted of hierarchical network model with two layers (Aoi et al. 2010). The rhythm generator network layer and pattern formation layer dictated timing information through phase oscillators and pulsatile activations dictating spatial activations of muscles, respectively. Phase-resetting was implemented as the sole source of sensory feedback to the rhythm generator network layer and was based on the foot contact information of heel strike and toe-off. Phase resetting in this model allows appropriate feed forward dictation of the typical muscle activations required for the locomotive cycle. This model performed much better in terms of stability when phase-resetting was implemented as simulations with phase resetting were more stable when changes in trunk mass were imposed, changes in incline of slope to be walked and during increased time delays. In the end, Aoi and colleagues see phase-resetting as a strategy for adaptive locomotion as it alleviates the effects of neural transmission delays as it can trigger those neuromuscular activations required for the locomotive cycle in a feed-forward manner.

In all, a few human studies explicitly studying phase-resetting in human locomotion have revealed it is possible to phase reset human locomotion with mechanical perturbations (with mixed results). Additionally, several modelers of human locomotion and designers of humanoid robots see phase-resetting as a critical neural control strategy that can be implemented in a simple manner.

These modelers believe that phase resetting may be implemented for feed-forward control and have proposed simple rules the nervous system may use to implement such a process. Such detail remains to be explored and verified in actual human locomotion.

Chapter 3: Function dictates the phase dependence of vision during human locomotion[1]

Introduction

It is generally held that sensory input influences locomotion in a phase-dependent manner. Evidence suggests that sensory inputs can be gated, by either facilitation or suppression, at certain phases of the locomotive behavior (Duysens et al. 2000; Rossignol et al. 2006). For example, the vertebrate Xenopus laevis (tadpole) has been shown to inhibit sensory pathways from modulating motor neurons at functionally relevant phases of its swimming cycle (Sillar and Roberts 1988). Such phase dependence may provide insight to the respective roles of different sensory modalities during locomotion.

Human (e.g., Capaday & Stein 1986; Duysens et al. 1990) and animal (e.g., Forssberg et al. 1975; Forssberg 1979) studies have emphasized phase dependence of somatosensory input, illustrating how responses to both tactile and proprioceptive stimuli are modulated during the gait cycle. The focus on proprioceptive/tactile inputs arises from the suppression or facilitation of their reflex pathways at different phases of the gait cycle to enable fast corrective responses to unexpected disturbances of balance and walking (Zehr & Stein 1999).

[1] This chapter has been recently published in the Journal of Neurophysioology.:
Logan D, Ivanenko YP, Kiemel T, Cappellini G, Sylos-Labini F, Lacquaniti F, Jeka JJ. Function dictates the phase dependence of vision during human locomotion. J Neurophysiol 112:165-80, 2014.

The use of vision has also been suggested to be dependent on the phase of the gait cycle. Patla and colleagues analyzed the use of visual cues at different phases of the gait cycle for subject-initiated modifications during the subsequent step (Patla 1991; Patla et al. 1991). Subjects were able to avoid small obstacles and alter step length or step width, but only when presented with visual cues up to the end of stance in the previous cycle. In contrast, change of direction must be cued prior to the end of mid stance. Additionally, denial of vision during a "critical period" of late stance has been shown to prolong stance duration during a task requiring subjects to step on light emitting "stepping stones" (Hollands & Marple-Horvat 1996). These studies use distinct tasks such as obstacle avoidance or alteration of foot placement to identify phases of the gait cycle in which vision is critical.

In addition to obstacle avoidance and foot placement, visual input is used for many other functions during walking. Using continuous optic flow stimuli, vision has been shown to be important for adjustments in speed (Konczak 1994), stride length (Prokop et al. 1997) and navigation (Warren et al. 2001). Immersive, oscillatory visual stimuli illustrate that visual inputs are critical for upright postural stability (Warren et al. 1996; Logan et al. 2010) during walking and that the nervous system makes greater use of visual information for the control of frontal-plane motion, which is thought to be more biomechanically unstable (O'Connor & Kuo 2009). The visual stimuli in the present study probed functions underlying the task of treadmill walking such as speed control for

maintaining position within the boundaries of the treadmill as well as upright postural stability.

Here we further investigate the phase-dependent effect of vision on walking with discrete disturbances of the visual scene towards or away from a subject walking on a treadmill. Transient ramp and hold virtual perturbations systematically probed control of treadmill walking while the right leg was in three different phases of the gait cycle (loading, mid stance and terminal stance). We examined segment angles and muscular activity to investigate the phase dependence of responses to visual perturbations. For the midline trunk segment we considered the perturbations at three phases, and recording of kinematic and muscle responses from both right and left lower limb allowed the analysis of 6 distinct phases of perturbation effects.

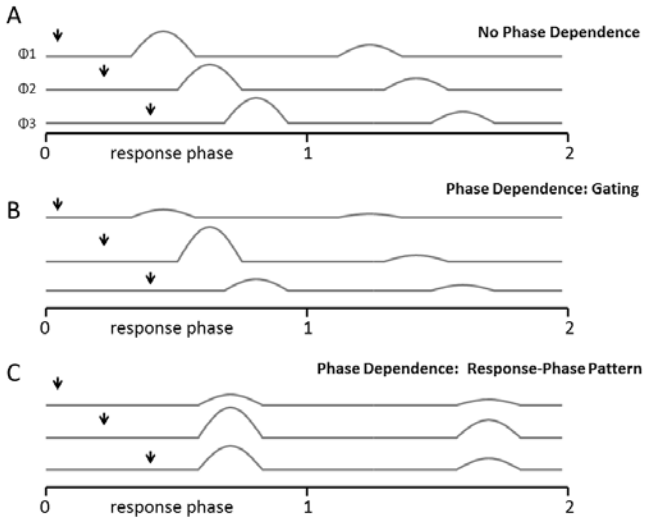

Figure 1. Phase Dependence Schematic. A hypothetical data set observed across response phases of a full cycle of a continuous behavior such as walking with three perturbation phase presentations (ϕ1,ϕ2 ϕ3) marked with arrows at perturbation onset. Responses can occur without phase dependence (A) while phase dependent responses such as gating (B) or a response-phase pattern(C) can occur. Response phase is indicated on the x-axes with the perturbation cycle and a cycle following the perturbation cycle. In this hypothetical data set of potential responses the transient response diminishes as it continues into the cycle following the perturbation cycle.

In studies of human locomotion, phase dependence more often takes the form of a response with fixed time delay and an amplitude dependent on the gait cycle phase of the perturbation (perturbation phase). This is due to the "local" nature of the perturbations typically used to probe phase-dependent responses. For example, investigations using somatosensory perturbations typically probe different phases of the gait cycle and observe phase dependence as the altered amplitude of a stereotyped waveform such as the H-reflex (Capaday & Stein 1986) or short-latency stretch reflex (Yang et al. 1991; SinkJær et al. 1996; Mazzaro et al. 2005), which are known to occur at a given response latency. Vision is clearly different. First, a "visual reflex" with fixed response latency during locomotion, if possible to elicit, has not been established. Second, visual pathways involve multiple neural structures which modify the response to a visual perturbation. Third, vision is a more "global" input, with the ability to affect all segments quasi-simultaneously.

With both the insight from studies of somatosensory input and the differences in vision noted above, we suggest a framework for understanding phase dependence of vision in human locomotion. Figure 1 presents three possible scenarios of phase dependence with these transient perturbations presented at three phases (Φ1, Φ2, Φ3) of the gait cycle. Figure 1A illustrates a linear response that has no phase dependence, that is, the response depends only on the time delay between perturbation and response. Figure 1B illustrates gating, in which the specific phase of the gait cycle during which a perturbation is presented will dictate the gait modifications (Duysens et al. 2000). An alternative

type of phase dependence, shown in Figure 1C, is when a response occurs at a characteristic phase of the gait cycle, a pattern we will refer to as a *response-phase pattern* of phase dependence. A response-phase pattern results from the state (position, velocity, etc.) of the limbs dictating when a response can be generated. As response-phase pattern intrinsically dictates the latency of response from a perturbation, the resulting variable time delay and its effect on response amplitude will be observed in the response.

The use of transient scene motion in this study is crucial as it allows us to distinguish between possible phase dependence scenarios (e.g. gating vs. response-phase pattern). Transient scene motion presented at specific perturbation phases of the gait cycle allows a determination of the effective perturbation phase or phases that is not clear during continuous (throughout gait cycle) perturbations. Evidence from previous work (Logan et al. 2010) using continuous scene motion led us to hypothesize that trunk segment responses to transient visual scene changes in this study would be at most weakly phase-dependent, whereas leg segment trajectories would be highly phase-dependent. Here we provide support for these hypotheses with the additional finding that *within-cycle* modulation of the leg segments and associated muscle activity are observed only when changes in visual scene occur at mid stance. This specific modulation due to visual input applied solely at mid stance, in addition to a leg response observed when vision is applied at all phases, suggests that phase dependence is not strictly dependent on the specific segment, but it also depends on the function of that visual input.

Methods

Ethical Approval

This study conformed to the Declaration of Helsinki and was approved by the Ethics Committee of the Santa Lucia Foundation. Informed consent was obtained from all participants according to the procedures of the Ethics Committee of the Santa Lucia Foundation.

Subjects

Eleven healthy subjects [6 males and 5 females, between 20 and 34 yrs of age with age 23.1 ± 4.3 (mean ± SD) yrs, weight 64.1 ± 11.0 kg] received modest monetary compensation for participating in this study. All subjects were self-reported to have normal (or corrected to normal) vision and no history of neurological disorders or surgical procedures involving the feet, ankles, knees, hips, back, brain, spinal cord or inner ear.

Apparatus

Virtual reality environment

Subjects walked at 3.6 km h^{-1} on a treadmill (EN-TRED 1475.911, Enraf-Nonius, Netherlands) one meter in front of a translucent screen (4x3m) with a rear-projected virtual display, as shown in Figure 2A. The display consisted of 500 randomly-distributed white triangles (3.7 x 3.7 x 3.5 cm) on a black background, updated at 60 Hz. The display was 3.7 m wide by 2.54 m high when static prior to trial initiation (position 0)**,** and subjects wore goggles with occluded

sides to prevent them from seeing the border of the visual display, allowing a 1.7 m wide by 1.7 m high field of view (about 81° of visual angle). The virtual display was created using CaveLib software (Mechdyne, USA) with projection through a digital projector (MP3135, HP,USA) synched to a desktop computer (Precision T5500, Dell, USA). Visual signals were created offline (Matlab, Mathworks, USA) and were generated via Labview (National Instruments, USA) on a desktop computer (Precision T5500, Dell, USA).

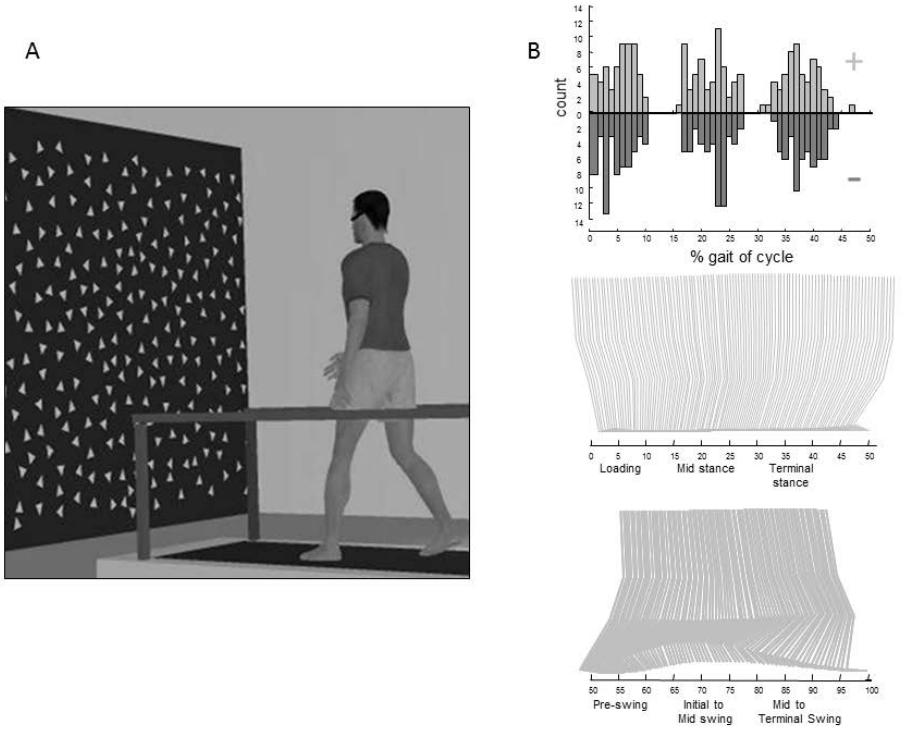

Figure 2. Experimental Setup. A: Subjects walked on a treadmill in front of a virtual display that would translate unpredictably in the sagittal plane using ramp and hold perturbations timed to RHS B: An exemplar histogram of the number of positive and negative stimuli at each phase of the gait cycle that were presented to a subject and representative stick diagrams below illustrating the position of the ipsilateral/ right (second row) and contralateral/left (third row) limbs at the times of perturbation. It is implicit in this exemplar stick figure that the foot lands at zero, or the ground, in the vertical plane.

Visual scene perturbations

During the experimental trials, the virtual scene either translated towards (negative/approaching) or away (positive/receding) from the subject in the anterior/posterior (A/P) direction. The perturbations were ramp and hold, reaching an amplitude of 13.5 cm in 60 msec. Direction from position 0 was chosen at random for all odd-numbered perturbations. A negative perturbation always followed a positive perturbation (and vice versa) in order to keep the range of scene motion between ±13.5 cm. The virtual scene was constructed with a fixed perspective point at the subject's eye height, with the assumption that the subject was 1 m from the screen. The scene was created so that subjects would see a fixed visual scene with the entire scene occasionally moving coherently towards or away from them. Perception of scene motion was not quantified in an objective manner in this study. Informally, subjects typically reported that something strange occasionally happened to the visual scene without clear indication of the direction of scene motion. The scene was constructed in this way as a probe to understand how fast changes in visual scene motion are used (via kinematics, EMG) at specific phases of the gait cycle. Visual display generation and data collection software were synchronized via an external trigger.

Kinematics

Body kinematics were measured using a nine camera VICON-612 motion analysis system (VICON, Inc, Oxford, UK). Reflective markers (diameter, 1.4 cm)

were placed on the right and left sides of the body at external landmarks corresponding to: base of the 5th metatarsal, posterior calcaneus (heel), lateral malleolus (ankle), lateral femoral condyle (knee), greater trochanter (hip), acromion process (shoulder), mastoid process (head) and frontal eminence (head). Additionally, markers were placed at the mediolateral center of the back of the head and the midline of the spine at the level of T1, T7 and L1 vertebrae. All markers were attached at the skin of these bony prominences, except those placed on the shoes at the 5^{th} metatarsal and heel. All kinematic data were collected at 100 Hz.

Our analysis focuses on the leg and trunk segments. Sagittal-plane foot, shank and thigh segment angles relative to the vertical were computed from angles formed by the fifth metatarsal to ankle, ankle to knee, and knee to hip with the most inferior point as the origin. We use segment angles rather than anatomical joint angles, based upon our interest in how the body maintains its orientation relative to the vertical during walking. Moreover, because joint angles can be computed from segment angles with a linear transformation, qualitatively similar results would be obtained with joint angles. As these segment angles are relative to the vertical, 0^0 in control waveform plots indicates that the superior marker on the segment is above and vertically aligned with the inferior marker on the segment. Positive values in these plots indicate that the superior marker on the segment is more forward of the inferior marker in the sagittal plane. Trunk orientation relative to the vertical in the sagittal plane was computed as the angle

formed by the L1 to T1 markers. To characterize whole body motion on the treadmill, A/P displacements of all markers were analyzed.

EMG

Muscular activity from both legs was measured using surface electromyographic (EMG) recordings (Zerowire, Aurion). Recordings of the following eight muscles were made from each side of the body: tibialis anterior (TA), gastrocnemius lateralis (LG), soleus (SOL), vastus lateralis (VL), rectus femoris (RF), biceps femoris (long head, BF), semitendinosus (ST), and erector spinae (ESL, recorded at L1-L2). Electrodes were positioned at the muscle belly with placement carefully chosen to minimize cross-talk (Cappellini et al. 2006). Recording sites were shaved, lightly abraded, and cleaned with isopropyl alcohol prior to electrode application. The EMG processing consisted of high-pass filtering, rectification and low-pass filtering with the same frequency cutoff values used in several previous studies of locomotion (Cappellini 2006; Cappellini et al. 2010a; Cappellini et al. 2010b; Maclellan et al. 2012). These EMG signals were band-pass filtered (analog, built in to Zerowire EMG system) between 10 and 1000 Hz and were sampled at 2000 Hz. Observation of low-frequency noise (< 20 Hz) in the recorded signal necessitated a high-pass digital filter prior to rectification. Using Matlab, these signals were high-pass filtered using a zero-lag forward-backward cascade of a 4^{th} order Butterworth filter with a 20-Hz cutoff frequency, full-wave rectified, and then low-pass filtered with a zero-lag forward-backward cascade of a 4^{th} order Butterworth filter with a 10-Hz cutoff frequency.

Procedures

Prior to experimental trials, subjects walked in front of a static visual display at the experimental locomotion speed in darkness with goggles on. This familiarization was followed by two trials 2 minutes long to determine mean gait period, which was used to create subject-specific timing of perturbations. Mean gait period was defined as the average time between each successive right heel strike (RHS) (see *Data Analysis*). In all trials, subjects were instructed to look straight ahead and were given approximately thirty seconds to reach steady state before recordings were made. For safety, an experimenter was behind the treadmill in close proximity with a push-button to immediately halt the treadmill if needed (never used).

Using subject-specific mean gait period, perturbation signals were designed so that onset of the ramp perturbations was timed to occur at about 0%, 16.66% or 33.33% of the gait cycle (see below). RHS was defined as 0% of the gait cycle. Subjects experienced fourteen experimental trials lasting approximately four minutes each, with approximately 24 perturbations in each trial. These 24 perturbations were 4 repeats of the six possible ramp and hold perturbations (2 directions x 3 perturbation phases) and were randomized within each trial, subject to the direction constraints mentioned above (see *Visual scene perturbations*). These perturbations were initiated via a footswitch whose force sensor was placed 1.25 cm anterior to the heel on the sole of the right foot. The footswitch used was a pressure-sensitive resistor (Zerowire, Aurion) that would indicate RHS and was integrated into the visual display system. As the motion

capture system was not integrated into the visual display system, the footswitch allowed initiation of the subject-specific perturbations designed to occur at specific phases of the gait cycle. Perturbations were applied pseudo-randomly throughout the trial. Across subjects, the mean number of gait cycles between perturbations was 8 cycles and the mean minimum and maximum gait cycles between perturbations were 4.3 and 27 cycles. There were never less than 3.6 cycles between perturbations.

Data Analysis

Perturbations

Prior to data analysis, the phase of the gait cycle where perturbation onset occurred (initiation of visual scene motion) was identified for each ramp and hold perturbation. The phase of the cycle when the perturbation occurs is the *perturbation phase*, while the *response phase* is the phase at which a response occurs after perturbation onset. Gait cycle phase of perturbation onset was identified as the percentage of the mean control cycle (see *Statistics*) elapsed between RHS prior to perturbation and perturbation onset. Each heel strike was computed as the local minimum of the heel marker in the vertical plane (Borghese et al. 1996; Ivanenko et al. 2004) occurring after each cycle's maximum angle formed by the fifth metatarsal-hip axis in the sagittal plane with the hip as the angle's origin.

Due to variability of right heel strike predicted by the foot switch relative to that measured from kinematics, ranges of perturbation onset were used. Those

perturbations which occurred at 0-10%, 16-26%, and 33-43% of the gait cycle were considered to occur at the 3 phases of perturbation onset. An exemplar histogram based on percentage of gait cycle from a single subject can be seen in Figure 2B, and the mean (SD) percentage of the gait cycle across subjects in these three phases was 6.1% (0.6), 22.5% (0.6), and 39.2% (0.6) for the 0-10%, 16-26%, and 33-43% groupings respectively. On average, 52, 49 and 52 perturbations occurred in these 0-10%, 16-26%, and 33-43% groupings for each perturbation direction for each subject.

Note that we applied perturbations in the first half of the gait cycle. To infer the effects of perturbations in the second half of the gait cycle, we assumed that walking has left-right spatio-temporal symmetry, namely that reversing left and right sides of the body is equivalent to shifting time by half a gait cycle. For example, we assumed that: (i) the right-side response to a perturbation at phases 50-60% with respect to RHS equals the left-side response to a perturbation at phases 50-60% with respect to left heel strike (LHS); and (ii) phases 50-60% with respect to LHS equals phases 0-10% respect to RHS, which corresponds to one of our experimental perturbations.

In this way, we were able to infer the responses of both sides of the body to perturbations at 6 phases of the gait cycle. In particular, left-side responses to perturbations at phases 0-10%, 16-26%, and 33-43% with respect to RHS were used to infer right-side responses to perturbations at phases 50-60%, 66-76%, and 83-93% with respect to RHS. The middle plot of Figure 2B shows an example control gait cycle trajectory of the right side of the body to illustrate the

normative configuration of the ipsilateral side of the body during the perturbation phases. In the final plot of Figure 2B, the configuration of the contra-lateral (left) side of the body at the same time is provided to illustrate the position of the contra-lateral limbs when these perturbations were to occur.

For clarity in presenting our results, we will refer to perturbation phases with respect to heel strike as loading (0-10%), mid stance (16-26%), terminal stance (33-43%), pre-swing (50-60%), initial to mid swing (66-76%) and mid to terminal swing (83-93%) (Perry, 1996). Percentages refer to the range of perturbation onsets.

Statistics

As seen in Figure 3A, large variability in a kinematic or EMG signal may mask the effect of the visual scene perturbation and how it depends on perturbation phase. Therefore, to quantify perturbation effects, we computed residual waveforms as follows. First, we defined a *perturbation cycle* as a gait cycle (heel strike to heel strike) during which a perturbation occurred and a *control cycle* as a gait cycle just prior to a perturbation cycle. We then used linear interpolation to compute response signals as a function of phase, where phase in increments of 0.005 ranged from -1 to 0 for control cycles, from 0 to 1 for perturbation cycles, from 1 to 2 for the first post-perturbation cycle, etc. For each trial, we averaged over all control cycles to obtain an unperturbed mean control waveform. For displacements, we computed a linear trend based on the first and last value of the mean control waveform and subtracted this trend from the mean

control waveform. EMG signals were normalized by the maximum value of the mean control waveform (Nieuwenhuijzen et al. 2000). For each gait cycle, the residual waveform as a function of phase was computed by subtracting the mean control waveform from the given signal (Fig. 3B). To correct for a slow drift in the subject's A/P position on the treadmill over the course of a trial, we computed the least-squares linear fit of the residual control cycle waveform of the L1 marker, extrapolated this linear fit over the perturbation and post-perturbation cycles, and then subtracted the linear fit from all A/P displacement signals. A residual waveform significantly different from 0 indicates that the visual perturbation had a significant transient effect (see *Effect of perturbations* below). The effect of visual perturbations on cycle periods, which is related to phase resetting, was analyzed separately (see *Change in gait measures* below).

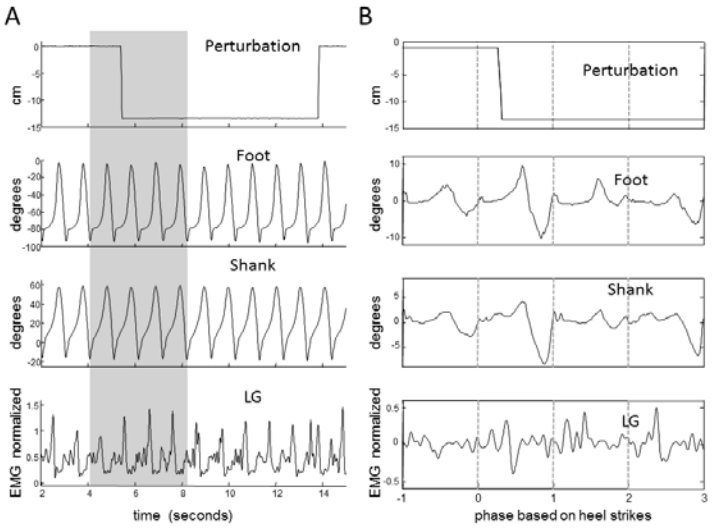

Figure 3. Epoch Extraction and Normalization. An example time series of perturbation, foot segment angle, shank segment angle, and rectified lateral gastrocnemius (LG) EMG recordings are observed in A. The shaded region in A is presented in B after normalization to the gait cycle and subtraction of mean control cycle waveforms (see *Methods*). Vertical dashed lines in B denote heel strikes. EMG has been normalized to control cycle maximum (see *Methods*). An abscissa value of 0 in C is the heel strike prior to visual scene motion. The perturbation isolated for observed responses in B occurs at mid stance and is towards the subject in the sagittal plane (-).

Phase dependence. To quantify phase dependence, we considered residual waveforms $r_k(\phi)$ as a function of delay ϕ from the perturbation in units of cycles, where the index $k = 1, \ldots, 6$ indicates the perturbation phase. We computed the mean $\bar{r}(\phi)$ of $r_k(\phi)$ across the six perturbation phases and defined $d_k(\phi) = r_k(\phi) - \bar{r}(\phi)$. Nonzero $d_k(\phi)$ correspond to phase-dependent responses. We defined R^+ and R^- as the root-mean-square (RMS) of $r_k(\phi)$ across positive delays $\varphi \in (0,2]$ and negative delays $\varphi \in [-2,0)$, respectively, and across the six perturbation phases. Since true responses to a perturbation occur at positive delays, a value of $R = R^+ - R^-$ significantly greater than 0 indicates a significant response. Similarly, we defined D^+ and D^- as the RMS of $d_k(\phi)$ for positive and negative delays, respectively. Then a value of $D = D^+ - D^-$ significantly greater than 0 indicates a significant *phase-dependent* response. To quantify the degree of phase dependence, we used the normalized measure $P = D/R$. $P = 0$ indicates no phase dependence and P approaches 1 as the degree of phase dependence increases. Thus, P evaluates phase dependence along a continuum. A low, but significant P characterizes a response as "weakly phase-dependent", which is synonymous with being primarily dependent on a time delay from the perturbation. We computed 95% confidence intervals for values of P using the bootstrap percentile-*t* method with 4,000 bootstrap resamples and 400 nested bootstrap resamples for variance estimation (Hall, 1988; Zoubir & Boashash, 1998).

Effect of perturbations. Significant deviations of the normalized residuals from 0 were considered the effect of the perturbation. Characterizing a

dependence on perturbation phase relies on observing the presence or absence of an effect for each perturbation phase. For each of the twelve perturbation types (2 directions x 6 perturbation phases), epochs of one cycle prior to the perturbation cycle and two cycles after the perturbation cycle were extracted from the normalized residual waveforms. For displacements, three cycles after the perturbation cycle and one cycle prior were extracted from normalized residual waveforms. These epochs were averaged within condition for each subject and binned in 5% intervals for two cycles after the end of each perturbation phase (e.g., from 10% for perturbations during loading). Because muscular activity shows more transient, shorter-lasting differences from 0, bin sizes of 1% for a single cycle after perturbation onset were used for EMG waveforms. Effects of the perturbation were considered significant if they were different from 0 using a *t*-test at each bin in each of the 12 perturbation conditions (2 directions x 6 perturbation phases). To test for asymmetry between the effects caused by positive and negative perturbations, post-perturbation data were summed across direction at each bin and then tested for significance from zero using a t-test at each bin. To account for multiple tests within each perturbation condition, we controlled the false discovery rate (FDR) at a level of 0.05 using the method of Benjamini and Hochberg (1995) applied to the *p*-values from the *t*-tests. This method is valid for independent *p*-values or *p*-values with positive dependency (Benjamini & Yekutieli, 2001).

Change in gait measures. Changes in the gait measures of stride length and gait period in each condition (2 directions x 6 phases) from pre-perturbation

control cycle values were computed. For changes in gait period, mean gait period (from heel strike to heel strike, in seconds) from pre-perturbation control cycles was subtracted from gait periods of the perturbation cycle (and successive cycles) for each subject prior to averaging across subjects. To observe changes in stride length over the same time period, deviations in A/P displacements of heel marker from pre-perturbation control cycles were computed in the same manner as above for segment angles. To compute change from mean displacement of the same foot (change in stride length), the deviation of heel displacement at each heel strike of the previous cycle was subtracted from deviation of heel displacement at each heel strike. RHS timing and deviations of A/P displacement of the right heel marker were used for the perturbation phases of loading, mid stance and terminal stance. Spatio-temporal symmetry was assumed and these calculations for the perturbation phases of pre-swing, initial to mid swing and mid to terminal swing were computed with LHS timing and deviations of the left heel marker. Changes in these gait measures were computed for the cycle the perturbation occurred and for two successive cycles. Correction for multiple tests within each condition was performed by controlling for FDR (as above).

Results

Four main results emerged in response to visual scene perturbations. First, translations of the visual scene that were towards the subject (approaching/negative) led to more consistent and larger deviations from mean

waveforms than the opposite translations (receding/positive), and are the focus of our results below. Second, significant deviations occurred in the trunk, but these deviations were not tied to a specific response phase or perturbation phase. Third, an additional, within-cycle gated response was observed in all leg segments when the perturbation was presented at mid stance (perturbation phase) and was accompanied by significant deviations in distal leg muscles. Finally, responses in the leg segments were found to be highly phase-dependent. More specifically, a response-phase pattern in the legs was observed as significant, stereotyped deviations of the foot and shank which consistently occurred prior to and after the stance to swing transition (response phase) of the gait cycle following the perturbation cycle.

Trunk shows little phase dependence, legs show strong phase dependence

We quantified the phase dependence of kinematic responses to approaching (negative) visual perturbations on a scale from 0 to 1 (see *methods*). The trunk (Fig. 4) had only a low phase dependence of 0.24 with a 95% confidence interval of [0.10, 0.31], indicating that perturbations at all phases of the gait cycle produced similar responses primarily as a function of the delay from the perturbation. Leg-segment responses (Fig. 5), however, were highly phase-dependent: 0.92 for the foot with a 95% confidence interval of [0.86, 0.96], 0.89 [0.84, 0.93] for the shank, and 0.91 [0.84, 0.97] for the thigh.

Approaching perturbations yield three distinct responses

Segment Angles. Figures 4A-C show responses of trunk orientation to perturbations applied at loading, mid stance and terminal stance. These trunk segment angles are aligned to the heel strike prior to the perturbation onset after removing mean waveforms from pre-perturbation gait cycles. These across-subject averages of the residual waveforms in Figures 4-6 are the effect of the perturbations and significant differences from zero are denoted with asterisks (FDR < 0.05, see *Statistics*). To view normative segment angles at all response phases, these figures also contain concatenated control cycle waveforms (mean of pre-perturbation cycles) below the residual waveforms.

Negative perturbations applied at all perturbation phases led to a decrease (i.e., backward tilt) in trunk orientation, but at no particular response phase. Looking at the control waveform, these decreases in trunk orientation (backwards tilt) occur when the trunk is in various states of the more positive flexion and less positive extension. Perturbations applied at mid stance (Figure 4B), for example, caused significant decrements in the response phase of pre-swing of the perturbation cycle until mid stance of the post-perturbation cycle and were largest at the stance to swing transition of the perturbation cycle. In comparison, decreases in trunk angle due to perturbations applied at terminal stance displayed in Figure 4C began and reached their largest point in the response phase of terminal swing of the perturbation cycle, and continued through mid stance of the following cycle. To supplement our quantification of phase dependence reported above, the latency of the trunk response was

quantified as the midpoint of significant bins in the initial backward trunk tilt response. As the trunk response is not a stereotyped waveform but does share a significant, initial backward tilt of varying width across perturbation phases, the measure best details a single point when the response specific to each perturbation phase has occurred. The midpoints of the initial, significant backward tilt in trunk orientation occur at .55, .62 and .6 cycle lengths from perturbation onset in loading, mid stance and terminal stance, respectively, and can be observed in Figure 4 amongst the significance asterisks. After correcting for gait period in each condition, these cycle length latencies correspond to response latencies of 633 ms, 713 ms and 693 ms for loading, mid stance and terminal stance, respectively. These are the values of response latencies we refer to in the remaining text. For reference, significant decrements first occurred in pre-swing (≈53%, Fig. 4A, midpoint of bin), pre-swing (≈54%, Fig. 4B) and terminal swing (≈91%, Fig. 4C) for loading, mid stance and terminal stance perturbations, respectively. Although we do not consider these values as response latencies, the first instances of significance corrected for gait period and stimulus onset correspond to 489 ms, 309 ms and 543 ms from perturbation onset for loading, mid stance and terminal stance, respectively. Overall, the subplots in Figure 4 are consistent with the phase dependence quantification presented above; for the trunk, phase does not dictate when a response happens and responses occur with a similar delay from stimulus onset.

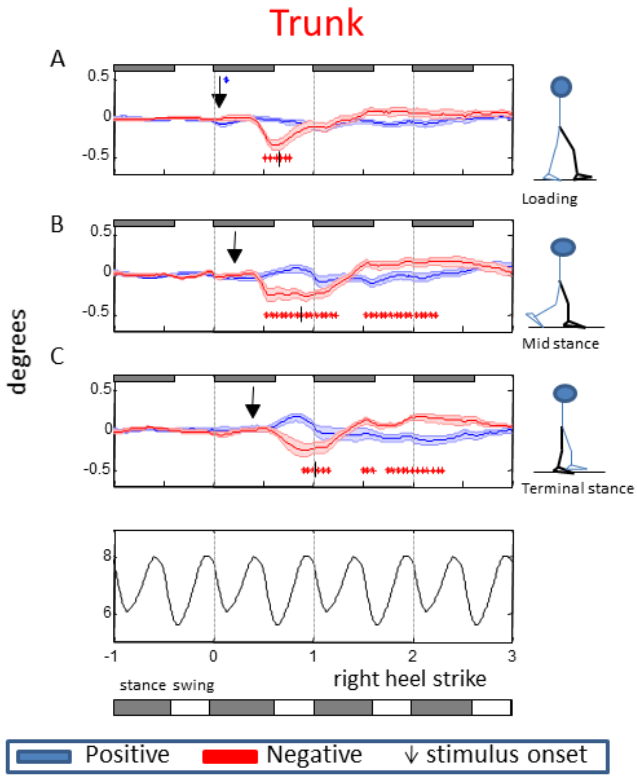

Figure 4. Trunk Orientation. Residual waveforms averaged across subjects are presented here for all directions and phases of visual scene motion. Arrows have been appropriately placed at the average stimulus phase for each condition, and stick figures represent position of the body during the three stimuli phases. The phase of perturbation is illustrated to the right of each plot. Blue/red asterisks denote that the positive/negative condition was different from zero at that bin, and these asterisks have been placed at the mid point of the bin, as these continuous traces were binned when performing statistics (n=11, FDR<.05). The vertical line within the asterisks for the negative perturbation denotes response latency for these trunk responses. An abscissa value of 0 is the heel strike prior to visual scene motion. Heel strike times of response phase are noted appropriately above or below each respective limb's response and inset bars represent stance phase. Shaded error bars correspond to standard error of the mean (s.e.m.). Across-subject means of the control cycle waveforms are concatenated and presented below residual waveforms. A more positive segment angle indicates a more forward deviation from vertical in the sagittal plane that could result in a more flexed trunk.

Assuming left-right spatio-temporal symmetry, bilateral kinematic and EMG responses to perturbations at three phases of the gait cycle were used to infer responses at a total of six perturbation phases (see *Methods*).

In contrast to responses observed in the trunk segment, responses in the leg segments occur at characteristic response phases and appear as two responses. First, significant *within-cycle* deviations of all leg segments were

observed when negative perturbations were applied solely at mid stance. At this perturbation phase specifically, the largest magnitude deviations across all perturbation phases in the foot, shank and thigh segment angles were observed in the gait cycle in which the perturbation occurred. As seen in the third row of plots in Figure 5, significant increases in the foot and shank segment angle peaked at the stance to swing transition (≈.6, Fig. 5C/I) while significant decreases followed and were at their greatest magnitude in the response phase of mid swing for both the foot (≈.79, Fig. 5C) and the shank (≈.84, Fig. 5I). Looking at control waveforms of foot and shank, it is clear that the negative perturbation presented at mid stance caused a heightened increase in the foot and shank angle until the stance to swing transition followed by larger decrease in these segment angles during mid swing. These deviations result in a net increased plantar-flexion of the foot prior to toe off and an increased dorsi-flexion after toe off while flexion of the shank increased prior to the stance to swing transition followed by net decreased flexion in swing until heel strike. A similar negative deviation was observed in the thigh angle in Figure 5O during the response phase of initial swing (≈.69) corresponding to a larger decrease in the thigh angle at this phase (when compared to the control waveform) resulting in a more pronounced thigh flexion throughout the swing phase of the perturbation cycle.

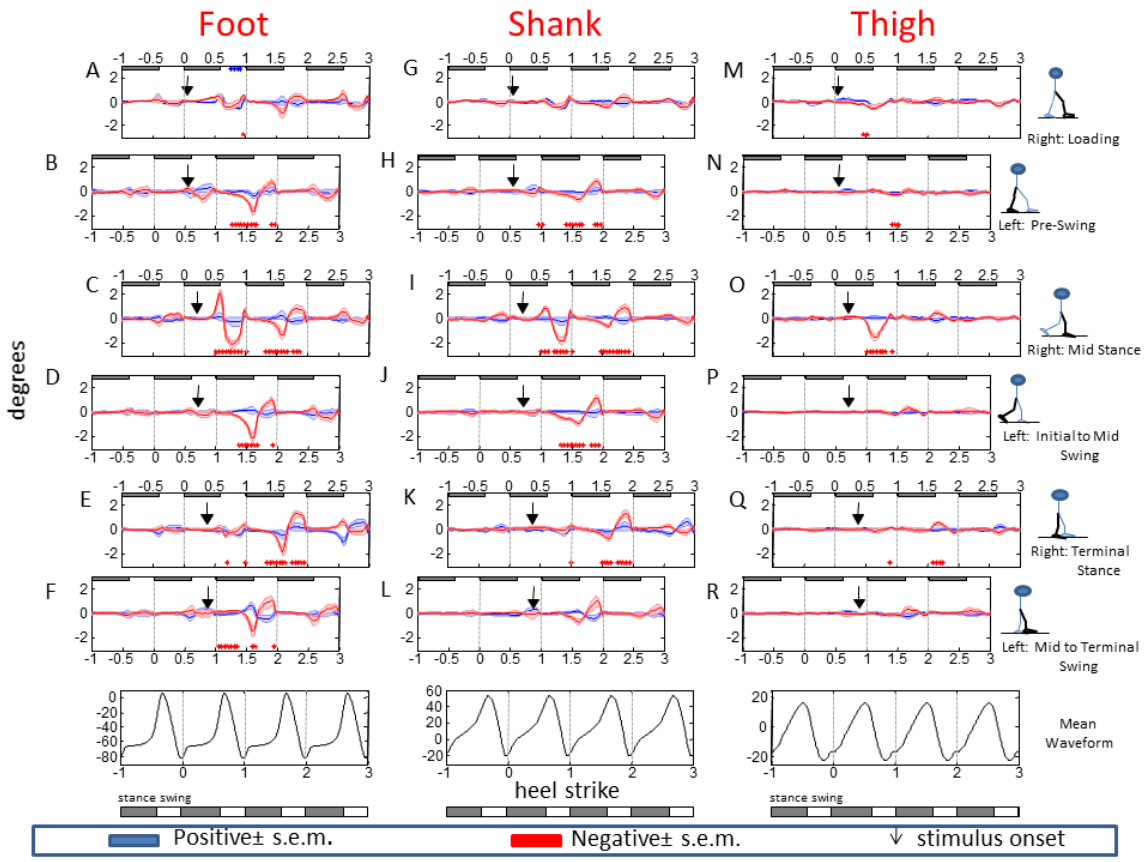

Figure 5. Leg Segment Angles. Residual waveforms averaged across subjects are presented here for all directions and phases of visual scene motion. Arrows have been appropriately placed at the average stimulus phase for each condition, and stick figures represent position of the body during these six stimuli phases. Underneath each stick figure is the limb used for that data and the gait cycle phase it was in when the perturbation occurred. Blue/red asterisks denote that the positive/negative condition was different from zero at that bin, and these asterisks have been placed at the midpoint of the bin, as these continuous traces were binned when performing statistics (n=11, FDR<.05). An abscissa value of 0 is the heel strike prior to visual scene motion. In this figure and others, subplots have been shifted so that the simultaneous effect of the perturbation on both limbs can be observed. Heel strike times of response phase are noted appropriately above or below each respective limb's response and inset bars represent stance phase. Shaded error bars correspond to standard error of the mean (s.e.m.). Across-subject means of ipsilateral right control cycle waveforms are concatenated and presented below residual waveforms. A more positive segment angle indicates a more forward deviation from vertical in the sagittal plane that could result in a more extended thigh, flexed shank or extended foot (plantarflexion).

Making up the second response of the leg segments, plots of the foot and shank angles illustrate that approaching (negative) visual perturbations across a range of perturbation phases caused deviations in the cycle following the deviation cycle. As seen in Figures 5B-F, in the gait cycle (heel strike to heel strike) following the perturbation cycle (post-perturbation cycle, heel strike 1-2,

Fig. 5) significant decreases and ensuing increments were observed in the foot angle when perturbations were applied at mid stance, terminal stance, pre-swing, initial to mid-swing, and mid to terminal swing. These decrements in the post-perturbation cycle are largest in magnitude at the response phase of the stance to swing transition (≈1.6 on the x-axis for all perturbation phases in Figures 5B-F). The significant increments which follow are all largest in magnitude in the response phase of mid to terminal swing (range: 1.83 -1.92 in Figures 5B-F). Although not significant, peak decrements occurred at the same response phase when perturbations were applied at loading (Figures 5A). Comparing the residual waveforms in 5B-F to the control waveform of foot angle (post-perturbation cycle, heel strike 1-2, Fig. 5), the effects of the perturbation correspond to a decrease in the increasing foot angle prior to and including the stance to swing transition and an increase in the decreasing foot angle during swing. These deviations translate to a net decreased plantar-flexion of the foot prior to toe off and a net decreased dorsi-flexion after toe off.

In the shank, significant decrements were observed when negative perturbations were applied at mid stance, terminal stance, pre-swing, and initial to mid-swing. Shown in Figures 5H-K, these decrements occurred in the post-perturbation cycle (heel strike 1-2, Fig. 5H-K), and were largest in magnitude at the stance to swing transition (≈1.6 in Figs. 5H-K). These decrements were followed by a more pronounced increment whose peak occurred during the response phase of terminal swing (≈1.9 in Figs. 5H-K, respectively) when perturbations were applied at mid stance, terminal stance, pre-swing, and initial

to mid-swing. Comparing these deviations to the control waveform of shank angle, the effects of the perturbation correspond to a decrease in the increasing shank angle prior to and including the stance to swing transition and an increase in the decreasing shank angle during swing. These deviations result in a net decreased flexion of the shank at the knee prior to the stance-swing transition followed by an increased flexion at the knee as the knee is extending in mid swing. In sum, negative perturbations, when applied across different phases of the gait cycle, characteristically alter the trajectories of the lower leg segments of foot and shank at specific response phases of the post-perturbation cycle (heel strike 1-2, Fig. 5H-K).

Muscle Activation. As observed in Figure 6, the largest deviations in EMG waveforms were observed after negative, mid stance perturbations. Non-significant increases in plantar-flexor muscles precede foot plantar-flexion, while significant decrements precede foot dorsi-flexion illustrating a coordination between kinematic and EMG responses to visual scene motion. As decrements in LG and SOL were significant, we focus on their functional role in causing a dorsi-flexion from mean waveform during mid stance perturbations. Significant decreases in both LG and SOL can be observed in Figures 6C and 6I. In both cases, these decreases were largest in magnitude during the response phase of terminal stance of the perturbation cycle with LG and SOL reaching sharp declines of -.094 (fraction of maximum control activity) and -.074 at 48% and 49% of the gait cycle, respectively. As seen in the control waveforms, these decrements in LG and SOL occur as the activity of these muscles is decreasing

in amplitude from peak activity suggesting an increased decline in activation of these muscles prior to push-off. Of these two muscles, soleus reliably decreased first, with the midpoint of the significant decrements occurring at 47% of the perturbation cycle (Figure 6I). When corrected for gait cycle timing and perturbation onset, this corresponds to a response latency of 300 ms to the midpoint of significant bins of this decrement. For comparison with a previous study (Marigold et al. 2007), the response latency of soleus decrements to the negative, mid stance perturbations of this study was 338 ms if each latency was computed on a single trial basis and deviations had to be greater than two standard deviations for at least 30 ms (method of Marigold et al. 2007). The negative perturbations applied at mid stance also elicited a significant increase in TA activity at the stance to swing transition of the perturbation cycle as shown in Figure 6O. In sum, perturbations applied only at mid stance modulated the amplitude of all of these distal leg muscles during late stance response phases of the perturbation cycle.

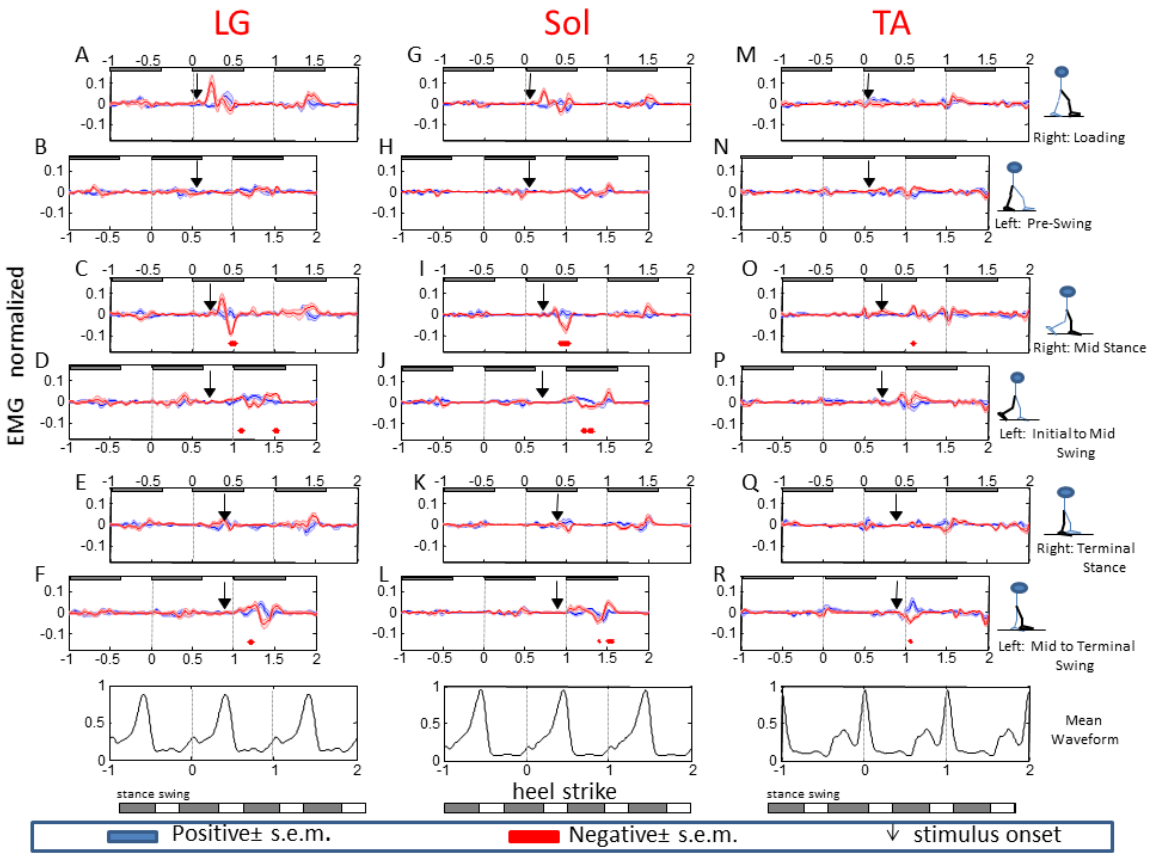

Figure 6. EMG Waveforms. Residual waveforms averaged across subjects are presented here for all directions and phases of visual scene motion. Arrows have been appropriately placed at the average stimulus phase for that condition, and stick figures represent position of the body during these six stimuli phases. Underneath each stick figure is the limb used for that data and the gait cycle phase it was in when the perturbation occurred. Blue/red asterisks denote that the positive/negative condition was different from zero at that bin, and these asterisks have been placed at the mid point of the bin, as these continuous traces were binned when performing statistics (n=11, FDR<.05). Lateral Gastrocnemius (LG), Soleus (Sol), and Tibialis Anterior (TA). An abscissa value of 0 is the heel strike prior to visual scene motion. Heel strike times of response phase are noted appropriately above or below each respective limb's response and inset bars represent stance phase. Shaded error bars correspond to standard error of the mean (s.e.m.). EMG values are in normalized units (to control cycle maximum for each trial). Across-subject means of the ipsilateral right control cycle waveforms are concatenated and presented below residual waveforms.

In addition to those observed in Figure 6, there were sporadic, significant deviations observed in ESL, BF, and ST due to these negative perturbations. In ESL, a decrease (-.078 at its lowest) was observed in pre-swing (54-58%) of the perturbation cycle when negative perturbations were applied at mid stance. There were three instances where significant deviations were observed in BF: an

increase (0.036 at its highest) was observed in mid swing (84-87%) of the perturbation cycle when perturbations were applied at pre-swing; an increase (.027 at its highest) was observed in loading (2-6%) of the post-perturbation cycle when negative perturbations were applied mid to terminal swing; and a decrease (-.041 at its lowest) was observed in terminal swing (87-91%) of the post-perturbation cycle when these negative perturbations were applied at mid to terminal swing. In ST, A decrement (-.036 at its lowest) was observed in early stance (9-14%) of the post-perturbation cycle when negative perturbations were applied at initial to mid swing. Although significant, these changes were generally much smaller than those observed in the distal leg muscles when perturbations were applied at mid stance, diminishing their functional significance.

Receding perturbations had little effect on segments angles and EMG

As shown by Figures 4-6, receding (positive) perturbations generally yielded smaller and inconsistent changes in segment angle trajectories and EMG waveforms compared to approaching (negative) perturbations. Figure 5A shows small, but significant, decrements in the foot angle observed during the swing phase of the perturbation cycle when positive perturbations were presented at loading (FDR<.05). In the trunk (Figure 4A), however, a single significant decrement was observed when positive perturbations were applied at loading. In all muscles, only a single instance of a significant deviation occurred during positive perturbations. A small but significant increase (.042 at largest) in ST

activity was observed in mid swing (85-87%) in the perturbation cycle followed by a significant decrease (-.038 at lowest) in late swing (91-94%) when positive perturbations were applied at loading.

When the effects due to the two directions were directly tested for asymmetry, significant differences were typically observed when negative perturbations caused significant deviations (FDR<.05). Overall, 88% (129/147) of those significant asymmetries in the leg and trunk segment angles were associated with significant responses to negative perturbations. Similarly, 71% (10/14) of asymmetries observed in the muscles were associated with significant responses to negative perturbations.

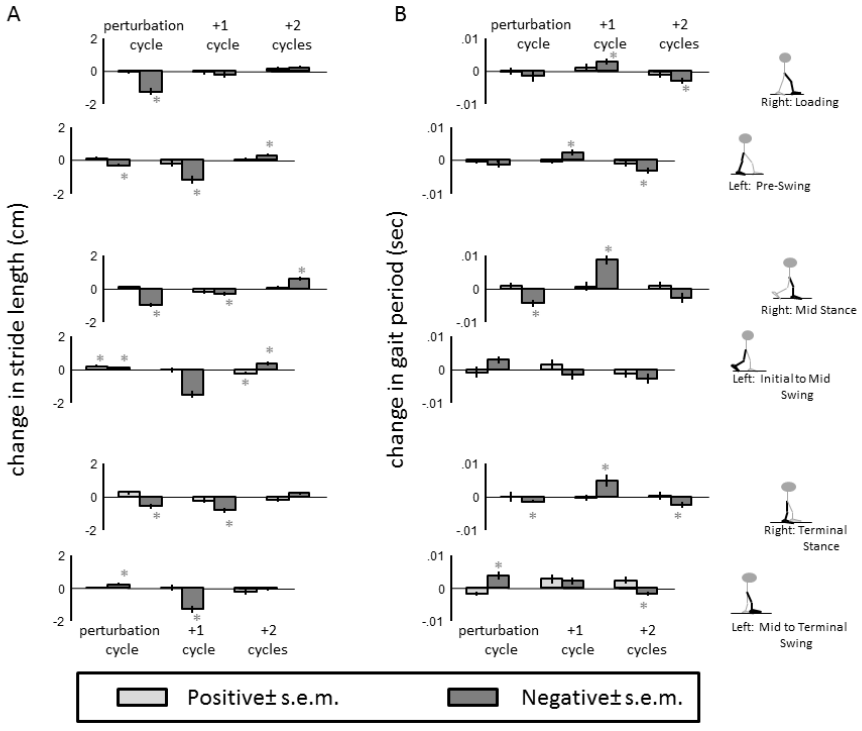

Figure 7. Changes in Gait Measures. Changes in stride length (A) and gait period (B) from mean pre-perturbation cycle are presented here for all phases of perturbation and direction. Underneath each stick figure is the limb used for that data and the gait cycle phase it was in when the perturbation occurred. Perturbation cycle corresponds to the gait/stride cycle in which the perturbation occurred and +1 cycle corresponds to the following cycle. Asterisks denote a significant change from mean pre-perturbation cycle (n=11, FDR<.05). Error bars correspond to standard error of the mean (s.e.m.).

Changes in stride length and gait period

Deviations from mean stride length and gait period are presented in Figure 7 illustrating that positive (receding) perturbations had little effect on the gait of subjects on the treadmill. Negative perturbations in the majority of perturbation phases caused a decreased stride length in both the cycle in which the perturbation occurred (perturbation cycle) and the cycle afterward (+1 cycle/post-perturbation cycle). As seen in Figure 7A, a decreased stride length was observed in the perturbation cycle in the first four perturbation phases with increases observed when perturbations were applied at initial to mid swing and mid to terminal swing. In the post-perturbation cycle, however, solely decreases in stride length were observed and four of these decreases were statistically significant. Figure 7B shows that the cycle after the perturbation (+1 cycle) was lengthened in time for the majority of phases in which a negative perturbation was used. Interestingly, both increases in gait period and decreases in stride length were observed in the +1 cycle during the three perturbation phases of mid stance, terminal stance and pre-swing. This combination of changes in stride length and gait period corresponds to a stride shorter in distance and longer in time, which effectively slows the subject on the treadmill in the post-perturbation cycle.

Displacement of the body on the treadmill

By assuming that responses in each leg would be the same if perturbations were presented at an identical phase of the gait cycle (spatio-

temporal symmetry), it has been shown above that the negative visual perturbations applied at many phases of the gait cycle result in slowing on the treadmill. To investigate this slowing further, displacements of the body with both legs and trunk on the same normalized time scale are plotted in Figure 8.

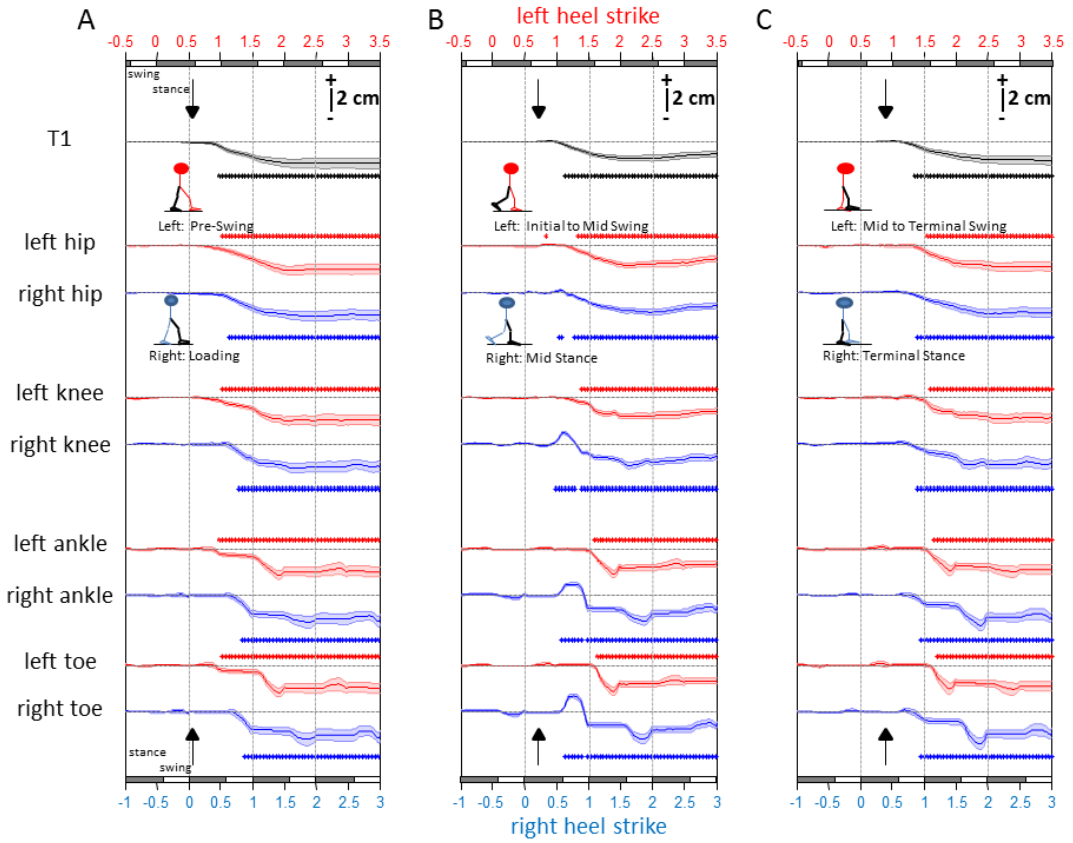

Figure 8. Whole Body Displacements during Negative Perturbations. Residual A/P displacements averaged across subjects are presented here for the three phases of negative (backward) visual scene motion. Displacements of right/left side of the body are in blue/red and midline displacement (T1) in black. Dashed horizontal lines denote 0 difference from mean displacement while the inset scale bar notes – /+ indicating a backward/forward displacement of the body on the treadmill. Arrows have been placed at the average perturbation phase as the right leg is in the gait cycle phase of loading (A), mid stance (B) and terminal stance (C) while the left leg is in pre-swing (A), initial to mid swing (B) and mid to terminal swing (C). Blue/red asterisks denote that the right/left side displacement was different from zero at that bin, and black asterisks denote that the midline marker on T1 was different from 0 at that bin. These asterisks have been placed at the midpoint of the bin, as these continuous traces were binned when performing statistics (n=11, FDR<.05). An abscissa value of 0 is the heel strike prior to visual scene motion. Shaded error bars correspond to standard error of the mean (s.e.m.). Heel strike timing for right/left legs is on the bottom/top abscissa of each subplot.

Figure 8 shows mean residual waveforms of displacements of both legs and trunk (T1). They were displaced backwards significantly by the negative perturbation at all three phases of perturbation. Similar to the weak phase dependence previously observed in the trunk orientation (Fig. 3), displacement of T1 backwards begins later as perturbations occur later. Significant backward deviations begin at ≈48% (midpoint of bin), ≈64% and ≈86% of the perturbation cycle with perturbations at loading (Fig. 8A), mid stance (Fig. 8B) and terminal stance (Fig.8C) of the right leg, respectively.

In the legs, backward displacements began in the left leg prior to the right leg when perturbations occurred at loading of the right leg (Fig. 8A) while backward displacements occurred first in the right leg when perturbations occurred during both mid stance (Fig. 8B) and terminal stance (Fig.8C) of the right leg. Interestingly, the largest backward deviations of all markers (ankle, toe) of both feet occurred when each leg was in its swing phase of the cycle following the perturbation cycle (post-perturbation cycle). Consistent with responses of segment angles, deviations observed in the right leg when the perturbation occurred during mid stance of the right leg were unique relative to the other phases of perturbation. As seen in Figure 8B, significant forward displacements in all markers of the right leg occurred at the stance to swing transition and, for most markers of the leg, continued throughout the entirety of the swing phase. In sum, all segments were eventually displaced backwards by the negative visual scene motion at all phases and the timing profile of displacement responses is consistent with responses observed in the segment angles.

Discussion

Transient visual-scene motion was used here to investigate phase-dependent responses to visual input during human locomotion. Trunk responses to approaching (negative) perturbations were only weakly phase-dependent and instead primarily depended on the delay from the perturbation. In contrast, leg responses were strongly phase-dependent. Leg responses during the same gait cycle as the perturbation exhibited gating, occurring when the perturbation was applied at mid stance. Leg responses during the post-perturbation gait cycle, however, exhibited a response-phase pattern over a range of perturbation phases. These two types of leg responses likely serve separate functions during the locomotion task used in this study. Overall, these results support the notion that the phase dependence of responses to visual input is determined by the functions, or subtasks, associated with vision during walking.

Directional Asymmetry

Across segments, responses to perturbations when the virtual scene was moving towards the subject (negative) were greater than responses, if they occurred at all, to visual perturbations moving away (positive) from the subject. These results are consistent with previous studies using continuous optic flow stimuli which show that visual perturbations approaching a subject on a treadmill have a larger effect on step velocity (Konczak 1994), stride length (Prokop et al. 1997), variability of ankle-knee relative phase and variability of center of mass

displacement (Guerin & Bardy 2008) when compared to perturbations moving away from the subject.

Although we have used transient perturbations in our study, the nervous system places an increased emphasis on approaching changes in visual scene motion, suggesting a functional aspect regardless of being a continuous flow or a transient change from fixed scene motion. Both approaching and receding visual scene motion are everyday occurrences during walking. It is normal for both directions of motion to occur, yet an approaching visual scene is more likely to require a functional change in the locomotive behavior. Transient changes in scene motion towards the subject in this study may be interpreted as an impending obstacle to avoid (due to large peripheral component), a wall that the approaching body will collide with or a change in position on the treadmill, necessitating a response. In the alternative case of receding perturbations, a response is functionally less critical.

Strong Phase Dependence of Leg Responses but not Trunk Responses

We quantified phase-dependence along a continuum in this study, and trunk responses were found to be weakly phase-dependent. To supplement this finding, latency to the midpoint of an initial, significant backward tilt was similar at all perturbation phases to approaching perturbations. Portions of stereotyped response waveforms have also been used to investigate phase-dependence during walking in other sensory systems. Modulation of waveforms such as the "medium latency response" (e.g., Iles et al. 2007; Blouin et al. 2011) for galvanic

vestibular perturbations or the H-reflex (e.g., Capaday & Stein 1986; Dietz et al. 1990) for perturbations to proprioceptive afferents support the use of a feature of responses to determine dependence on phase of gait cycle. The midpoint of a stereotyped backward trunk tilt was used here to supplement the quantification of phase-dependence, and it shifted later as perturbations were applied later. In sum, the trunk's response is primarily dictated by the time delay from a change in scene motion and is most similar to the "no phase dependence" scenario in Figure 1A rather than the gating (Fig. 1B) or response-phase pattern (Fig. 1C) scenarios.

The weak phase dependence of trunk responses in the present study is consistent with the responses of the trunk to *continuous* visual perturbations found in a previous study, which could be approximated with linear, time-invariant frequency response functions (Logan et al. 2010). In the task of treadmill walking and most forms of walking, there is a critical underlying subtask of maintaining postural control upright that the nervous system must continually perform to keep the oscillating trunk from toppling over the legs as they propel the body from place to place. Previous studies have shown that oscillatory motions of the trunk couple with oscillatory visual scene motion to stabilize the motion of the trunk at low frequencies (Warren et al. 1996; Logan et al. 2010). The long-lasting and weakly phase-dependent responses observed to these transient perturbations support the notion that trunk responses in this experiment also reflect a continuous, time-invariant maintenance of postural equilibrium during bipedal locomotion.

Responses observed in the leg, on the other hand, were strongly phase-dependent, in two distinct ways. First, a phase-dependent response was observed in all leg segments within the same cycle as the visual perturbation. As seen in the third row of Figure 5, *within-stride* deviations of the foot, shank and thigh angles are observed when perturbations are presented *solely* at mid stance indicating that this response is gated (as in Figure 1B). In the foot, the visual perturbation yielded a net increased plantar-flexion prior to toe off and an increased dorsi-flexion after toe off. At the same time, deviations in the shank render an increased flexion of the shank prior to the stance to swing transition followed by decreased flexion at the knee as the shank is extending in swing until heel strike. The thigh also displays more pronounced flexion throughout the swing phase of the perturbation cycle. Such flexion of the thigh and foot coupled with extension of the shank reveal a combination of segment angles that result in an overall higher position of the leg segments during swing. Significant decreases in soleus and gastrocnemius activation observed in the response phase of pre-swing (row 3 of Figure 6) likely account for the net decreased angle (dorsi-flexion) of the foot in ensuing swing when perturbations occur at mid stance. Additionally, the significant increases in tibialis anterior observed in early swing (Fig 6O) also likely play a role in this dorsi-flexion observed in the foot during swing. In sum, the combined action of a decrease in lower limb plantar-flexor muscle activity and increased dorsi-flexor activity cause the eventual foot dorsi-flexion that occurs in mid swing when perturbations occur during mid stance perturbations.

This early phase-dependent response observed in the leg segments serves a within-cycle function in response to mid stance perturbations. Mid stance may mark a visually sensitive period where a fast pathway "hazard detector" (Marigold, 2008) is activated to avoid or accommodate hazards such as impending collisions with a wall or obstacles in the ensuing swing phase. Although there has been work in animal models (Sherk & Fowler 2001; Graziano & Cooke 2006; Simmons et al. 2010) regarding defensive postures prior to collisions, there is not, to our knowledge, a definitive account of kinematic or muscular strategies in response to an incoming whole-body collision during human locomotion. It is premature to assume that fast pathways which may initiate obstacle avoidance and whole-body collision avoidance are separable. However, common responses observed in this study and those studies reported below suggest that fast, approaching changes in visual scene motion trigger a fast, generalized hazard accommodation response regardless of the features (wall, obstacle, etc) of the visual scene motion.

As responses in the leg segments to these types of perturbations have not been reported elsewhere, studies of obstacle avoidance support the idea that the kinematic features and timing of this response is a response to an approaching hazard. Both the foot dorsi-flexion and thigh flexion observed in the swing response phase in this investigation (in response to mid stance perturbations) are main components of the "elevating strategy" for avoiding small obstacles occurring within the same gait cycle (Eng et al. 1994; Patla 1991). Although our attention to gait cycle phase dictates normalizing by gait cycle, mean response

latencies calculated for muscular activity in real time reveal latencies with comparable timescales to those found in a previous study whose focus was avoidance of actual obstacles (Marigold et al. 2007). Despite no “real” obstacles in this study, our approach is similar to that of Marigold and colleagues as both studies introduce a dramatic change in the peripheral visual field with responses observed in the same cycle. They found that the biceps femoris (BF) is a reliable first muscle to be activated with a mean response latency of 134 ms when obstacles are released in late stance. In our study, the soleus (SOL) was the most reliable first muscle to be activated with a mean response latency of 338 ms (method of Marigold et al. 2007) when negative visual scene perturbations were presented at mid stance. In the Marigold study, response latencies grew larger as obstacles were presented earlier in the gait cycle. With this caveat in mind, the 134 ms BF response latency to a late stance obstacle could be extrapolated to a 314 ms latency for a mid stance obstacle in our study (obstacle presentation 15% earlier in the cycle), suggesting muscle response latencies on similar timescales. Thus, the kinematic features and muscular timing of the responses to the approaching, mid stance perturbations display a response that is functionally distinct from other trunk and leg responses we observed, indicating an alteration of leg segment trajectory *within-cycle* in a manner resembling a hazard accommodation/avoidance response.

An alternative explanation to this proposed hazard accommodation/avoidance response would be that this response is caused purely by a visual startle during walking. This distinct, within-cycle response

observed in the leg segments to a transient perturbation is reminiscent of auditory startle and its interaction with obstacle avoidance in human locomotion (Nieuwenhuijzen et al. 2000; Queralt et al. 2008). An auditory startle paired with an obstacle has been shown to improve the obstacle avoidance response and associated modulation of EMG amplitude (Queralt et al. 2008), indicating that startle to sensory perturbations can have functional implications and may play a role in the response observed in this study when mid stance perturbations are presented. Auditory startle responses in the musculature have been shown to occur at all perturbations, however, with amplitude modulated by perturbation phase without changes to the fast (<150 ms) response latencies (Nieuwenhuijzen et al. 2000). Here we observe little consistency across perturbation phases in measuring the existence of significant EMG responses. The additional response in leg segments that does not rely on time from stimulus, but instead shows a response-phase pattern, indicates that we have not measured a modulation of fixed latency startle response for the whole body. Interestingly, auditory startle has been shown to shorten the gait period of both the perturbation and post perturbation cycle while decreasing both the maximal peak flexion and extension of both the ankle and knee (Nieuwenhuijzen et al. 2000). The increases in both the maximal extension and flexion of foot and shank angles observed here (Figs 5C, 5I) are actually opposite of that found in auditory startle. Moreover, the gait period of the post perturbation cycle (+1 cycle in 3rd row of Fig 7B) is increased. These discrepancies suggest that the response to mid stance perturbation is not a visual startle response.

For this specific response in the legs, the time-domain measures we used allowed us to observe an EMG response to visual scene motion that precedes a kinematic response during mid stance perturbations. However, we did not observe clear EMG responses during the additional phase-dependent response of the legs or the response in the trunk. There could be different reasons for this discrepancy. It is well known that muscle activation patterns for unperturbed walking show large inter-subject variability in addition to variability stride to stride while kinematics remain relatively invariant (Winter & Yack 1987). Indeed, the results reported here also show more consistent, interpretable results in responses of kinematics compared to EMG during walking with perturbed visual scene motion. The lack of a systematic relationship for all responses could be due to missing action of muscles that were not recorded, not performing enough perturbations, and the potential of synergistic co-activation of muscles for function.

The second phase-dependent response occurred when perturbations presented at all phases elicited consistent responses of the leg segments in the gait cycle subsequent to the cycle in which a perturbation occurred (post-perturbation cycle, heel strike 1-2 in Fig. 5). As seen in the post-perturbation cycle in Figures 5B-F, deviations in the foot segment angle translate to a net decreased plantar-flexion of the foot prior to toe off and a net decreased dorsi-flexion after toe off. Meanwhile, shank angle deviations translate to a net decreased flexion of the shank at the knee prior to the stance-swing transition followed by an increased flexion at the knee as the knee is extending in mid

swing. We consider this to be indicative of a *response-phase* pattern and in line with Figure 1C as it consistently occurred at the same response phase with characteristic waveforms in the foot and shank. Together, these deviations illustrate decreased range of motion of the lower leg on both sides of the stance to swing transition in the cycle following the perturbation. In other words, the legs adjust to slow the subject so that a central position can be maintained after a forward translation is determined from approaching scene motion. Such changes occur in the post-perturbation gait cycle, which is consistent with previous studies that show subjects use vision for changes in planned stepping adjustments approximately two steps, or a full gait cycle, in advance of a change in ground terrain (Patla & Vickers 2003; Marigold & Patla 2007).

This interpretation is also supported by the changes in stride length and gait period presented in Figure 7. Various combinations of stride length and gait period allow maintenance of the same speed during treadmill walking (Dingwell & Cusumano 2010). Increasing stride length could be counteracted with increasing gait period (as well as both decreasing) to not change the subject's speed or position on the treadmill. In the post-perturbation cycle (+1 cycle in Fig. 7), the two gait measures never changed in the same direction, indicating that the approaching (negative) visual scene motion caused a change in position on the treadmill. Five of the six perturbation phases yielded either a decreased stride length or increased gait period to slow subjects in the post-perturbation cycle (+1 cycle in Fig.7). Furthermore, there were three perturbation phases (mid stance, terminal stance, pre-swing) with *both* decreases in stride length *and* increases in

gait period. This combination of changes in stride length and gait period strongly supports slowing on the treadmill. These results coupled with the backward displacements of leg segments in the post-perturbation cycle (heel strike 1-2) observed in Figure 8 further support the notion that the major adjustments in speed occur primarily in the post-perturbation cycle regardless of perturbation phase.

Smaller stride lengths coupled with counteracting shorter gait periods (or increases in both), however, would maintain similar speed on the treadmill. Indeed, significant changes of both stride length and gait period in the same direction are observed in the perturbation cycle (perturbation cycle in Fig. 7) in three perturbation phases (mid stance, terminal stance, mid to terminal swing) while the other three perturbation phases are accompanied by non-significant trends of gait period in the same direction which aid in counteracting significant changes in stride length. These findings are generally consistent with the lack of positional-maintenance changes in segment angles observed in Figure 5 in the perturbation cycle (0-1 in Fig. 5) and consistent with little change in displacements in the perturbation cycle (0-1 in Fig. 8). Although changes in segment angles occur in the perturbation cycle when perturbations occur at mid stance (Figs. 5C, 5I, 5O), the deviations in leg displacements occurring in the perturbation cycle are corrected within cycle (Fig 8B, blue lines), further supporting the notion that the within-cycle responses to mid stance perturbations do not support the function of changes in speed over a stride. Additionally, changes in gait measures and displacements inform as to why deviations in the

post-perturbation cycle are not significant in the legs during perturbations presented at loading (Figs. 5A, 5G, 5M). Decreases in stride length in the perturbation cycle in addition to increases in gait period in the post perturbation cycle (first row of Figs. 7A, 7B) coupled with the backward displacements in the perturbation cycle (Fig.8A, 0-1, blue lines) in addition to the post perturbation cycle suggest that adjustments for maintaining position is spread across both the perturbation cycle and post-perturbation cycle when perturbations were presented at loading. We speculate that this is the reason for a lack of significant, stereotyped kinematic deviations in the post-perturbation cycle (1-2 in Figs. 5A, 5G, 5M) when perturbations were applied at loading. Further experimentation will be needed to test this idea that adjustments in speed are enacted across both the perturbation and post-perturbation cycle when visual scene motion is presented at the onset of the gait cycle.

Phase dependence of vision dependent on function

Visual perturbations delivered at different phases of the gait cycle revealed several responses in the trunk and legs which reflect distinct functions during locomotion. Changes in visual scene motion were shown to: 1) modulate trunk orientation for upright equilibrium; 2) alter leg motion for hazard accommodation/ avoidance; and 3) alter leg motion to control position on the treadmill. Such results are consistent with perturbations using other modalities during locomotion. For example, Bent et al (2004) showed distinct leg and trunk responses due to galvanic vestibular stimulation; foot placement responses were

dependent on phase of perturbation while trunk responses showed no such dependence. Bent and colleagues suggest that these responses are indicative of independent upper and lower body control during walking (Bent et al. 2004, 2005). As distinct responses were observed both within the legs and between the trunk and leg segments in this study, the nature of phase dependence cannot simply be ascribed to the level of segments, but relies on the functional subtask for which vision was used.

Subtasks, or necessary elements underlying the task of safe walking, typically consist of support maintenance by the stance limb, control of posture upright in sagittal and frontal planes, and proper foot trajectory control (Winter 1989). In more dynamic environments, however, additional subtasks such as hazard accommodation/avoidance or positional maintenance on a treadmill must be successfully performed. Recently, there has been renewed support for the idea that subtasks of human locomotion are modular in nature, and are enacted by distinct combinations of muscle activations (McGowan et al. 2010; Neptune et al. 2009). Such studies echo previous work in human locomotion suggesting that the muscular activations performing the “subtasks” of locomotion are a few, underlying temporal components (Ivanenko et al. 2004).

Such subtasks often occur within the same gait cycle of the overarching task of bipedal walking, and visual input at a phase of the gait cycle critical for one subtask is not necessarily relevant for another subtask. Subtask-dependent timing is likely mediated by separate neural control pathways. For example, the within-cycle subtask and the subtask occurring in the post-perturbation cycle of

the leg observed in this study are accomplished through parallel online feedback and slower, feed-forward pathways (Marigold 2008), respectively. Candidate pathways for parallel activations are cortical area MST and associated areas VIP and CSv, which have been found to have varying degrees of egocentric and allocentric tuning to visual scene motion (Wall & Smith 2008). Such pathways may underlie the distinction between changes in self-motion and motion of hazards in the external world. As these neural control pathways are further explored in animal models and patient populations, it is critical to take gait cycle phase into account. The nervous system's modulation of responses to sensory perturbations throughout the gait cycle are particularly important when using sensory inputs such as vision to aid in the restoration of specific motor functioning (subtasks) underlying locomotion.

Chapter 4: Sensory reweighting for human walking control

Introduction

Previous studies in human walking have clearly shown that human locomotive control makes use of vision for many functions. Vision has been shown to aid the maintenance of posture upright (Warren et al. 1996; Kay & Warren 1998; Kay & Warren 2001), alter gait parameters such as speed (Konczak 1994) and stride length (Prokop et al. 1997), assist in foot placement (Hollands and Marple-Horvat 1996), provide information for navigation (Warren et al. 2001) and be critical for obstacle avoidance (e.g., Patla 1997; Grasso et al. 1998; McFadyen et al. 2007) during walking. Less clear, however, is how changing the properties of this critical sensory input directly translates to changes in control of the various segments and muscular activity for the many functions of locomotion.

One potential process used for control in changing sensory environments is “sensory reweighting”, in which sensory inputs that are more reliable indicators of self-motion will be used for control of the musculoskeletal system (Horak & MacPherson 1996). Within the context of standing postural control, sensory reweighting has been formalized using linear time-invariant (LTI) approaches (Peterka & Benolken 1995; Oie et al. 2002; Mahboobin et al. 2005). Such studies show that, for example, proportional decreases (i.e., downweighting) in the use of visual input occur with a large increase in amplitude of visual scene motion (Peterka & Benolken 1995; Kiemel et al. 2005) or when an alternate source of

sensory information is more reliable (Oie et al. 2002). Surprisingly, there have been few studies (Varraine et al. 2002; Deshpande & Patla 2005; Berard et al. 2012) which suggest sensory reweighting is a critical mechanism contributing to the flexible control of locomotion.

In this study, we characterized input-output relationships with harmonic transfer functions (HTFs) (Werely 1991). The HTFs presented here represent an innovative methodological approach to investigate how perturbations affect human locomotion. We have previously shown that broad-band stimuli can be used to probe responses of trunk kinematics to visual stimuli during walking (Logan et al. 2010; Anson et al. 2014) with use of traditional LTI frequency response functions (FRFs). We would now like to extend these investigations to the more time-varying response variables of lower-limb kinematics and muscular activity. The use of HTFs allows the use of a continuous, broad-band stimulus to identify input-output relationships with fluctuations in visual scene motion as input and segment angles, body displacement and surface electromyography (sEMG) as outputs. Furthermore, the transformation of these HTFs into the time domain as phase-dependent impulse response functions (pd-IRFs) allows us to visualize how these input-output relationships change as a function of the phase of the gait cycle.

Here we analyzed multiple body segments during treadmill walking during two types (translation and rotation) of visual scene motion. Amplitude of scene motion was increased with the expectation of a proportionally smaller response (gains of HTFs), which we interpret as a downweighting of visual input for

walking control. An additional interest in the type of scene motion is supported by evidence that rotating and translating visual scene motion is differentially processed by the visual system (reviewed by Britten et al. 2008). Both translating and rotating visual scene motion were used here, and both provide cues regarding self-motion on the treadmill. A previous study (Logan et al. 2010) using only translating visual scene motion indicated that response (gain) of a single kinematic marker such as on the shoulder, which translates in the anterior-posterior direction, was stronger than the response of a segment such as the trunk, which rotates in the sagittal plane.

If responses vary depending on the type of visual movement and body motion, it is expected that the degree of sensory reweighting is dependent on the type of scene motion. We predicted that a larger reweighting (ratio of responses to low amplitude scene motion over responses to high amplitude scene motion) of trunk orientation responses was expected with use of rotating visual scene motion compared to translating scene motion. Likewise, a larger reweighting of whole body position would be observed when translating visual scene motion was used compared to rotating scene motion. Support for these hypotheses would provide evidence that the nervous system uses sensory reweighting in a manner that benefits the subtasks, or underlying functions, of the overarching walking task. That is, sensory reweighting changes the emphasis of rotational motion cues for maintenance of orientation relative to the vertical in addition to changing the emphasis of translation scene motion for maintenance of position on the treadmill.

Methods

Subjects

Ten healthy subjects [5 males and 5 females, between 23 and 36 yrs of age, 64.2 ± 11.2 kg (mean ±SD)] received modest monetary compensation for participating in this study. All subjects were self-reported to have normal (or corrected to normal) vision. The studies conformed to the Declaration of Helsinki, and informed consent was obtained from all participants according to the procedures of the Ethics Committee of the Santa Lucia Foundation.

Apparatus

Virtual reality environment

Subjects walked at 5 km h^{-1} (EN-TRED 1475.911, Enraf-Nonius, Netherlands) one meter in front of a translucent screen (4x3m) with a rear-projected virtual display (as in Logan et al. 2014). The display consisted of 500 randomly-distributed white triangles (3.7 x 3.7 x 3.5 cm) on a black background, updated at 60 Hz. The display was 3.7 m wide by 2.54 m high when static prior to trial initiation (position 0)**,** and subjects wore goggles with occluded sides to prevent them from seeing the border of the visual display, allowing a 1.7 m wide by 1.7 m high field of view (about 81° of visual angle).The virtual display was created using CaveLib software (Mechdyne, USA) with projection through a digital projector (MP3135, HP,USA) synched to a desktop computer (Precision T5500, Dell, USA). Visual signals were created offline (Matlab, Mathworks, USA)

and were generated via Labview (National Instruments, USA) on a desktop computer (Precision T5500, Dell, USA).

Visual scene signals

These driving visual signals were either a high or low amplitude filtered white noise signal that translated or rotated in the sagittal plane. For each trial of each subject, a different seed was used to generate a white noise signal using a random number generator. High-amplitude signals had a one-sided spectral density of 600 cm^2/Hz while low-amplitude signals had a spectral density of 156.8 cm^2/Hz. These signals were then filtered using a first-order Butterworth low-pass filter with a cutoff of .02 Hz and an eighth-order Butterworth low-pass filter of 5 Hz. In doing so, power of scene motion was smoothed and limited to lower frequencies. Across subjects, the high-amplitude translation signal had an average root mean square error (RMSE) of 4.33 cm and 6.99 cm/s while the low-amplitude signal had an average RMSE of 2.19 cm and 3.49 cm/s. The high-amplitude rotation signal had an average root mean square error (RMSE) of 4.39 deg and 7.02 deg/s while the low-amplitude signal had an average RMSE of 2.17 deg and 3.50 deg/s. A positive/negative signal corresponded to an anterior-posterior (A-P) translation or forward/backward rotation into the screen from position 0. Figure 9A shows an example of the time series of low and high amplitude translation signals presented to subjects with positive being translating scene motion away from subject, or into the screen. A one cm negative translation of the visual scene corresponded to an expansion of the triangles to

3.4 x 3.4 x 3.2 cm. The virtual scene was constructed so that the focus of expansion was at the subject's eye height, with the assumption that the subject was 1 m from the screen. These visual scene motion signals were constructed so that both rotation and translation scene motion produced the same AP translation of the visual scene relative to the head, assuming small-angle approximations for deviations from vertical. Visual display generation and data collection software were synchronized via an external trigger.

Kinematics

Body kinematics were measured using a nine camera VICON-612 motion analysis system (VICON, Inc, Oxford, UK). Reflective markers (diameter, 1.4 cm) were placed on the right and left sides of the body at external landmarks corresponding to: base of the 5th metatarsal, posterior calcaneus (heel), lateral malleolus (ankle), lateral femoral condyle (knee), greater trochanter (hip), acromion process (shoulder), mastoid process (head) and frontal eminence (head). Additionally, markers were placed at the mediolateral center of the back of the head and the midline of the spine at the level of T1, T7 and L1 vertebrae. All markers were attached at the skin of these bony prominences except those placed on the shoe at the 5^{th} metatarsal and heel. All kinematic data were collected at 100 Hz.

Our analysis focuses on the leg and trunk segments. Sagittal foot, shank and thigh segment angles relative to the vertical were computed from angles formed by the fifth metatarsal to ankle, ankle to knee, and knee to hip with the

most inferior point as the origin. Trunk orientation relative to the vertical in the sagittal plane was computed as the angle formed by the L1 to T1 markers.

Muscle Activity (EMG)

Muscular activity of the right leg and lower trunk was measured using surface electromyographic (sEMG) recordings. Recordings of the following fifteen muscles were made: tibialis anterior (TA), gastrocnemius lateralis (LG), gastrocnemius medialis (MG), soleus (Sol), vastus medialis (Vmed), vastus lateralis (Vlat), rectus femoris (RF), sartorius (SART), tensor fascia latae (TFL), biceps femoris (BF, long head), semitendinosus (ST), gluteus maximus (Gmax), gluteus medius (Gmed), rectus abdominus (RAS, superior portion) and erector spinae (ESL, recorded at L1-L2). Electrodes were positioned at the muscle belly with placement carefully chosen to minimize cross-talk (Cappellini et al. 2006). Recording sites were shaved, lightly abraded, and cleaned with isopropyl alcohol prior to electrode application. The EMG data were recorded at 2000 Hz using the wireless Zerowire system (Aurion, Milan, Italy). The recording system bandwidth was 20–1,000 Hz with an intrinsic gain of 1,000. The EMG processing consisted of high-pass filtering, rectification and low-pass filtering with the same frequency cutoff values used in several previous studies of locomotion (Cappellini 2006; Cappellini et al. 2010a; Cappellini et al. 2010b; Maclellan et al. 2012). Using Matlab, these signals were high-pass filtered using a zero-lag forward-backward cascade of a 4^{th} order Butterworth filter with a 20-Hz cutoff frequency, full-wave

rectified, and then low-pass filtered with a zero-lag forward-backward cascade of a 4th order Butterworth filter with a 10-Hz cutoff frequency.

Procedures

Prior to experimentation, subjects experienced a static visual display at the experimental locomotion speeds in darkness with goggles on. An experimenter was always behind the treadmill in close proximity to the subject to ensure safety in case of falling (never occurred). Additionally, there was a push-button close to hand so that the subject and/or experimenter could immediately halt the treadmill (never used).

Subjects began each experimental trial by looking straight ahead at the visual display screen. Once they were ready, subjects said "Go" and the experimenter initiated treadmill movement for approximately 30 seconds for the subject to reach steady-state. At this point, the subject would declare if he or she was ready for the trial to begin. The experimenter then initiated data acquisition/scene motion with variable delays to avoid start-up effects. Each trial was 180 seconds in duration with a rest of 60 seconds between trials. The experimental design consisted of two amplitudes of visual scene motion (low, high) and two types of scene motion (translation/ rotation) for a total of four conditions presented in randomized blocks. Each block contained one trial of each condition. All subjects were presented with five trials of each condition.

Data Analysis

Frequency Response Functions

To transition into use of harmonic transfer functions we show trunk orientation responses to changes in visual scene rotation using LTI frequency response functions (LTI FRFs). LTI FRFs have been previously shown to be useful approximations of the input-output mapping of visual scene motion input to trunk kinematics output (Logan et al. 2010; Anson et al. 2014). To measure the sensitivity of trunk kinematics to the visual stimulus, gain was computed. Gain was taken from the frequency response functions (FRFs) of visual scene motion input to trunk orientation output.

These FRFs were computed in the same manner as in Logan et al. 2010. Briefly, Fourier transforms of A/P visual scene motion and de-meaned trunk orientation were calculated. One-sided power spectral densities (PSDs) and cross spectral densities (CSDs) using Welch's method (Bendat & Piersol, 2000) with a 20 second Hanning window and one-half overlap were then calculated with these transforms. These PSDs and CSDs were then averaged within condition for each subject. For each subject, PSDs and CSDs of stimulus frequencies up to 3.7 Hz were binned to create ten frequency bins. Binning these stimulus frequencies yielded bin averages of .05, .1, .15, .25, .4, .6, .925, 1.4, 2.1 and 3.125 Hz. Using these binned PSDs and CSDs, complex coherence was calculated as $C_{xy}(f) = P_{xy}(f) / \sqrt{P_{xx}(f) P_{yy}(f)}$, where $P_{xy}(f)$ is the CSD of the stimulus (x) and kinematic response variable (y). Across subjects, the FRF was defined as $\overline{H}_{xy}(f) = \overline{C}_{xy}(f) \sqrt{\overline{P}_{yy}(f) / \overline{P}_{xx}(f)}$ where $\overline{C}_{xy}(f)$ is the mean complex

coherence and $\overline{P}_{yy}(f)$ and $\overline{P}_{xx}(f)$ are geometric mean PSDs (Kiemel et al. 2008). Gain is the absolute value of the FRF, $\overline{H}_{xy}(f)$.

Harmonic transfer functions and phase dependent impulse response functions

Harmonic transfer functions (HTFs) of visual scene velocity as input and response variables of segment angles, L1 displacements and rectified sEMGs as outputs were computed. Here we describe the analysis steps used to compute harmonic transfer functions (HTFs) and phase-dependent impulse response function (PD-IRFs). A fuller description with equations and expanded motivation can be found in the APPENDIX. The goal of the analysis is to describe the effect of *u*(*t*), visual scene velocity, on *y*(*t*), a kinematic or sEMG response variable. **The majority of results presented in this chapter are calculated in step 4 as the modes of the transient HTF of individual response variables.** Computing the HTF and PD-IRF consists of six steps:

1. ***Approximate phase*****.** First we compute heel-strike times t_k $(k = 1,\dots,K)$ for a reference leg. Then we compute $\bar{T}$, the mean of the stride times $t_{k+1} - t_k$ $(k = 1,\dots,K-1)$, and compute the estimated gait frequency as $f_0 = 1/\bar{T}$. Next we define a discontinuous approximation of phase as $\theta_{\mathrm{d}}(t) = k + f_0(t - t_k)$ for $t_k \le t < t_{k+1}$. To obtain a continuously-differentiable approximation of phase, $\theta(t)$, we apply a second-order low-pass filter to $\theta_{\mathrm{d}}(t)$:

$$\ddot{\theta}(t) + 2d(\dot{\theta}(t) - f_0) + d^2\theta(t) = d^2\theta_{\mathrm{d}}(t).$$

Note that in the absence of perturbations, approximate phase $\theta(t)$ matches the usual definition of the phase of the gait cycle.

2. *Replace time with approximate phase*. Let *p* be the inverse of *θ*: $p(\theta(t)) = t$ and $\theta(p(\vartheta)) = \vartheta$. Let approximate phase ϑ take the place of time $t = p(\vartheta)$ as the independent variable and compute $\tilde{u}(\vartheta) = u(p(\vartheta))$, $\tilde{y}(\vartheta) = y(p(\vartheta))$, and $\tilde{d}(\vartheta) = \dot{\theta}\big(p(\vartheta)\big)/f_0$. (We use the symbol ϑ to distinguish approximate phase as an independent variable from approximate phase as a function of time.)

3. *Compute output variables for HTF analysis*. For each ϑ, let $y_0(\vartheta)$ be the mean of $\tilde{y}(\vartheta)$. Then compute the deviations $\tilde{y}^{(1)}(\vartheta) = \tilde{y}(\vartheta) - y_0(\vartheta)$ and $\tilde{d}^{(1)}(\vartheta) = \tilde{d}(\vartheta) - 1$.

4. *Compute transient and phase-derivative HTFs.* To account for shifts in phase that affect all response variables, both a transient and phase-derivative HTF are computed. We compute the *transient HTF* from $\tilde{u}(\vartheta)$ to $\tilde{y}^{(1)}(\vartheta)$, denoted $\widetilde{H}_y$, and the *phase-derivative HTF* from $\tilde{u}(\vartheta)$ to $\tilde{d}^{(1)}(\vartheta)$, denoted $\widetilde{H}_d$, as follows. Let $z(\vartheta)$ be either $\tilde{y}^{(1)}(\vartheta)$ or $\tilde{d}^{(1)}(\vartheta)$. Compute the power spectral density (PSD) $p_{\tilde{u}\tilde{u}}(f_1)$ and the double-frequency cross-spectral density (CSD) $p_{\tilde{u}z}(f_1, f_2)$ (Bendat & Piersol 2000). The two sided power spectral density $p_{\tilde{u}\tilde{u}}(f_1)$ of a low and high amplitude condition is observed in Figure 9B. The double-frequency CSD describes the

relationship between the input signal $\tilde{u}(\vartheta)$ at input frequency f_1 and the output signal $z(\vartheta)$ at output frequency f_2. The PSD and CSD are computed using Welch's method with 40-cycle Hanning windows (aligned to start at an integer value of ϑ) and 50% overlap. The *k*-th mode of the HTF H_z from $\tilde{u}(\vartheta)$ to $z(\vartheta)$ is computed as $H_{z,k}(f_1) = p_{\tilde{u}z}(f_1, f_1 + kf_0)/p_{\tilde{u}\tilde{u}}(f_1)$. Note that H_z is a function of both the mode index *k* and the input frequency f_1.

5. *Compute transient and phase IRFs*. For an LTP mapping from $\tilde{u}(\vartheta)$ to $z(\vartheta)$, its HTF H_z can be converted to its phase-dependent IRF h_z using a Fourier series constructed from an inverse Fourier transform of each mode of the HTF. The IRF h_z is a function of response phase ϑ_r and stimulus phase ϑ_s and can be used to represent the LTP mapping from $\tilde{u}(\vartheta)$ to $z(\vartheta)$ as

$$z(\vartheta_\mathrm{r}) = \int_{-\infty}^{\vartheta_\mathrm{r}} h_z(\vartheta_\mathrm{r}, \vartheta_\mathrm{s})\, \tilde{u}(\vartheta_\mathrm{s}) d\vartheta_\mathrm{s}.$$

Using this procedure, compute the *transient IRF* $\tilde{h}_y$ and *phase-derivative IRF* $\tilde{h}_d$ from $\tilde{H}_y$ and $\tilde{H}_d$, respectively. Then compute the *phase IRF* by integrating the phase-derivative IRF:

$$h_\theta(\vartheta_\mathrm{r}, \vartheta_\mathrm{s}) = \int_{\vartheta_\mathrm{s}}^{\vartheta_\mathrm{r}} \tilde{h}_d(\tau, \vartheta_\mathrm{s}) d\tau.$$

6. Compute IRFs. The IRFs $\tilde{h}_y$ and h_θ can be combined to obtain the IRF from *u*(*t*) to *y*(*t*) that is a function of response time t_r and stimulus time t_s. Here t_r and t_s are expressed in normalized time: time divided by the mean

gait period and aligned so that stimulus time t_s equals true stimulus phase.

Steps 1-4 were computed on a trial by trial basis with averages of PSDs and CSDs taken across trials for each condition of each subject for completion of the HTF analysis. Spectral densities were averaged across trials for each subject and then binned in .125 Hz total size groupings symmetric around 0 Hz input frequency (0 Hz is in the middle of the middle bin) prior to calculation of HTF modes. If we ignore the effects of phase-resetting, HTF theory predicts that for walking with gait frequency f_0, a sensory or mechanical input at frequency f will produce outputs at all output frequencies $f + kf_0$, where k is an integer. For example, for a gait frequency of 1 Hz, a 0.2 Hz sensory perturbation will produce outputs at 0.2 Hz, 1.2 Hz, 2.2 Hz, etc., and also at 0.2 – 1 Hz = -0.8 Hz, 0.2 – 2 = -1.8 Hz, etc. Thus, HTF modes and comparisons (i.e. gain ratios described below) are plotted with negative to positive input frequency ranges. For each k, the mapping from input frequency f to output frequency $f + kf_0$ is described by the k-th mode of the HTF. Six ($k=0,1,\ldots5$) modes of the HTF between visual scene velocity and each response variable were computed. The FRF and 0^{th} mode of the HTF both map responses at the same output frequency as the perturbation input frequency, but the 0^{th} mode of the HTF is a function of approximate phase not time and windows of the HTF are lined up at integer values of phase.

The HTF analysis described in step 4 above is used in this chapter to investigate the majority of condition effects. To measure both the sensitivity and timing of the response variables to the visual stimulus, gain and phase were

computed. Gain is the absolute value of each mode of the HTF and phase is the argument of each mode of the HTF, converted to degrees. Measures of gain and phase were plotted as a function of input frequency.

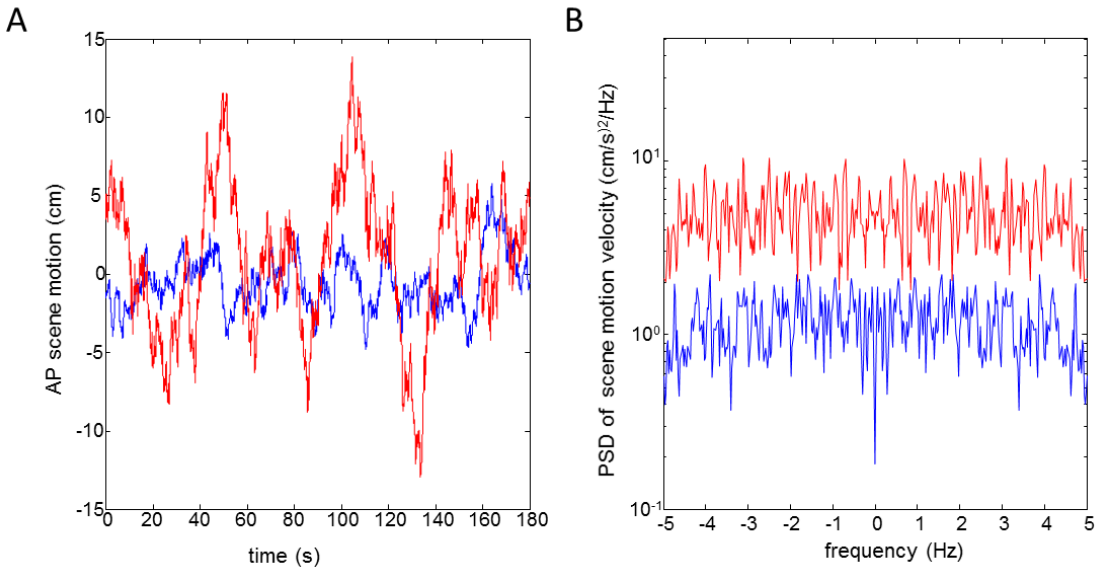

Figure 9. Time series and PSD of translation perturbation. A: Signals used in separate trials of high and low amplitude A-P translating visual scene motion for a single subject. B: Double-sided PSD of the velocity of the same signals in A.

Statistics

Statistical tests of HTFs were performed in the complex plane at each frequency bin of each mode for all response variables. To test that each response was different from 0, each bin of each mode was tested with Hotelling's T^2 test for difference from 0 (α=.05). If both amplitude conditions at a given frequency bin were different from zero, they could then be tested for conditional differences in gain to test for amplitude-dependent sensory reweighting. To test for condition differences in gain, 95% bootstrap confidence intervals were computed for differences in log gain at each frequency bin using the bootstrap

percentile-*t* method with 4000 bootstrap resamplings and 400 nested bootstrap resamplings for variance estimation (Hall, 1988; Zoubir & Boashash, 1998). A significant difference between two amplitudes was found when the confidence interval of differences in log gain, or gain ratios, did not include one. This same procedure was applied to gain of trunk orientation FRFs shown in Figure 10. The interaction of amplitude and scene motion type was determined by calculating the difference in log gain of amplitude conditions for each response variable within each scene motion type, and then computing the log gain difference of these log gain differences from each scene motion type. These ratios of differences in log gain, or ratio of gain ratios, were calculated after initial tests that all 4 conditions were different from zero were satisfied at that bin.

We also tested PD-IRFs to investigate if conditional effects such as amplitude-dependent reweighting changed across phases of the gait cycle. To investigate a dependence of amplitude-dependent sensory reweighting on phase of the gait cycle, permutation tests (1,000, Manly 1997) based on the t-statistic between the two conditions at all combinations of stimulus phase and normalized response time were tested simultaneously and family-wise error rate (FWER) was controlled for each response variable. The tmax method (Blair & Karnisky 1993) was used to adjust the p-value for each combination of stimulus phase and normalized response time ($\alpha = .05$). These tests were performed in Matlab using functions written by Groppe (Groppe et al. 2011). These tests are non-parametric and suited for this study as FWER control is strong compared to other methods

(e.g. cluster-based permutation testing, false discovery rate) allowing us to determine where effects are reliable (Groppe et al. 2011) in the PD-IRFS.

Results

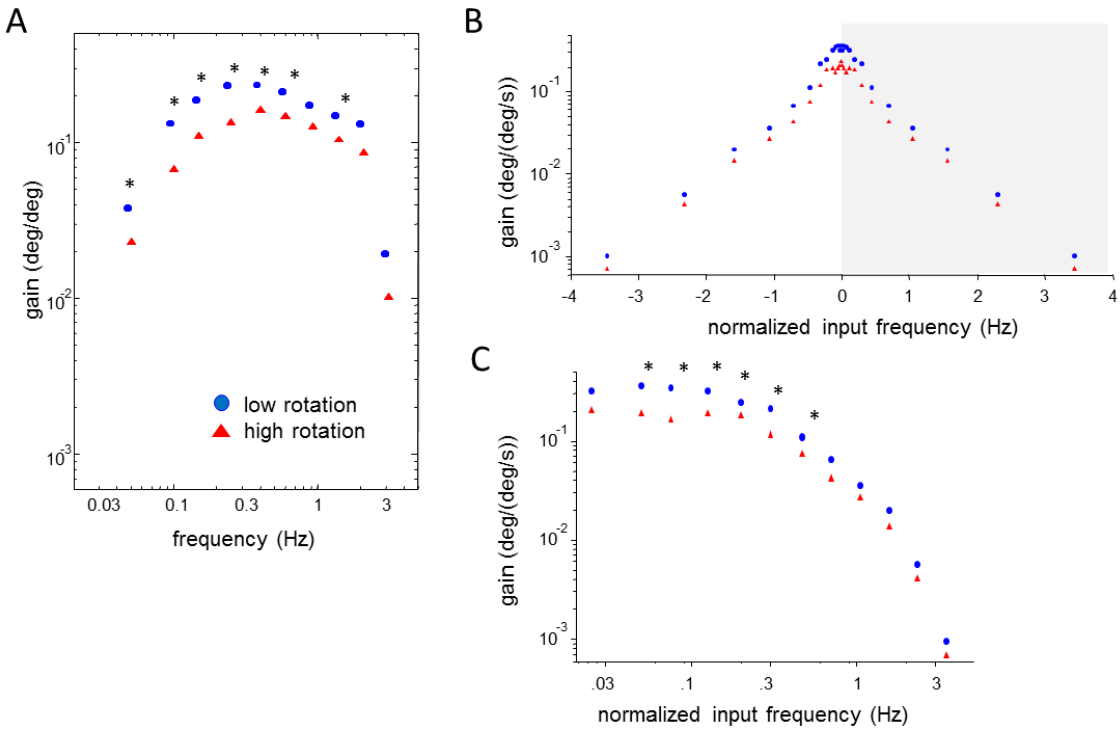

Figure 10. Trunk Orientation FRF and HTF. A) Gain of trunk orientation from change in visual scene rotation using FRFs(as in Logan et al. 2010). B. 0th mode of the HTF of trunk orientation from visual scene velocity. C. The shaded region in B is shown in C for comparison between A and B at the same frequency range. A and C have identical axes and bin ranges are approximately the same for those in A and the last 10 bins in C. Asterisks denote significant ($p<.05$) differences in responses between different amplitude conditions at that frequency bin (see *Methods*).

We begin by illustrating a dependency of trunk orientation response magnitude on changes in visual scene amplitude using both LTI FRFs and HTF analyses. Marking a transition in methods for studying sensory reweighting during walking, Figure 10 shows trunk orientation responses to vision showing

both a FRF and comparable 0^{th} mode of a HTF for the same data. Negative and positive frequencies are shown in Figure 10B to introduce the HTF mode plots, and present value of output frequency (in Hz) as the input frequency added or subtracted to the product of the mode order and gait cycle frequency (see *Methods*). Figure 10B is the 0^{th} mode of the HTF, so it describes how input at any given frequency f produces a response at the same frequency. This allows comparison between the common frequency range in Figure 10A and 10B. This common frequency range is noted with a shaded box in Figure 10B and is presented in Figure 10C. Verified with gain ratios at individual frequency bins (see *Methods*), a clear amplitude dependency was observed in both analyses (Figs 10A and 10C). Gains of trunk orientation to scene motion in both analyses increased as visual scene motion amplitude decreased, and are noted in Figures 10A and 10C with an asterisk.

To take into account the limit-cycle dynamics of gait, we show the relationship of all response variables (kinematics and sEMG) in the frequency domain at higher modes in addition to the 0^{th} mode. As highlighted by Figures 11 and 12, there were responses observed across several modes in all response variables. These figures show frequency bins where gain and phase were different from zero in the complex plane ($p<.05$, see *Methods*) in the low amplitude, rotational scene motion condition for trunk orientation, foot segment angle, normalized ES sEMG and normalized LGAS sEMG. Gain and phase are plotted dependent on input frequency, and the output frequency (in Hz) is the input frequency added or subtracted to the product of the mode order and gait

cycle frequency (see *Methods*). Phase is shown for complete description of the HTF mode, but our focus is on gain as we investigate a dependency on amplitude. The first mode describes how input at any given frequency f produces output at frequency f + f_0, where f_0 is the gait frequency while the second mode describes how input at any given frequency f produces output at frequency f + $2f_0$. For example, the responses in foot angle observed at non-zero modes are strong evidence that an LTI FRF, which does not take into account the limit-cycle dynamics of gait, is a poor approximation of the input-output mapping of visual scene motion input to foot segment motion output.

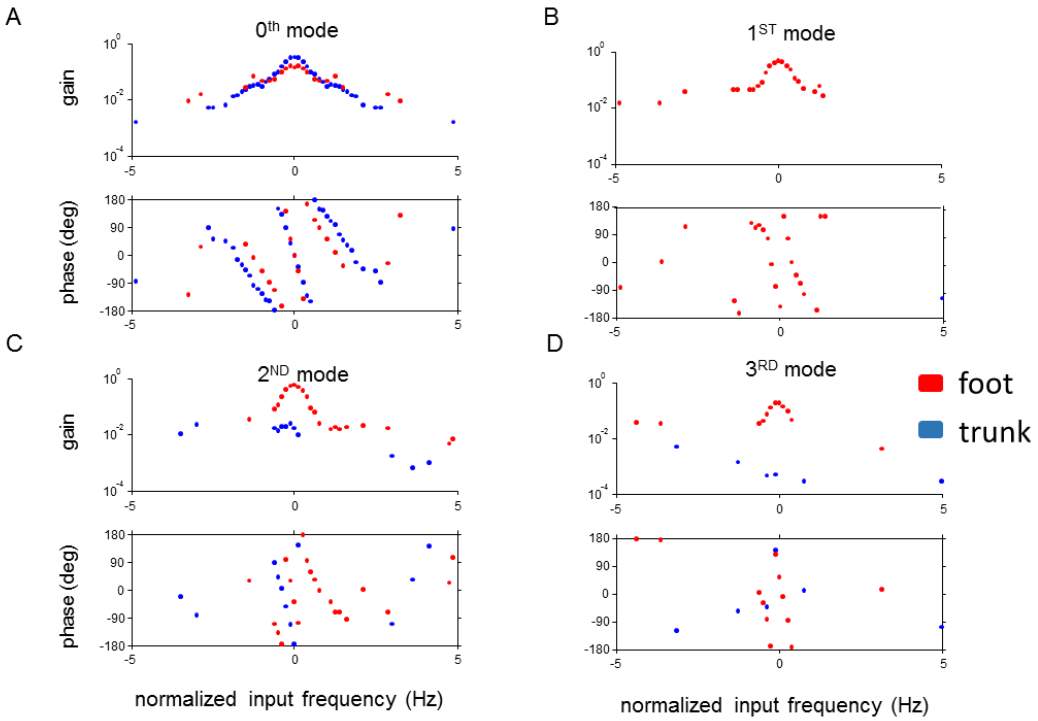

Figure 11. Segment Angle HTFs. Gain and phase of HTFs of foot (red) and trunk (blue) segment angles from visual scene velocity. These data are means across subjects in the low amplitude, rotating scene motion condition. Only those bins passing initial statistical tests in complex plane are shown (see *Methods*). Gain and phase of modes 0 through 3 are shown in subplots A-D. Value of output frequency (in Hz) is the input frequency added to the product of the mode order and gait cycle frequency (see Methods).

Responses of kinematic response variables to visual scene motion generally took either the form of a trunk or leg segment response. Figure 11 shows HTFs of trunk orientation responses to visual scene velocity in blue. Trunk responses were more prevalent and larger in magnitude in the 0th mode while leg segment responses were higher in magnitude in the 1st and 2nd mode compared with the 0th mode. Gains of foot segment response were observed to be larger in the 1st and 2nd mode compared to the 0th mode while retaining the same shape of response. As observed in Figure 11, the peak magnitude of the foot segment angle response, in addition to gains at other frequency bins, declined from the 2nd to 3rd mode and remained in a similar magnitude range as mode order increased from 3 to 5 (not pictured). These patterns of gain were similar across all leg segment angles calculated.

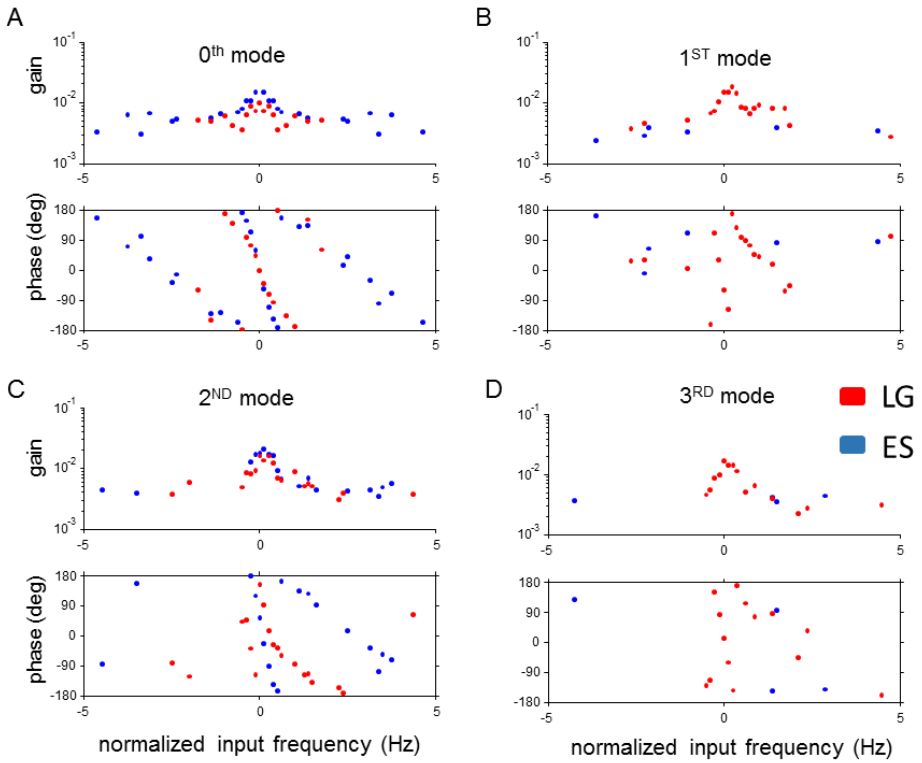

Figure 12. sEMG HTFs. Gain and phase of HTFs of normalized Erector Spinae (ES) and Lateral Gastrocnemius (LG) sEMGs from visual scene velocity. These data are means across subjects in the low amplitude, rotating scene motion condition. Only those bins passing initial statistical tests in complex plane are shown (see *Methods*). Gain and phase of modes 0 through 3 are shown in subplots A-D. Value of output frequency (in Hz) is the input frequency added to the product of the mode order and gait cycle frequency (see Methods).

Like kinematics, sEMGs also show two typical patterns of responses across modes of HTFs. Similar to patterns observed in the trunk segment angle, responses of normalized erector spinae (ES) sEMG shown in Figure 12 in blue were most abundant in the 0^{th}, 2^{nd} and 4^{th} mode of the HTF. Shown in red in Figure 12, gains are higher in the 1^{st} through 3^{th} mode than observed in the 0^{th} mode for LG. Patterns of gain are generally the same in modes 1-4. Responses in the remaining muscles were similar to LGAS; larger gains were observed in the 1^{st} to 4^{th} mode with respect to the 0th mode. RAS was an exception, with few responses observed across input frequencies and modes.

Amplitude dependence for both types of visual scene motion

Gains decreased with increasing amplitude of scene motion for both types of scene motion in segment angles and L1 A-P displacement. Figure 13 shows gain ratios significantly different than one, which were typically found at lower input frequencies. Across kinematic response variables, there was only a single instance of increased gain to visual scene motion upon increasing visual scene motion amplitude, which was observed in the shank response to rotating scene motion in the 1^{st} mode at the 2.125 Hz input frequency bin. Overall, there are more instances of amplitude-dependent changes to gain during rotation

conditions in the leg segment angles with more dispersion across modes while amplitude-dependence in the trunk orientation and L1 displacement are more concentrated in the 0^{TH} mode.

Figures 13A/B/C show how foot, shank and thigh segment angles show similar dependencies on changes in rotating scene motion amplitude. These three segment angles had similar amounts of amplitude-dependent changes in gain spread across HTF modes 0-3 with 8.8(± 3.1), 7.5 (±1.9) and 6.8(±2.2) mean across mode instances (# of frequency bins) of reweighting in foot, shank and thigh, respectively. At higher modes (4^{th} and 5^{th}), fewer instances of amplitude dependence were observed in the thigh compared to lower modes while the lower- limb foot and shank segments continued to display amplitude-dependent relationships.

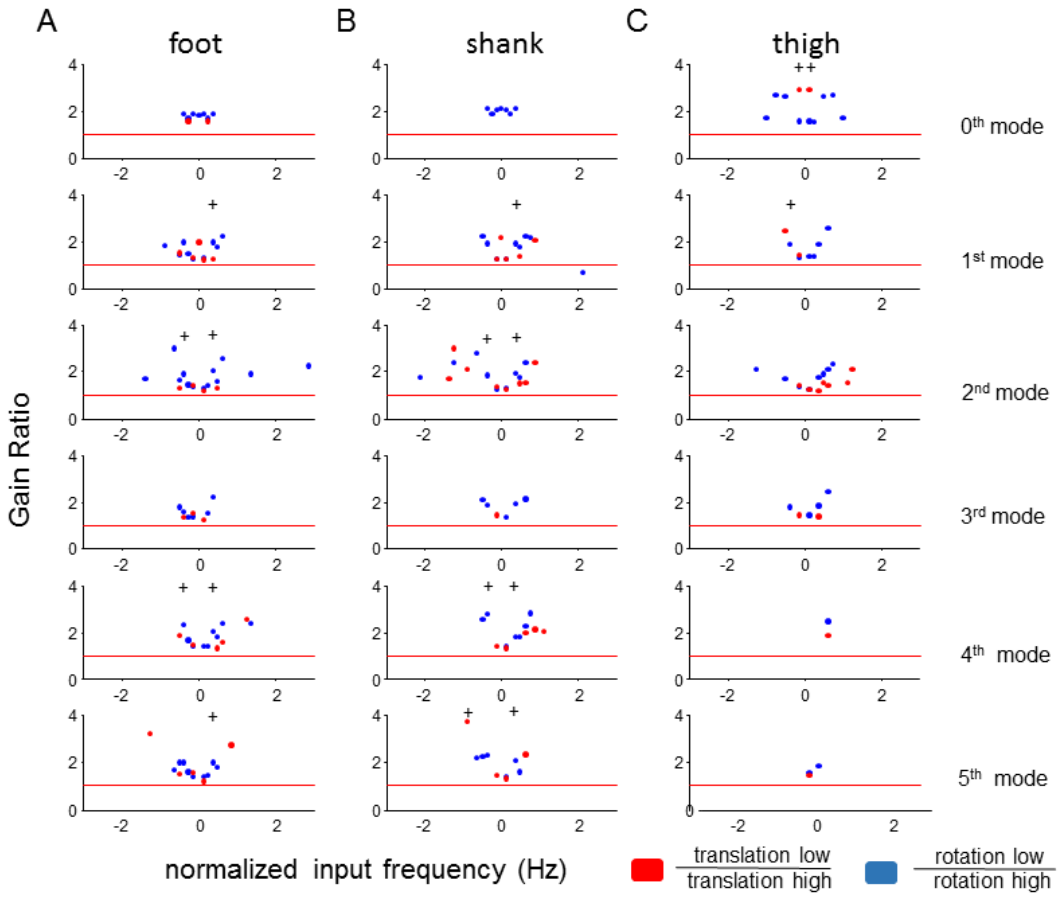

Figure 13. Leg Kinematics gain ratios. Ratios of low amplitude gains to high amplitude gains of sagittal plane foot segment angle (A), shank segment angle (B), and thigh segment angle(C) in translation and rotation conditions. Gain ratios plotted here are those gain ratios which are significantly different from 0 ($p<.05$). The red line denotes a gain ratio of one. Only those bins passing initial statistical tests in complex plane could be compared (see *Methods*). Gain ratios of modes 0 through 5 are shown in different rows. Value of output frequency (in Hz) is the input frequency added to the product of the mode order and gait cycle frequency (see Methods). Significant interactions between gain ratios and visual scene motion type are noted with a + above, requiring the ratio of gain ratios to be different from 0 and that all four responses at that bin initially different from zero in the complex plane ($p<.05$, see *Methods*).

In the trunk segment angle, the majority (27 out of 43 total) of instances of amplitude dependence observed in the trunk were in the 0^{th} mode with another large portion (12/43) observed in the 4^{th} mode. L1 A-P displacement, which is an indicator of whole body motion in the anterior-posterior plane, also had a large proportion (22/49) of amplitude dependence in the 0^{th} mode with additional

instances observed in the 2nd (12/49), 3rd (3/49) and 4th(12/49) mode. In contrast to trunk orientation, more (28/49) instances of L1 A-P amplitude-dependent changes in gain were observed during rotating scene motion than observed during translating scene motion. In sum, trunk orientation and L1 A-P displacement have similar dispersion of significant gain ratios across modes with more amplitude dependent changes in gain observed in trunk orientation to translating scene motion while amplitude dependence in L1 A-P displacement responses is more often observed to rotating stimuli.

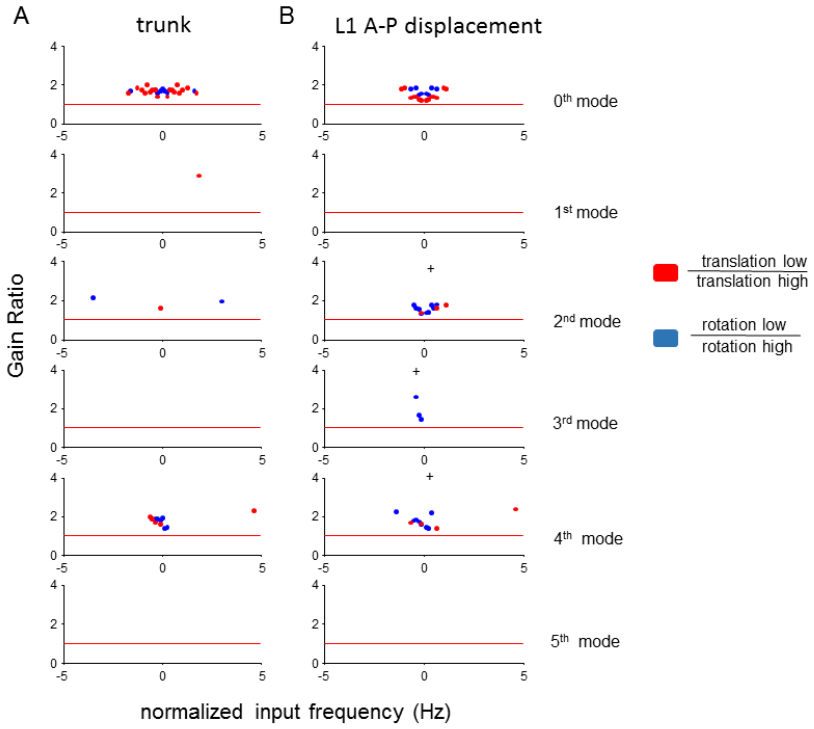

Figure 14. Trunk kinematics gain ratios. Ratios of low amplitude gains to high amplitude gains of sagittal plane trunk orientation (A)and A-P displacement of the L1 marker (B) in translation and rotation conditions. Gain ratios plotted here are those gain ratios which are significantly different from 0 ($p<.05$). The red line denotes a gain ratio of one. Only those bins passing initial statistical tests in complex plane could be compared (see *Methods*). Gain ratios of modes 0 through 5 are shown in different rows. Value of output frequency (in Hz) is the input frequency added to the product of the mode order and gait cycle frequency (see Methods). Significant interactions between gain ratios and visual scene motion type are noted with a + above, requiring the ratio of gain ratios to be different from 0 and that all four responses at that bin initially different from zero in the complex plane ($p<.05$, see *Methods*).

The interaction of scene motion and amplitude dependency was also tested at each frequency bin, and larger amplitude dependencies (gain ratio) of one type of scene motion compared to the other is noted with a + symbol in Figures 13 and 14. Larger gain ratios reveal that increasing scene-motion amplitude caused a proportionally larger decrease in gain for one scene-motion type than the other. As seen in Figures 13A and 13B, the frequency bins and modes of this interaction are identical for the foot and shank with the exception of a greater amplitude dependence of translating scene motion for the shank in the 5th mode at the -.875 frequency input bin. In 18 of 19 instances, increasing scene-motion amplitude caused a proportionally larger decrease in gain to rotational scene motion than to translating scene motion. Although this interaction was sporadic across modes, there is consistency in the input frequency as the larger gain ratio for rotational scene motion was observed primarily (16 of 18 instances) at either -.375 or .375 Hz input frequency for the segment angles shown in Figure 13.

In addition to kinematic response variables, changes in gain due to changes in amplitude were also observed in muscle activity (sEMG). As observed in Figure 15 and indicative of most muscles recorded, significant gain ratios were typically observed in the 1st through 4th modes with rotating scene motion. The exception to these trends was the RAS muscle, in which no evidence of reweighting was observed for either type of visual scene motion. Like kinematics, significant gain ratios in the musculature were observed at input frequencies closer to 0. Significant gain ratios of rotating scene motion ranged

from 1.26 observed in SOL in the 4th mode with -.125 Hz input frequency to 3.61, which was observed in RF at the 4th mode with .375 Hz input frequency. For translation, significant gain ratios ranged from 1.27 observed in MG at the 1st mode with the .25 Hz input frequency to 5.44, which was observed in TFL at the 2nd mode with the input frequency of 1.125. Critically, there were no instances of gains being higher in a high amplitude condition compared to a low amplitude condition.

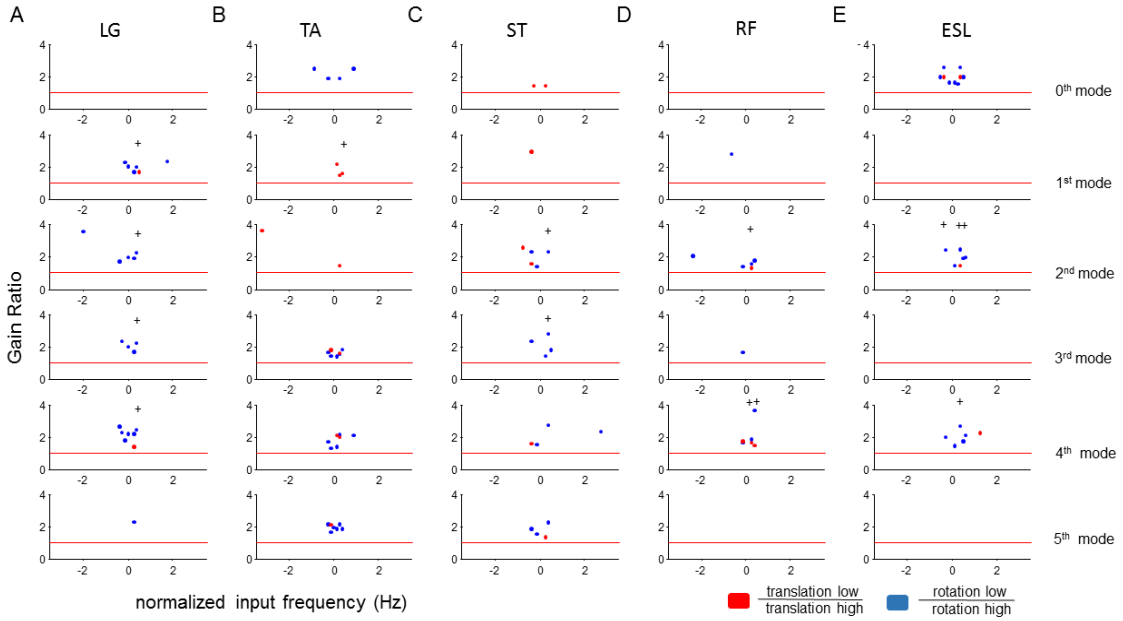

Figure 15. Muscle activity gain ratios. Ratios of low amplitude gains to high amplitude gains of lateral gastrocnemius (A), tibialis anterior (B), semitendinosus (C), rectus femoris (D) and lumbar erector spinae (E) in translation and rotation conditions. Gain ratios plotted here are those gain ratios which are significantly different from 0 ($p<.05$). The red line denotes a gain ratio of one. Only those bins passing initial statistical tests in the complex plane could be compared (see *Methods*). Gain ratios of modes 0 through 5 are shown in different rows. Value of output frequency (in Hz) is the input frequency added to the product of the mode order and gait cycle frequency (see Methods). Significant interactions between gain ratios and visual scene motion type are noted with a + above, requiring the ratio of gain ratios to be different from 0 and that all four responses at that bin initially different from zero in the complex plane ($p<.05$, see *Methods*).

Also seen in Figure 15, interactions of scene motion and amplitude dependency were observed for sEMG. Greater increases in gains when

decreasing visual scene amplitude (gain ratios) were observed during rotational scene motion compared to translating scene motion at 25 combinations of input frequency and modes in the 15 muscles recorded. In addition to those interactions shown in Figure 15 with a +, greater gain ratios to rotational scene motion were observed in Gmed (-.25 Hz input frequency in 3rd mode, .375 Hz in 4th mode), SART (.25 Hz in 4th mode), Gmax (-.25 and .25 in 3rd mode), MG (-.25 in 1st mode, -.375 in 2nd and 3rd mode) and Sol (-.25 in 1st and 4th mode, .25 in 1st and 2nd mode). Similar to kinematics, a large portion (13 of 25) of these interaction effects were observed at input frequency of -.375 or .375. There were two instances of greater amplitude dependence on translational scene motion; these were at the .125 bin of the 1st mode of TA responses (Fig. 15B) and the .125 bin of the 3rd mode of Gmax responses. No interactions of reweighting based on type of scene motion were observed for RAS, TFL, BF, VMed or Vlat muscles.

No evidence for differential amplitude dependence by gait cycle phase

We also tested computed PD-IRFs from these HTFs to investigate if conditional effects such as amplitude-dependent reweighting changed across phases of the gait cycle. As observed in Figure 16, taking these HTFs into the time domain (normalized by the gait cycle) allows visualization of the responses dependent on phase of the gait cycle. The phase at which the stimulus occurred (stimulus phase) is on the x-axis and the phase at which a response may occur is

on the y-axis (normalized response time). Consistent with frequency domain responses being more concentrated in the 0^{th} mode, responses in trunk orientation to rotating stimuli shown in Figure 16A form a band parallel to stimulus onset line indicating a large portion of the overall response to be time-invariant. Intensity of the PD-IRF on the whole in the high amplitude condition appears weaker than observed in the low amplitude condition, which echoes the amplitude dependency observed in the HTF analyses. Figure 16B shows the PD-IRF of LG, showing stimulus phase-dependent responses similar to that previously observed with transient ramp stimuli in A-P translation (Logan et al. 2014) as visual scene perturbations (~.2 on x-axis) elicit changes in activation within cycle in the response time of pre-swing (.5 on y-axis). Testing for differences between amplitudes at each combination of stimulus phase and normalized response time revealed no differences in the response variables in Figure 13 in addition to all other kinematics and sEMGs. Evidence for the gait cycle phase altering the amplitude dependence was not observed in translation conditions either. Significant differences between amplitude conditions at specific locations of stimulus phase and normalized response time with the strong FWER control used could have provided strong evidence for an amplitude-dependence which changes base on gait cycle phase, or even subtask.

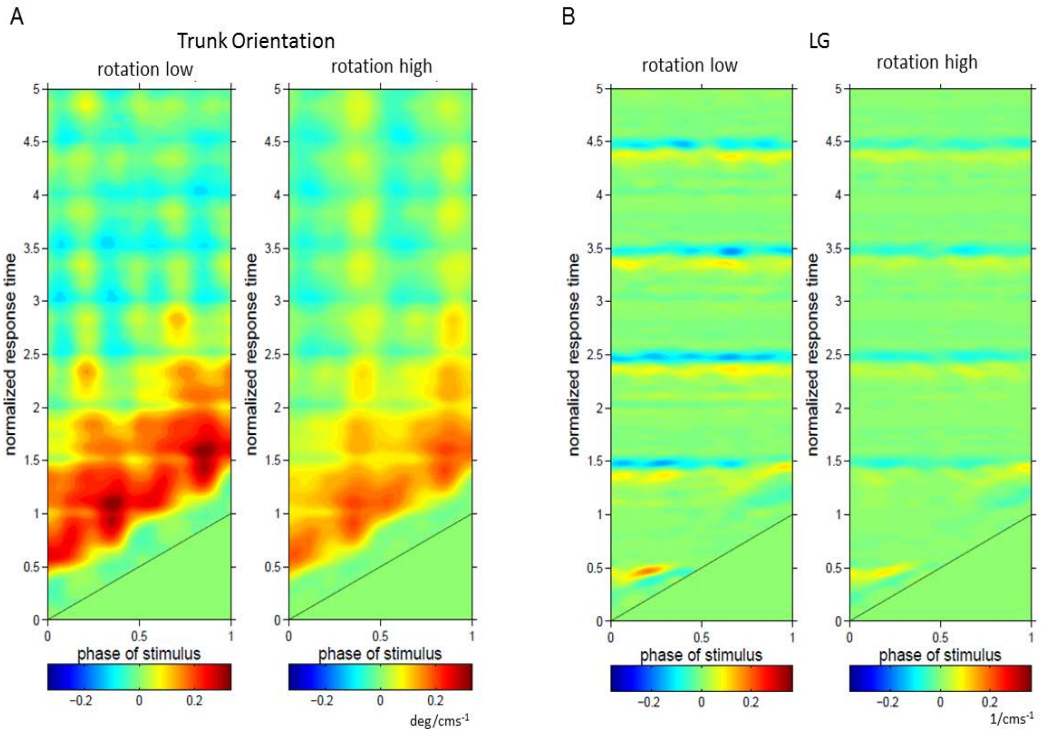

Figure 16. Phase-dependent impulse response functions. PD-IRFs from visual scene velocity to trunk orientation (A) and normalized LG sEMG (B). Maximum values in the contour plot of both plots were dictated by maximum value found across both conditions for each response variable. ($p<.05$, see

Discussion

A dependence on amplitude of visual scene motion was observed in the responses of multiple segment angles and muscle activations to both rotating and translating visual scene motion. The decrease in proportional use of visual scene motion as it increased in amplitude was observed in multiple modes at low input frequencies, providing substantial evidence that the sensor fusion process of sensory reweighting supported in studies of standing postural control (Peterka & Benolken 1995; Oie et al. 2002; Mahboobin et al. 2005) is used in walking control. When possible to compare, larger reweighting of rotational scene motion compared to translational scene motion was observed, suggesting a greater

reliance on rotational motion cues by the nervous system for locomotive control. Finally, transformation of these HTFs in the time domain reveal that this sensory reweighting likely does not change based on the phase of the gait cycle when the visual scene motion occurs. To our knowledge, our use of HTFs and PD-IRFs in this study has provided the first investigation of sensory reweighting of vision during human walking that can be applied to the legs and musculature in addition to the trunk.

Sensory reweighting observed in multiple modes

Application of HTFs to human walking has allowed us to investigate sensory reweighting and more fully characterize responses in the weakly time-varying response variables of trunk orientation and whole body translation during walking. LTI FRFs have been previously shown to be useful approximations of the relationship between visual scene motion and trunk kinematics (Logan et al. 2010; Anson et al. 2014). LTI FRFs of trunk motion in those studies correspond to the responses observed to positive input frequencies in the 0^{th} mode shown in Figure 10. Larger magnitude and more consistent responses are observed at the 0^{th} mode, yet there are still small, significant responses observed at higher modes for both trunk orientation and L1 A-P displacement with reweighting relationships uncovered with HTFs. In other words, visual scene motion at a specific input frequency elicits responses of the trunk at additional frequencies beyond the frequency of input. The weakly time-varying nature of these responses of the trunk is more fully characterized by the use of HTF over LTI FRFs, yet these new findings do not undermine previous work (Logan et al.

2010; Anson et al. 2014) as a much larger portion of actual responses and reweighting relationships are observed in the 0^{TH} mode.

In response variables such as leg segment angles and sEMG which intrinsically change in magnitude and direction across the phases of the gait cycle it was predicted that use of HTFs was critical due to the potential for responses to sensory input to vary based on the phase of the gait cycle. In fact, there is a large and growing body of evidence supporting the notion that responses in leg segments and muscle activity to input from sensory systems is used for function in a phase-dependent manner (e.g., Forssberg et al. 1975; Forssberg 1979; Capaday and Stein 1986; Duysens et al. 1990; Patla 1991; Hollands and Marple-Horvat 1996; Zehr and Stein 1999; Bent et al. 2004). For vision specifically, a single previous study (Logan et al. 2010) investigated responses of leg motion to broad-band visual scene motion. Cross-covariance analysis revealed a phase-dependent response in the thigh segment to vision which effectively disallowed the use of LTI FRFs for investigating input-output relationships of vision to leg segments. As the 1^{st} mode and greater in Figures 11 and 12 show the majority of responses of leg kinematics and muscle activity, it is clear that an analysis was needed that takes into account responses at an output frequency that is different from the input frequency of perturbation. More instances of reweighting were observed in these higher modes than observed in the 0^{th} mode in the leg segments, as seen in Figure 13. Finally, the sensory reweighting observed in the leg muscles in Figure 15 would not have been observed with the LTI FRF analysis used in previous studies of amplitude-

dependent changes in muscle responses in standing postural control (Kiemel et al. 2011; Logan et al. 2014b).

Few studies have investigated sensory reweighting as a process for locomotive control. Also using virtual scene motion, Warren and colleagues (1996) have shown that sinusoidal stimuli with and without a constant flow field show decreased “excursion gains” of a marker placed at the neck to increased amplitude (Warren et al. 1996). Our study expands on that study as we now show that amplitude-dependent changes are ubiquitous in the kinematics and muscle activations of multiple segments. The notion of reweighting was not discussed by Warren et al (1996), but has been supported in more recent work in steering control. Deviations in Center of mass (CoM) displacement in overground walking elicited by a head mounted display are larger in older adults compared to younger adults, reflecting a poor ability to downweight erroneous visual cues for locomotive steering (Berard et al. 2012).

Studies of interactions between sensory systems have also provided further support that sensory reweighting is used for locomotive control. Evidence for intersensory reweighting has been provided by Varraine and colleagues (2002) in the form of a higher PSD of walking velocity at a visual stimulus frequency during a combined visual and mechanical perturbation that provided additional, somatosensory input at the foot compared to a visual stimulus alone. Deshpande and Patla (2005) used prism goggles and galvanic vestibular stimulation (GVS) to show an increased effect of GVS on CoM displacement in the early approach to a target followed by a dominance of vision for CoM

displacement later in approach (Deshpande and Patla, 2005). Although instances of sensory reweighting studies are few during walking, these studies support the nervous system's flexible use of sensory input for function. Furthermore, future intersensory reweighting studies which make use of broad-band sensory stimuli and HTF methods are supported by these previous studies and are logical extensions of our initial study of reweighting in a single sensory system.

Subtask control

Rotating visual cues inform the nervous system that a change in the body's orientation has occurred while translating visual cues inform that a change in position has occurred. It was expected that the nervous system would use visual cues in a subtask dependent manner. That is, greater reweighting of rotational cues would be used by trunk orientation for the subtask of orientation to vertical while a greater reweighting of translation cues would be used by whole body translation for maintaining position on the treadmill. A differential emphasis on processing of scene motion based on kinematic variable was not observed as predicted. When possible to compare, larger reweighting of rotational scene motion compared to translational scene motion was observed, suggesting a greater reliance on rotational motion cues by the nervous system for locomotive control. The emphasis on type of scene motion was not observed in an overwhelming majority for either response variable, however, leaving how sensory reweighting changes based on subtask, if at all, an open question.

Perhaps a more nuanced view of how to determine the use of sensory reweighting for specific subtasks is needed. One potential route could be for an

emphasis on common input frequencies which yield significant reweighting relationships. In this initial study of sensory reweighting during walking there is at least one speculative observation with regards to subtask control that can be made. Almost all amplitude by scene motion interaction effects observed favor reweighting orientation cues over translation cues and the majority of these interaction effects are observed at the .375 Hz input frequency bin. This suggests that this input frequency range is a “sweet spot” for neural control that makes use of rotating visual cues for upright postural control during walking. Although our focus is typically on trunk orientation when discussing the subtask of maintenance of postural control upright during walking (Logan et al. 2010; Logan et al. 2014; Anson et al. 2014), combinations of muscle activations and leg segment angles could contribute to this subtask as well. One could speculate that processing of orientation cues is emphasized across the segments and musculature when frequencies of stimuli occur at this specific frequency, and it is possible that responses are coordinated across the segments for decreasing the use (gain) of more destabilizing, larger amplitude rotational cues.

Likewise, transformation of these responses into the time domain to investigate differential reweighting based on gait cycle phase did not provide support for changes in sensory reweighting due to subtask. Phase-dependent responses to visual scene motion were observed in Figure 16 as in a previous study (Logan et al. 2014), which allow characterization of muscular and kinematic responses to vision into subtasks performed during walking. However, no differences at specific combinations of stimulus phase and normalized response

time were observed for any response variable between low and high amplitude conditions. These findings support the conclusion that all subtasks of human walking use sensory reweighting to inhibit the use of erroneous or incongruent visual information and can be observed throughout the kinematics and muscle activity enacting those subtasks.

Chapter 5: Fast and slow time scales for control for human walking

Introduction

Virtual scene motion has been used in treadmill walking experiments to provide insight into how visual information is used in human locomotion (Warren et al. 1996; Prokop et al. 1996). Recent studies have also made use of virtual visual environments to gain a better understanding of the neural control of human walking (O'connor & Kuo, 2009; O'connor et al. 2012). By imposing variability in the walking behavior, visual scene perturbations revealed that control of the body's motion in the frontal plane is a much more active, neural process compared to the sagittal plane (O'connor & Kuo, 2009), and that increased energy expenditure is correlated with the increased control effort (O'connor et al. 2012). Thus, visual perturbations can be used to understand the control of walking as probes to control in addition to being used to understand the role of vision per se.

Our goal in this work was to learn about the control of human walking by probing the underlying functions, or subtasks, of walking with visual scene motion perturbations. Continuous visual scene motion has been shown to enact whole body translations of subjects walking on a treadmill (Warren et al. 1996; Logan et al. 2010). To perform the subtask of positional maintenance on the treadmill during these whole body translations to visual scene perturbations, subjects have been shown to have small, but significant, advances or delays in the timing of gait cycle phase (Kiemel et al. 2010). With a limit cycle approximation of the response variables of treadmill walking, there can be deviations away from the

limit cycle or there can be a shortening/ lengthening of the cycle period induced by the perturbation. This shortening/ lengthening of the gait cycle is deemed "phase resetting". Thus, subjects in these experiments "reset" the phase, or shift the timing of the gait cycle, to ensure that the body stays on the treadmill.

Such phase-resetting to a visual perturbation shows how a sensory probe reveals a control strategy for the subtask of positional maintenance on the treadmill. Modeling approaches have supported phase-resetting as a strategy employed for stable adjustments in speed control following perturbations as it has improved convergence back to the locomotive cycle after external force disturbances (Yamasaki et al. 2003; Aoi et al. 2008), improved phase estimation (Nakanishi et al. 2004) and kept center of mass velocity within acceptable ranges during force disturbances, increased trunk mass or changes in walking slope (Aoi et al. 2010).Understanding how the nervous system controls walking where relative position needs to be maintained simultaneously with other subtasks is imperative for understanding situations such as how one maintains position and avoids collisions with others within a crowd while simultaneously navigating his or herself to a desired location.

Here we imposed experimental constraints on the nervous system to gain insight into the control strategy for positional maintenance. Walking was constrained in two ways. First, treadmill walking requires that subjects do not fall off the treadmill so they must maintain the same average speed as the treadmill over the course of the trial. A second constraint used was dictating cadence on the treadmill with a metronome. By limiting the temporal variability in taking a

step (step period), we predicted that: 1) the nervous system would not employ a phase-resetting strategy in response to perturbations; and 2) vision would be less important for the subtask of speed control.

Methods and Materials

Subjects

Twenty healthy subjects [11 males and 9 females, between 20 and 27 yrs of age, 68.2 ± 9.5 kg (mean ±SD)] participated in this study. All subjects were self-reported to have normal (or corrected to normal) vision. The studies conformed to the Declaration of Helsinki, and informed consent was obtained from all participants according to the procedures of the Institutional Review Board at the University of Maryland, College Park.

Apparatus

Virtual reality environment

Subjects walked at 5 km h^{-1} on a treadmill (Cybex Trotter 900T, Cybex International, Inc., USA) surrounded by three screens (width, 3.05 m; height, 2.44 m; Fakespace, USA), one in front of the subject and one on either side. Subjects wore goggles with occluded top shield to prevent them from seeing motion capture cameras mounted above the screen in front of them. Visual displays were rear projected to the screens at a frame rate of 60 Hz by JVC projectors (model DLA-M15U; Victor Company of Japan). CaveLib software (Mechdyne, USA) was used to generate a virtual moving visual scene consisting

of three walls attached at right angles that coincide with the screens when the visual scene is not moving. Each wall consisted of 500 non-overlapping white small triangles (3.4 x 3.4 x 3.0 cm) with random positions and orientations on a black background. To reduce aliasing effects in the fovea region, no triangles were displayed on the front wall within a 30- cm-radius circular region directly in front of the participant's eyes. The display on each screen was varied with time to simulate sagittal plane rotation of the visual scene about the axis through the subject's ankles with a focus of expansion at eye level, with the assumption that the subject was 1 m from the screen. The visual signals were created offline (Matlab, Mathworks, USA) and were generated via Labview (National Instruments, USA) on a desktop computer (Precision T5500, Dell, USA).

Visual scene signals

Visual signals were a filtered white noise signal used to simulate rotating scene motion in the sagittal plane. For each trial of each subject, a different seed was used to generate a white noise signal using a random number generator. Signals had a one-sided spectral density of 600 deg^2/Hz. These signals were then filtered using a first-order Butterworth low-pass filter with a cutoff of .02 Hz and an eighth-order Butterworth low-pass filter of 5 Hz. In doing so, power of scene motion was smoothed and limited to lower frequencies. Across subjects, these driving signals had an average root mean square error (RMSE) of 4.08 deg and 6.89 deg/s. Signals were generated to be 250 s in length with the initial and final 5 s of each signal multiplied by increasing and decreasing ramps,

respectively, to insure that the value of the signal at the beginning and end of the trial would be 0. Only the middle 240 s of each trial was analyzed. A positive/negative signal corresponded to a forward/backward rotation into the screen from position 0. Visual display generation and data collection software were synchronized via an external trigger.

Metronome

Our interest in using a metronome here is for auditory entrainment of the step period to diminish phase resetting. The metronome was broadcast through two satellite speakers (Altec Lansing, USA) via Labview and synched with data collection software. The two satellite speakers were placed two meters behind the treadmill, and had a sound intensity of approximately 75 decibels (verified with sound level meter). A 300 Hz cosine wave was amplitude modulated by a square wave to yield a beats per minute (bpm) metronome signal specific to each subject (see *Procedures*). The average ±S.D. bpm used in this study was 116.6±4.8 bpm.

Kinematics

Body kinematics were measured using a ten camera VICON-MX motion analysis system (VICON, Inc, Oxford, UK). Reflective markers (diameter, 1.4 cm) were placed on the right and left sides of the body at external landmarks corresponding to: base of the 5th metatarsal, posterior calcaneus (heel), lateral malleolus (ankle), lateral femoral condyle (knee), greater trochanter (hip),

anterior superior iliac spine (ASIS), posterior superior iliac spine (PSIS), iliac crest, superior acromion process (shoulder), mastoid process (head) and frontal eminence (head). Additionally, markers were placed at the mediolateral center of the back of the head and the midline of the spine at the level of T1, T7 and L1 vertebrae. All markers were attached at the skin of these bony prominences except those placed on the shoe at the 5th metatarsal and heel. All kinematic data were collected at 120 Hz.

Our analysis focuses on the leg and trunk segments as well as whole-body sagittal plane displacements. Anterior-posterior (A/P, sagittal plane) foot, shank and thigh segment angles relative to the vertical were computed from angles formed by the fifth metatarsal to ankle, ankle to knee, and knee to hip with the most inferior point as the origin. Trunk orientation relative to the vertical in the A/P plane will be computed as the angle formed by the L1 to T1 markers. Whole-body sagittal plane displacement was approximated as the displacement of L1 in the sagittal plane. Trunk orientation relative to the vertical in the A/P plane was computed as the angle formed by the L1 to T1 markers.

Muscle Activity (sEMG)

Muscular activity of the right leg and trunk was measured using surface electromyographic (sEMG) recordings. Recordings of the following sixteen muscles were made: tibialis anterior (TA), gastrocnemius lateralis (LG), gastrocnemius medialis (MG), soleus (Sol), vastus medialis (Vmed), vastus lateralis (Vlat), rectus femoris (RF), sartorius (SART), tensor fascia latae (TFL),

biceps femoris (BF, long head), semitendinosus (ST), gluteus maximus (GM), gluteus medius (Gmed), erector spinae (ESL, recorded at L1-L2), anterior deltoid (ADELT) and posterior deltoid (PDELT). Electrodes were positioned at the muscle belly with placement carefully chosen to minimize cross-talk (Cappellini et al. 2006). Recording sites were shaved, lightly abraded, and cleaned with isopropyl alcohol prior to electrode application. The sEMG data were recorded at 2160 Hz using the wireless TRIGNO system (DELSYS, USA). This recording system has built in bandwidth of 20–450 Hz and gain of 909 V/V. Using Matlab, these signals were high-pass filtered using a zero-lag forward-backward cascade of a 4^{th} order Butterworth filter with a 20-Hz cutoff frequency, full-wave rectified, and then low-pass filtered with a zero-lag forward-backward cascade of a 4^{th} order Butterworth filter with a 10-Hz cutoff frequency.

Procedures

Prior to experimentation, subjects experienced a static visual display at the experimental locomotion speed. An experimenter was always behind the treadmill in close proximity to the subject to ensure safety in case of falling (which never occurred). During this period subjects selected their preferred cadence (in bpm) using a single iteration of a step up-step down staircase procedure with a metronome software application (Mobile Metronome). During the Metronome condition subjects were instructed to walk comfortably and “match their heel strikes with the metronome beat”. After selecting the preferred bpm, the software

application was no longer used as the appropriate bpm was relayed via speakers placed behind the subject (see *Metronome* above).

Subjects began each experimental trial by looking straight ahead at the visual display. Once they were ready, the experimenter initiated treadmill movement for approximately 30 seconds for the subject to reach steady-state. At this point, the subject would declare if he or she was ready for the trial to begin. The experimenter then initiated data acquisition/scene motion/metronome (in Metronome trials) with variable delays to avoid start-up effects. Subjects were reminded prior to each Metronome trial to ""match their heel strikes with the metronome beat" and prior to each No Metronome trial they were instructed to "walk comfortably". Each trial was 250 seconds in duration with a rest of at least 60 seconds between trials. The experimental design consisted of two conditions of Metronome or No Metronome presented in randomized blocks. Visual scene motion occurred in all trials. Subjects were presented with seven trials of the Metronome condition and six trials of the No Metronome trial. A Metronome condition was always the first trial and data from this trial was discarded for all subjects. Some subjects found this first trial with the metronome difficult to perform at the beginning of the trial, but these subjects did not report difficulty in performing the experiment after the beginning of this first Metronome trial.

Data Analysis

Metronome Following

Analog recordings of the metronome sound wave synchronized with kinematic data collection allowed us to determine if a subject was able to follow

the metronome. Heel strike (HS) was determined as successive minima of each heel marker, and error from the metronome beat was measured as deviations of successive heel strikes from onset of successive metronome beats in metronome time (using subject-specific bpm). To be a follower, subjects had to maintain their error from the metronome within ±.5 metronome periods for the majority of the Metronome trials (e.g., 4 of 6).

Phase-dependent impulse response functions

Here we describe the analysis steps used to compute phase-dependent impulse response function (PD-IRFs). A fuller description with equations and expanded motivation can be found in the APPENDIX. The goal of the analysis is to describe the effect of *u*(*t*), visual scene velocity, on *y*(*t*), a kinematic or sEMG response variable. **The majority of results presented in this chapter are calculated in steps 5 and 6 as the full PD-IRF and the phase PD-IRF.** Computing the full PD-IRF consists of six steps:

1. *Approximate phase*. First we compute heel-strike times t_k $(k = 1, \ldots, K)$ for a reference leg. Then we compute $\bar{T}$, the mean of the stride times $t_{k+1} - t_k$ $(k = 1, \ldots, K-1)$, and compute the estimated gait frequency as $f_0 = 1/\bar{T}$. Next we define a discontinuous approximation of phase as $\theta_{\mathrm{d}}(t) = k + f_0(t - t_k)$ for $t_k \leq t < t_{k+1}$. To obtain a continuously-differentiable approximation of phase, $\theta(t)$, we apply a second-order low-pass filter to $\theta_{\mathrm{d}}(t)$:

$$\ddot{\theta}(t) + 2d(\dot{\theta}(t) - f_0) + d^2\theta(t) = d^2\theta_{\mathrm{d}}(t).$$

Note that in the absence of perturbations, approximate phase $\theta(t)$ matches the usual definition of the phase of the gait cycle.

2. *Replace time with approximate phase*. Let *p* be the inverse of *θ*: $p(\theta(t)) = t$ and $\theta(p(\vartheta)) = \vartheta$. Let approximate phase ϑ take the place of time $t = p(\vartheta)$ as the independent variable and compute $\tilde{u}(\vartheta) = u(p(\vartheta))$, $\tilde{y}(\vartheta) = y(p(\vartheta))$, and $\tilde{d}(\vartheta) = \dot{\theta}\big(p(\vartheta)\big)/f_0$. (We use the symbol ϑ to distinguish approximate phase as an independent variable from approximate phase as a function of time.)

3. *Compute output variables for HTF analysis*. For each ϑ, let $y_0(\vartheta)$ be the mean of $\tilde{y}(\vartheta)$. Then compute the deviations $\tilde{y}^{(1)}(\vartheta) = \tilde{y}(\vartheta) - y_0(\vartheta)$ and $\tilde{d}^{(1)}(\vartheta) = \tilde{d}(\vartheta) - 1$.

4. *Compute transient and phase-derivative HTFs.* To account for shifts in phase that affect all response variables, both a transient and phase-derivative HTF are computed. We compute the *transient HTF* from $\tilde{u}(\vartheta)$ to $\tilde{y}^{(1)}(\vartheta)$, denoted $\widetilde{H}_y$, and the *phase-derivative HTF* from $\tilde{u}(\vartheta)$ to $\tilde{d}^{(1)}(\vartheta)$, denoted $\widetilde{H}_d$, as follows. Let $z(\vartheta)$ be either $\tilde{y}^{(1)}(\vartheta)$ or $\tilde{d}^{(1)}(\vartheta)$. Compute the power spectral density (PSD) $p_{\tilde{u}\tilde{u}}(f_1)$ and the double-frequency cross-spectral density (CSD) $p_{\tilde{u}z}(f_1, f_2)$ (Bendat & Piersol 2000). The double-frequency CSD describes the relationship between the input signal $\tilde{u}(\vartheta)$ at input frequency f_1 and the output signal $z(\vartheta)$ at output frequency f_2. The

PSD and CSD are computed using Welch's method with 40-cycle Hanning windows (aligned to start at an integer value of ϑ) and 50% overlap. The *k*-th mode of the HTF H_z from $\tilde{u}(\vartheta)$ to $z(\vartheta)$ is computed as $H_{z,k}(f_1) = p_{\tilde{u}z}(f_1, f_1 + kf_0)/p_{\tilde{u}\tilde{u}}(f_1)$. Note that H_z is a function of both the mode index *k* and the input frequency f_1.

5. *Compute transient and phase IRFs*. For an LTP mapping from $\tilde{u}(\vartheta)$ to $z(\vartheta)$, its HTF H_z can be converted to its phase-dependent IRF h_z using a Fourier series constructed from an inverse Fourier transform of each mode of the HTF. The IRF h_z is a function of response phase ϑ_r and stimulus phase ϑ_s and can be used to represent the LTP mapping from $\tilde{u}(\vartheta)$ to $z(\vartheta)$ as

$$z(\vartheta_\mathrm{r}) = \int_{-\infty}^{\vartheta_\mathrm{r}} h_z(\vartheta_\mathrm{r}, \vartheta_\mathrm{s})\, \tilde{u}(\vartheta_\mathrm{s}) d\vartheta_\mathrm{s}.$$

Using this procedure, compute the *transient PD-IRF* $\tilde{h}_y$ and *phase-derivative IRF* $\tilde{h}_d$ from $\widetilde{H}_y$ and $\widetilde{H}_d$, respectively. Then compute the *phase PD-IRF* by integrating the phase-derivative IRF:

$$h_\theta(\vartheta_\mathrm{r}, \vartheta_\mathrm{s}) = \int_{\vartheta_\mathrm{s}}^{\vartheta_\mathrm{r}} \tilde{h}_d(\tau, \vartheta_\mathrm{s}) d\tau.$$

6. Compute full PD-IRFs. The PD-IRFs $\tilde{h}_y$ and h_θ can be combined to obtain the full PD-IRF from *u*(*t*) to *y*(*t*) that is a function of response time t_r and stimulus time t_s. Here t_r and t_s are expressed in normalized time: time divided by the mean gait period and aligned so that stimulus time t_s equals true stimulus phase.

Steps 1-4 were computed on a trial by trial basis with averages of PSDs and CSDs taken across trials for each condition of each subject for completion of the HTF analysis and steps 5-6 to compute the PD-IRFs. To account for and characterize phase-resetting between the two conditions, the phase PD-IRF calculated in step 5 for each condition is presented in Figure 20. The full PD-IRFs in Figures 18, 19 and 21 are computed in step 6 above and are the sum of the transient PD-IRF computed for each response variable and the phase PD-IRF. In the remaining text, the terms PD-IRF and phase PD-IRF are used for the full PD-IRF and phase PD-IRF defined above.

Statistics

Statistical tests between No Metronome and Metronome conditions of these PD-IRFs of all response variables were performed at each combination of stimulus phase and normalized response time. Permutation tests (1,000, Manly 1997) based on the t-statistic between the two conditions at all combinations of stimulus phase and normalized response time were tested simultaneously and family-wise error rate (FWER) was controlled for each response variable. The tmax method (Blair & Karnisky 1993) was used to adjust the p-value for each combination of stimulus phase and normalized response time with alpha = .05. These tests were performed in Matlab using functions written by Groppe (Groppe et al. 2011). These tests are non-parametric and suited for this study as FWER control is strong compared to other methods (e.g. cluster-based permutation testing, false discovery rate) allowing us to determine where effects are reliable (Groppe et al. 2011) in the PD-IRFS.

Results

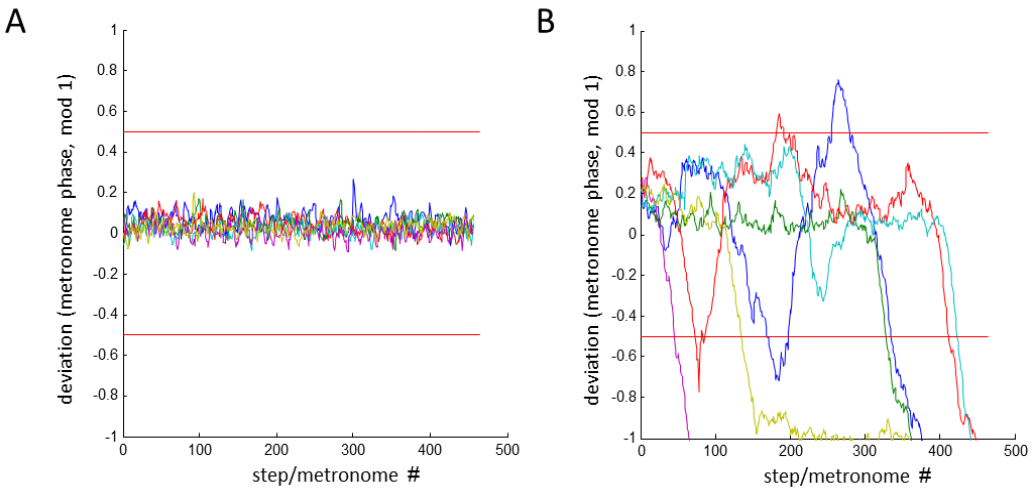

Figure 17. Exemplar deviations in step timing from metronome. A: Separate trials of a single subject that was able to minimize the difference of his or her step timing from the timing of the metronome within one metronome period. B: Separate trials of a single subject that was not able to minimize the difference of his or her step timing from the timing of the metronome within one metronome period. Different color traces represent different trials. 1 or -1 on the y-axis would dictate the subject was either one metronome step period ahead or one metronome step period behind the metronome beat, respectively.

The main focus of this experiment was to investigate if phase-resetting due to visual scene motion was altered by the Metronome condition. A preceding concern, however, was to ensure that subjects were actually following the metronome during the Metronome condition. As can be seen in Figure 17 there was a clear difference in deviations of step timing with respect to metronome phase between subjects: there were those who were able to follow the metronome and those who were not.

Figure 17A shows a single subject whose deviations in step timing were well below the “following” threshold (see *Methods*). His or her mean deviation was observed to be .04 metronome beats after averaging across trials and steps.

Figure 17B shows a subject who crosses the threshold of non-following multiple times on multiple Metronome trials. This subject was considered a non-follower and had a mean deviation of -.95 metronome beats across trials and steps.

The majority (>3/6) of trials in 13 of the 20 subjects followed the metronome in a similar manner to that observed in Figure 17A. The remaining 7 subjects had a mean overall deviation of -.76 and did not remain within the following margin of 1 beat period throughout the majority of trials. The overall mean deviation in step period of the13 subjects who always remained within the following margin of 1 beat period was .04 across subjects. As these 13 subjects were able to follow the metronome during the Metronome condition, we focus on their data in the remaining analysis.

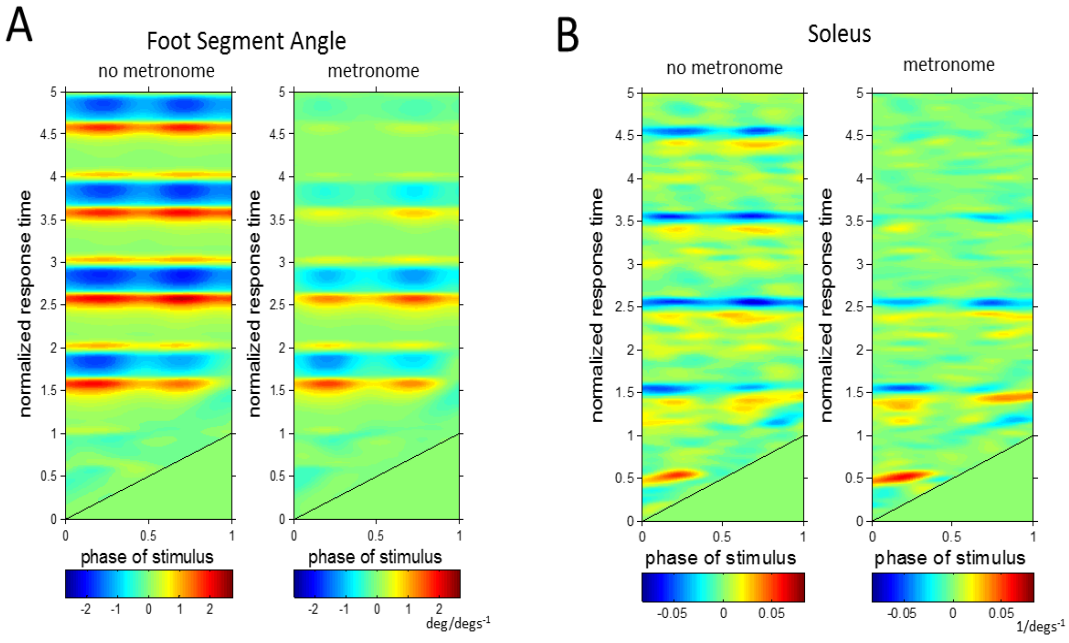

Figure 18. Foot segment and soleus PD-IRFs. PD-IRFs from visual scene velocity to foot segment angle (A) and rectified soleus sEMG (B). Maximum values in the contour plot of both plots were dictated by maximum value found across both conditions for each response variable.

As observed in Figure 18, differences in the PD-IRFs between conditions is suggested in several response variables. In the No Metronome condition, rectified soleus sEMG and foot angle show clear bands in the PD-IRFS at normalized response times specific to each response variable that demonstrate kinematic and muscular features of phase resetting. These horizontal bands observed late in the 3rd cycle of normalized response time are markedly diminished in the No Metronome condition.

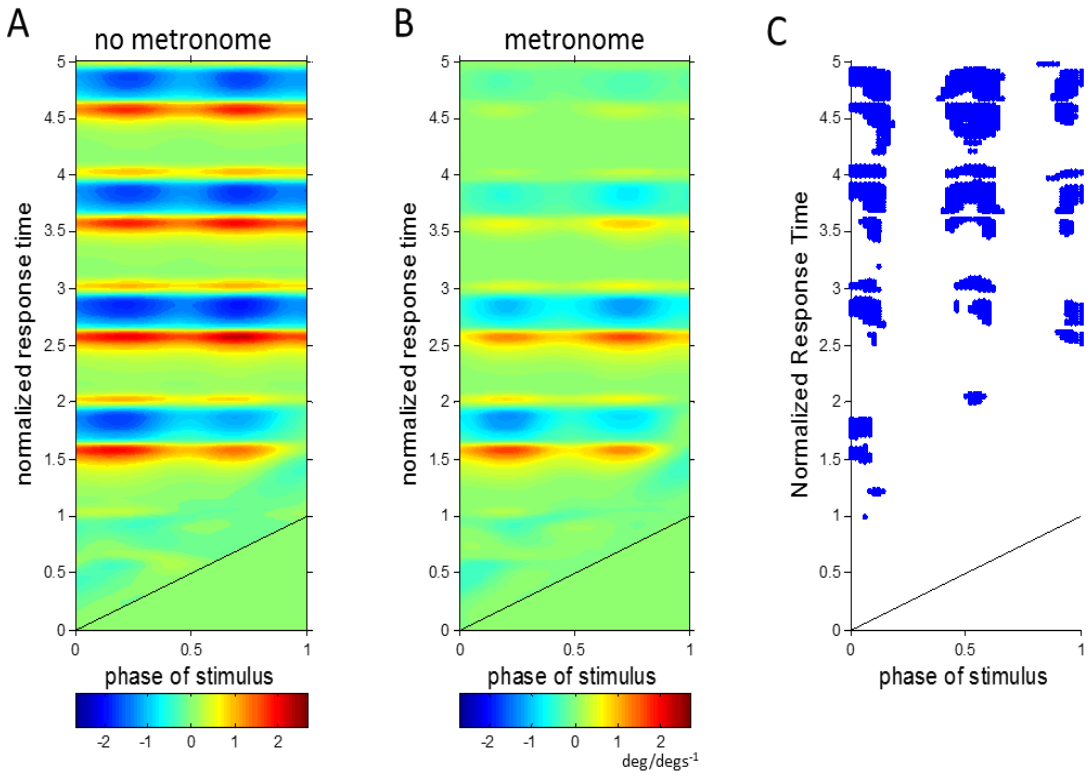

Figure 19. Foot segment PD-IRFs. PD-IRFs from visual scene velocity to foot segment angle in Metronome (A) and No Metronome (B) conditions. Maximum values in the contour plot of both plots were dictated by maximum value found across both conditions. Asterisks plotted in C correspond to a significant difference between A and B at the same plotted combination of stimulus phase and normalized response time.

Statistical tests of these PD-IRFs reveal, however, that only lower limb kinematics and phase PD-IRFs are different between the two conditions, as

observed in Figure 19C for the foot segment angle. Asterisks denote the phase locations, or specific combination of stimulus phase and normalized response time, of significant differences between the two conditions in the foot segment angle. As seen in Figure 19C, significant differences between conditions are observed in stimulus phases centered around heel strikes (e.g. 0-12%, 44-62% and 94-100% at normalized response time of 3.92) and at normalized response times occurring during pre-swing (50-60%) and the entire swing phase. Similar patterns of significant differences were observed for shank and thigh segment angles.

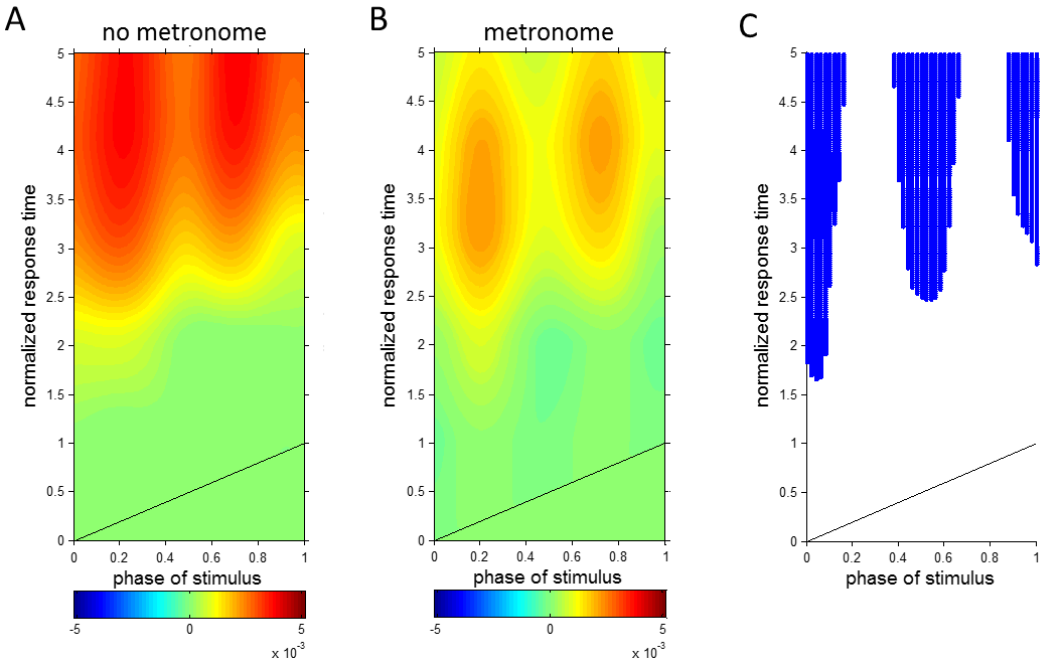

Figure 20. Phase PD-IRFs. Phase PD-IRFs from visual scene velocity to estimated phase in Metronome (A) and No Metronome (B) conditions. Maximum values in the contour plot of both plots were dictated by maximum value found across both conditions. Asterisks plotted in C correspond to a significant difference between A and B at the same plotted combination of stimulus phase and normalized response time.

Phase PD-IRFs of visual scene motion shown in Figure 20 show how the actual measured change in phase due to change in visual scene motion is eliminated in the Metronome condition. Figure 20A shows a persistent phase advance at all stimulus phases Asterisks at specific locations in Figure 20C demonstrate that the phase shift due to the visual scene motion is eliminated in the Metronome condition at several stimulus phases.

To observe how this elimination in phase-resetting affects positional maintenance on the treadmill, anterior-posterior (A-P) motion of L1 as an indicator of whole-body motion on the treadmill is shown in Figure 21. Contour plots in both conditions show a red intensity at all stimulus phases, with maximum responses observed at similar combinations of stimulus phase and normalized response time; 1.52 cm/cms^{-1} for No Metronome condition at stimulus phase .74 and response time 3.02 and 1.53 cm/cms^{-1} for Metronome condition at stimulus phase .78 and response time 3.02. These plots indicate motion of the body in the same direction as the visual scene motion that is equally persistent across the two conditions. Interestingly, Figure 21C shows that there are no phase locations showing a difference between conditions even though there is a clear suppression in persistent phase resetting observed in Figure 20.

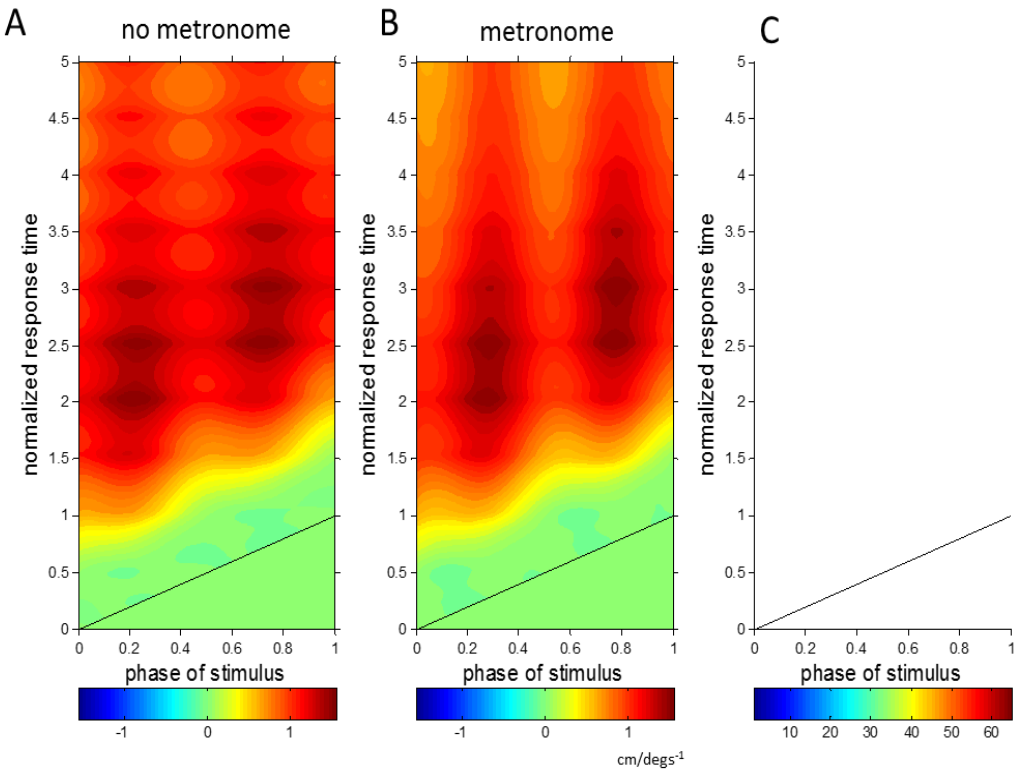

Figure 21. A-P L1 displacement PD-IRFs. PD-IRFs from visual scene velocity to Anterior Posterior Displacement of L1 in Metronome (A) and No Metronome (B) conditions. Maximum values in the contour plot of both plots were dictated by maximum value found across both conditions. Asterisks plotted in C correspond to a significant difference between A and B at the same plotted combination of stimulus phase and normalized response time.

To investigate the relationship between phase-resetting and positional maintenance further, Figure 22 plots the phase PD-IRF and PD-IRF of L1 A-P motion at the 14% stimulus phase. Figure 22A shows a phase advance due to visual scene motion occurring in both Metronome and No Metronome conditions beginning in the first cycle after the stimulus. Yet, the phase advance in the Metronome condition does not persist. The phase PD-IRF response abruptly drops off in the Metronome condition while it plateaus in the No Metronome condition. Comparison tests ($p<.05$) reveal differences between conditions beginning 3.66 cycles from stimulus onset. In contrast, Figure 22B shows that the

indicator of whole-body translation on the treadmill (A-P L1 displacement) is not different between the Metronome and No Metronome condition.

In sum, a phase advance due to visual scene motion was initiated within the first cycle in both conditions, and plateaued at approximately 3-4 gait cycles from perturbation onset. This phase advance was suppressed in the Metronome condition beginning late in the 3rd gait cycle denoted by the diminishing of persistent phase-resetting. Responses of A-P L1 displacement were not changed between the two conditions, however, indicating similar positional maintenance even though phase-resetting properties were clearly different.

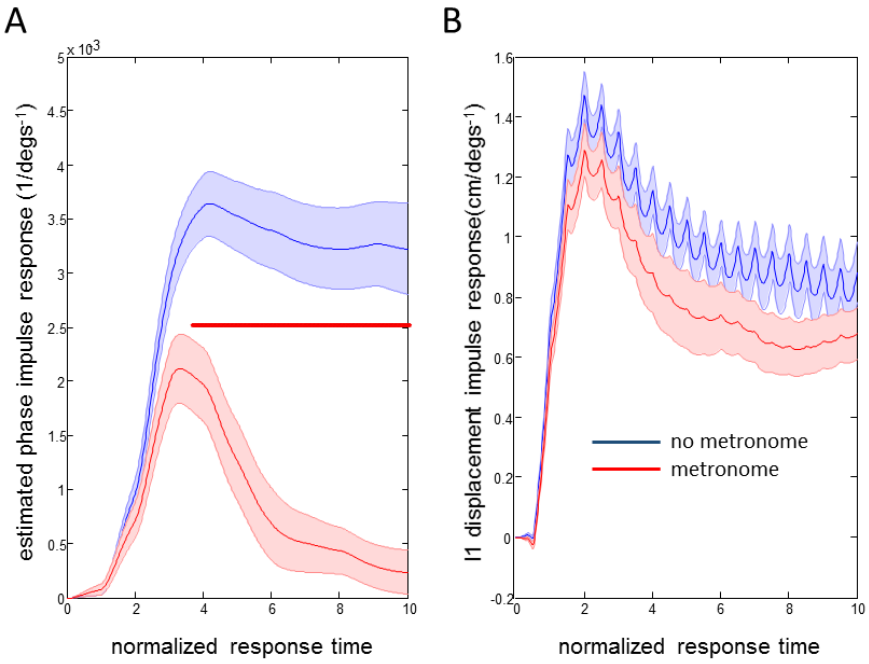

Figure 22. Impulse response functions of estimated phase and L1 displacement. Impulse response functions of estimated phase (A) and L1 displacement (B) at the 14% stimulus phase in both No Metronome and Metronome conditions. Error bar is ± s.e.m. Asterisks denote normalized response times where a difference was observed between Metronome and No Metronome condition ($p<.05$, see *Methods*).

Discussion

In this study we used constraints on the locomotive behavior of walking coupled with perturbations of virtual scene motion to investigate how the subtask of positional maintenance is controlled on the treadmill. As hypothesized, use of a metronome to dictate cadence diminished subjects' use of phase-resetting to maintain position on the treadmill. Interestingly, both change in position due to visual scene motion and phase-resetting due to visual scene motion were not initially different between conditions. As time progressed from the perturbation, the phase advance due to visual scene motion differed between the two conditions while the shift in the body's position did not. In sum, maintaining position on the treadmill was linked to phase resetting on a short time scale while being unlinked on a longer time scale.

Two time scales for control

The separation of phase-resetting and positional maintenance reveals two timescales of control for human locomotion: 1) a fast control initiated in the first cycle after the perturbation cycle that serves the subtask of speed control (i.e., positional maintenance on the treadmill) and 2) a slow control initiated several cycles after a perturbation to suppress phase shifts when maintaining a fixed cadence.

Visual scene motion initiates changes in positional maintenance and phase-resetting on a similar time scale. As seen in Figure 21, the initiation of changes in whole body positioning on the treadmill is approximately parallel with the line that signifies onset of visual scene perturbations, with a delay of

approximately one cycle. Phase-resetting is enacted in the same post-perturbation cycle as a strategy for correcting the changes in position of the body brought on by changes in visual scene motion. This can be visualized in the horizontal bands of PD-IRFs presented in Figures 18 and 19 as visual scene motion alters kinematic trajectories and sEMG in a similar manner during the first full cycle (1-2 in normalized response time) after the visual perturbation. Furthermore, changes in the phase PD-IRF shown in Figure 22 show how a phase advance is clearly initiated during this time frame.

We hypothesized that the use of a metronome would significantly diminish or remove phase-resetting initiated by visual scene motion. Unexpectedly, as seen in Figure 22a, phase-resetting still occurred during the Metronome condition, and did not appreciably diminish until late in the third full cycle after the cycle in which the visual perturbation occurred. The nervous system does not continue to coordinate this change in phase-resetting with whole body motion, indicating a different control scheme on a different time scale several cycles removed from the perturbation.

Making use of a treadmill to constrain subjects' speed has been used previously to investigate walking control, and has provided insight into timescales of control. Dingwell and colleagues (2010) have found that subjects sub-optimally overcorrect deviations in position on the treadmill to maintain stride speed (SS) through stride to stride alterations in a combination of stride length (SL) and stride period (SP) forming a goal equivalent manifold (GEM). Using detrended fluctuation analysis (DFA), goal relevant deviations away from the GEM were

found to be corrected quickly (anti-persistent) on a stride to stride basis while goal equivalent deviations along the GEM were found to persist for several strides (Dingwell et al. 2010).

Terrier and Deriaz (2012) found that adding a metronome to treadmill walking made all gait parameters (SS,SL,SP) anti-persistent. These authors argue that cross-regulation of SL and SP occurred which led to an absence of redundancy among the gait parameters. In accordance with Dingwell and colleague's (2010) proposal of the GEM for SS, dictating both SP with metronome and SS with treadmill will indirectly cause control of SL for subjects to accomplish the goal of staying on the treadmill (Terrier & Deriaz 2012). In a related study, Terrier (2012) found that the Metronome condition yielded a low non-stationarity Index (NSI) of SS,SP and SL, which confirmed low consistency in local averages. Terrier concluded that the locally consistent means (low NSI) and statistical anti-persistence observed previously result from a "lost" degree of freedom; there is no longer redundancy between step length and step period for flexible control (Terrier 2012).

Echoing Dingwell, Terrier (2012) proposed that gait control has two modes: a long-range, fractal-like mode for a "steady gait" across many strides and a more conscious, tightly controlled mode indicated by anti-persistent patterns in short-range stride to stride corrections (Terrier 2012). To further support this claim, a follow-up experiment showed that adding a metronome to treadmill walking enhanced long term (4-10 strides from perturbation, as in Dingwell & Cusamano 2000) local dynamic stability (LDS) of the center of

pressure while having comparatively smaller effects on short term (up to one step) LDS (Terrier & Deriaz 2013).

In our study visual input shifted both the body's position and gait cycle phase on a short time scale while use of metronome interfered with the effect of vision on gait cycle phase on a longer time scale. Visual scene motion was used as a probe here, and its shifting of cycle phase was not immediately inhibited by the metronome condition. In common with the work of Terrier and Deriaz (2013), the metronome condition in our study had an effect on control in the long term and not in the short term. The secondary task of walking to a fixed cadence was given a lower priority by the nervous system, and not allowed to interfere with the primary task of positional maintenance for several cycles. In line with the ideas of Dingwell and colleagues (2010), we can speculate that the nervous system allowed deviations due to the metronome task as long as it assisted with the primary positional maintenance task, and later allowing correction for control. This is informative for how multiple functions are performed during walking; suggesting that the alterations due to less important, secondary tasks (e.g. imposed marching) which interfere with primary subtasks of walking will be executed on longer time scales.

Clinical implications and future directions

Our use of a perturbation to walking in conjunction with auditory metronome could inform the growing use of a metronome as a rhythmic auditory cue (RAC) to improve walking function in neurodegenerative disease and recovery from major neural insult. Interventions making use of rhythmic auditory

cues have been found to be effective in improving walking speed in Parkinson's disease (Thaut et al. 1996; Lim et al. 2005) and Huntington's disease (Thaut et al. 1999). Use of RAC in stroke survivors has shown RAC to increase gait symmetry (Roerdink et al. 2007), velocity and stride length (Thaut et al. 1997). These rehabilitation approaches using RAC could potentially be improved by taking into account the notion that walking control is occurring on two time scales. The two time scales could be exploited in simple ways such as instructing patients to actively monitor their velocity stride to stride while keeping cadence with a metronome that will inform them of the timing of every fourth stride. Doing so could improve clinical measures (symmetry, speed) of the overall behavior that encompasses the two tasks which individually tap into the two timescales for control.

An additional potential direction of this work in neuro-rehabilitation could be to alter gait cycle phase where subjects should synchronize with the RAC, and determine beneficial phases for improving specific ailments such as foot drop. Recent work using mechanical perturbations at the ankle entrained gait cycle period and found that subjects phase locked at the end of terminal stance/beginning of pre-swing where the perturbation could be leveraged for enhanced propulsion into swing (Ahn & Hogan 2012). Tapping into phases that could elicit functional improvements in conjunction with consideration of time scales for control could lead to therapies which positively affect both the features of a function and the timescale of its initiation. In all, manipulating subtasks and

timing requirements with respect to the gait cycle have potential for improving the beneficial outcomes of RAC in rehabilitation.

Chapter 6: The interaction of upright posture and positional maintenance during human locomotion

Introduction

Treadmill walking is often used to investigate locomotive control. It provides the opportunity for controlled experiments with a fixed speed and several consecutive strides conducive to various types of recording and stimulating equipment. Treadmill walking is also very useful to those interested in the neural control of locomotion as it constrains locomotive behavior so that subjects, at minimum, have to fulfill two requirements for successful walking behavior. First, treadmill walking dictates that subjects must not fall off of the treadmill so they must, on average, maintain the same average speed as the treadmill. Second, as in any walking task unaided by weight support, subjects must maintain orientation relative to vertical and not allow the proportionally massive trunk to topple over the legs.

How the nervous system performs these two subtasks which underlie the overarching task of walking simultaneously is the focus of this study. As the response variables which indicate whole body positional changes in the anterior posterior (A-P) plane for speed control and trunk orientation are physically linked, there is certainly the possibility that these two subtasks interact. For example, if one accelerates forward on treadmill to correct his/her position, then the trunk may lean forward.

In this study we use visual and mechanical perturbations simultaneously as probes to investigate the interactions of these two subtasks. Both visual and

mechanical perturbations have been used successfully to learn about how subtasks are enacted during walking. Changes in virtual visual scene motion were used here, and have been previously used to alter speed (Konczak, 1994), trunk orientation to vertical (Logan et al. 2010), stride length (Prokop et al. 1997), translation of the body on the treadmill (Warren et al.1996; Logan et al. 2010), and the speed of the walk-run transition (Mohler et al. 2007) and its kinematic and energetic features (Guerin and Bardy, 2008). In one such study, visual scene motion was used in standing posture and walking conditions to show that visual scene motion perturbations affected trunk orientation similarly between the two behaviors while trunk translation responses were much larger during walking, reflecting the simultaneous use of vision for orientation upright and positional maintenance on the treadmill (Logan et al. 2010).

Mechanical perturbations during walking have also been used to investigate many subtasks of walking. An early investigation by Nashner made use of support surface perturbations to show that stabilizing muscle activations during walking mimicked those occurring during standing posture (Nashner 1980), reflecting postural control within locomotion. Further investigation into postural control during walking revealed that subjects will first stabilize posture prior to performing an additional, planned lever pulling task (Nashner & Forsberg 1986). Mechanical perturbations have also been used to study the subtask of obstacle avoidance/ accommodation during walking, and have revealed an elevating or lowering strategy depending on phase of the gait cycle (Eng et al. 1994) or mixture of the two (Forner-Cordero et al. 2003). More recently, Ahn and

Hogan used torque perturbations at the ankle and found that the gait period will entrain to the perturbation when advantageous for propulsion, supporting a neuro-mechanical oscillator for propulsion control (Ahn & Hogan, 2012). The authors suggested that these findings support a separation in control of low level propulsion and higher level "episodic supervisory control of a semi-autonomous periphery" when needed for cases such as irregular footholds or obstacle avoidance, suggesting a control scheme enacted in a subtask-dependent manner. In all, mechanical perturbations are clearly useful for providing insight into how the nervous system controls the subtasks of walking.

A concern in use of visual and mechanical perturbations during walking is that effects of perturbations may vary throughout the phases of the gait cycle. This concern is supported in studies which have shown gait-cycle phase-dependent responses to imposed mechanical perturbations (Nashner 1980; Nashner & Forsberg 1986; Eng et al. 1994; Forner-Cordero et al. 2003) and changes in visual scene motion (Logan et al. 2014). To satisfy this concern, we use small independent, broad-band stimuli to characterize the mapping between perturbation (input) to response variables such as trunk orientation (output) using phase-dependent impulse response functions (PD-IRFs). Doing so allows unique mappings between each perturbation and response variables at each phase of the gait cycle in which the stimulus has occurred.

Independent mechanical and visual perturbations were used here to investigate the interaction of trunk orientation and positional maintenance throughout the gait cycle. A mechanical perturbation was designed to create a

distributed pulling at the upper trunk which would elicit active (neural-driven) responses that correct movements of the body imposed by the perturbation. Being a sensory perturbation, both motions of the body imposed by the visual perturbation and corrective responses, if required, are neural-driven. Although these perturbations have different routes to active responses, both eliciting the same strategy for simultaneous subtask control would be very strong evidence for that strategy being used by the nervous system for walking. Supported by the finding that postural corrections are initiated prior to performance of an additional, mechanically destabilizing task (Nashner & Forsberg 1986) and a more recent study (Logan et al. 2014) showing that corrections of trunk orientation are initiated prior to positional maintenance corrections, we hypothesized that both perturbations would elicit a control strategy that prioritized control of trunk orientation for staying upright over positional maintenance for staying on the treadmill in terms of time.

Methods and Materials

Subjects

Twenty healthy subjects [8 males and 12 females, between 19 and 30 yrs of age, 67.9 ± 12.9 kg (mean ±SD)] participated in this study. All subjects were self-reported to have normal (or corrected to normal) vision. The studies conformed to the Declaration of Helsinki, and informed consent was obtained from all participants according to the procedures of the Institutional Review Board at the University of Maryland, College Park.

Apparatus

Virtual reality environment

Subjects walked at 5 km h^{-1} on a treadmill (Cybex Trotter 900T, Cybex International, Inc., USA) surrounded by three screens (width, 3.05 m; height, 2.44 m; Fakespace, USA), one in front of the subject and one on either side. Subjects wore goggles with occluded top shield to prevent them from seeing motion capture cameras mounted above the screen in front of them. Visual displays were rear projected to the screens at a frame rate of 60 Hz by JVC projectors (model DLA-M15U; Victor Company of Japan). CaveLib software (Mechdyne, USA) was used to generate a virtual moving visual scene consisting of three walls attached at right angles that coincide with the screens when the visual scene is not moving. Each wall consisted of 500 non-overlapping white small triangles (3.4 x 3.4 x 3.0 cm) with random positions and orientations on a black background. To reduce aliasing effects in the fovea region, no triangles were displayed on the front wall within a 30- cm-radius circular region directly in front of the participant's eyes. The display on each screen was varied with time to simulate rotation of the visual scene about the axis through the subject's ankle, assuming a fixed perspective point at the average position of the participant's eyes. The signals specifying scene rotation were created offline (Matlab, Mathworks, USA) and were generated via Labview (National Instruments, USA) on a desktop computer (Precision T5500, Dell, USA).

Mechanical Perturbation

As seen in Figure 23, a weak continuous mechanical perturbation was applied to the subject from behind as a spring with one end attached to a modified trunk harness worn by the subject and the other end attached to a linear motor (LX80L; Parker Hannifin Corporation). The actual displacement of the motor in the anterior posterior (A-P) direction was used as the mechanical perturbation signal. The spring had a spring constant of 0.0175 N/mm and was attached in series with a 45.7 cm rigid plastic cable fixed to the back of the harness. The harness was adjusted for each subject so that the point of attachment was at mid-scapula height centered on the midline of the upper trunk.

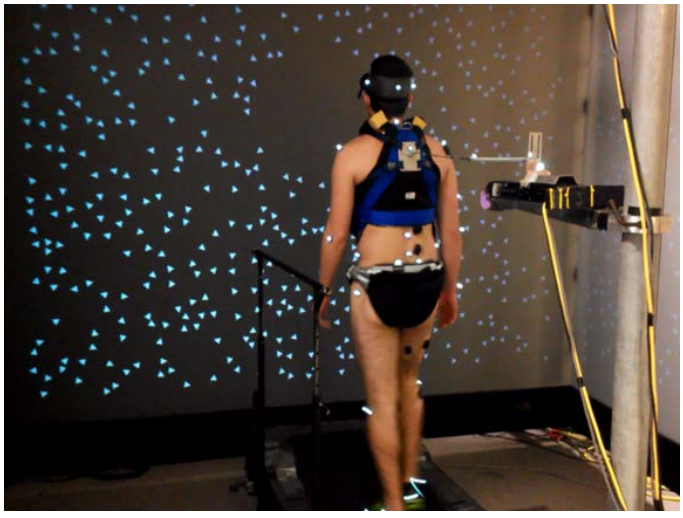

Figure 23. Experimental setup. Subjects walked on a treadmill located within a three panel virtual "cave" providing rotating visual scene motion in the sagittal plane. Subjects were also attached to a motor through a spring and rigid cable in series.

Perturbation Signals

Both visual and motor signals were filtered white noise signals. For each trial of each subject and each perturbation type, a different seed was used to generate a white noise signal using a random number generator. The initial and final 5 s of each 250 s signal were multiplied by increasing and decreasing ramps, respectively, to insure that the value of the signal at the beginning and end of the trial would be 0. Only the middle 240 s of each trial was analyzed. Visual signals had a one-sided spectral density of 150 deg^2/Hz. These signals were then filtered using a first-order Butterworth low-pass filter with a cutoff of .02 Hz and a second-order Butterworth low-pass filter of 5 Hz. Across subjects, these driving signals had an average root mean square error (RMSE) of 2.13 deg and 3.62 deg/s. A positive/negative signal corresponded to a forward rotation into the screen/backward rotation towards the subject. The virtual scene was constructed so that the focus of expansion was at the subject's eye height, with the assumption that the subject was 1 m from the screen. Motor signals had a one-sided spectral density of 1.1 cm^2/Hz. These signals were filtered using an eighth-order Butterworth low-pass filter with a cutoff frequency of 4 Hz. Across subjects, these driving signals had an average root mean square error (RMSE) of 1.30 cm and 19.40 cm/s. These parameters were used for the motor signal as a balance between ensuring a flat power spectrum up to highest frequency possible and staying within travelling distance and velocity limits of the motor. A pilot study (n=5) showed that using the first smoothing filter (as in vision) to limit power at relatively high frequencies would diminish ability to observe responses,

supporting the nonuse of this smoothing filter for the motor perturbation. Visual display generation, motor motion and data collection software were synchronized via an external trigger.

Kinematics

Body kinematics were measured using a ten camera VICON-MX motion analysis system (VICON, Inc, Oxford, UK). Reflective markers (diameter, 1.4 cm) were placed on the right and left sides of the body at external landmarks corresponding to: base of the 5th metatarsal, posterior calcaneus (heel), lateral malleolus (ankle), lateral femoral condyle (knee), greater trochanter (hip), anterior superior iliac spine (ASIS), posterior superior iliac spine (PSIS), iliac crest, superior acromion process (shoulder), mastoid process (head) and frontal eminence (head). Additionally, markers were placed at the medio-lateral center of the back of the head and the midline of the spine at the level of C6, T10 and L1 vertebrae. All markers were attached at the skin of these bony prominences except those placed on the shoe at the 5^{th} metatarsal and heel. All kinematic data were collected at 120 Hz.

Our analysis focuses on the trunk segment in the sagittal plane as well as whole-body displacements in the A-P direction. Trunk orientation relative to the vertical in the sagittal plane was computed as the angle formed by the L1 to T1 markers. Whole-body displacement in the A-P direction was measured as the displacement of L1 in the A-P direction.

Muscle Activity (sEMG)

Muscular activity of the right leg and trunk was measured using surface electromyographic (sEMG) recordings. Recordings of the following sixteen muscles were made: tibialis anterior (TA), gastrocnemius lateralis (LG), gastrocnemius medialis (MG), soleus (Sol), vastus medialis (Vmed), vastus lateralis (Vlat), rectus femoris (RF), tensor fascia latae (TFL), biceps femoris (BF, long head), semitendinosus (ST), gluteus maximus (GM), gluteus medius (Gmed), rectus abdominus (RA), lumbar erector spinae (ESL, recorded at L1-L2), thoracic erector spinae (EST, recorded at T9) and posterior deltoid (PDELT). Electrodes were positioned at the muscle belly with placement carefully chosen to minimize cross-talk (Cappellini et al. 2006). Recording sites were shaved, lightly abraded, and cleaned with isopropyl alcohol prior to electrode application. The sEMG data were recorded at 2160 Hz using the wireless TRIGNO system (DELSYS, USA). This recording system has built in bandwidth of 20–450 Hz and gain of 909 V/V. Using Matlab, these signals were high-pass filtered using a zero-lag forward-backward cascade of a 4^{th} order Butterworth filter with a 20-Hz cutoff frequency, full-wave rectified, and then low-pass filtered with a zero-lag forward-backward cascade of a 4^{th} order Butterworth filter with a 10-Hz cutoff frequency. Although consistent sEMG responses were observed in many muscles to the visual perturbation, we focus on erector spinae muscles (EST and ESL) in the results presented below as consistent responses were observed solely in these muscles for both perturbations

Procedures

Prior to experimentation, subjects experienced a static visual display at the experimental locomotion speed. An experimenter was always behind the treadmill in close proximity to the subject to ensure safety in case of falling (never occurred). Subjects began each experimental trial by looking straight ahead at the static visual display at the experimental treadmill speed (5 km/h) for approximately 30 seconds to reach steady-state treadmill walking. At this point, the subject would declare if he or she was ready for the trial to begin. The experimenter then initiated data acquisition, scene motion and the motor simultaneously with variable delays on each trial to avoid start-up effects. Each trial was 250 seconds in duration with a rest of at least 60 seconds between trials. The initial and final 5 s of each 250 s signal were multiplied by increasing and decreasing ramps, respectively, to insure that the value of the signal at the beginning and end of the trial would be 0. Only the middle 240 s of each trial was analyzed. The experimental design consisted of 10 trials of visual scene and motor motion. Upon inspection of a kinematic marker on the spring attached to the motor there were instances where the spring obviously went slack during the trial. This resulted in 13 of the 200 trials recorded across subjects to be shortened.

Data Analysis

Phase-dependent impulse response functions

Here we describe the analysis steps used to compute phase-dependent impulse response function (PD-IRFs). A fuller description with equations and

expanded motivation can be found in the APPENDIX. The goal of the analysis is to describe the effect of *u*(*t*), a visual scene velocity or motor position perturbation, on *y*(*t*), a kinematic or sEMG response variable. **The majority of results presented in this chapter are full PD-IRFs, and are calculated in step 6.** Computing the full PD-IRF consists of six steps:

1. ***Approximate phase*.** First we compute heel-strike times t_k $(k = 1, \ldots, K)$ for a reference leg. Then we compute $\bar{T}$, the mean of the stride times $t_{k+1} - t_k$ $(k = 1, \ldots, K-1)$, and compute the estimated gait frequency as $f_0 = 1/\bar{T}$. Next we define a discontinuous approximation of phase as $\theta_{\mathrm{d}}(t) = k + f_0(t - t_k)$ for $t_k \leq t < t_{k+1}$. To obtain a continuously-differentiable approximation of phase, $\theta(t)$, we apply a second-order low-pass filter to $\theta_{\mathrm{d}}(t)$:

$$\ddot{\theta}(t) + 2d(\dot{\theta}(t) - f_0) + d^2\theta(t) = d^2\theta_{\mathrm{d}}(t).$$

Note that in the absence of perturbations, approximate phase $\theta(t)$ matches the usual definition of the phase of the gait cycle.

2. ***Replace time with approximate phase*.** Let *p* be the inverse of θ : $p(\theta(t)) = t$ and $\theta(p(\vartheta)) = \vartheta$. Let approximate phase ϑ take the place of time $t = p(\vartheta)$ as the independent variable and compute $\tilde{u}(\vartheta) = u(p(\vartheta))$, $\tilde{y}(\vartheta) = y(p(\vartheta))$, and $\tilde{d}(\vartheta) = \dot{\theta}\big(p(\vartheta)\big)/f_0$. (We use the symbol ϑ to distinguish approximate phase as an independent variable from approximate phase as a function of time.)

3. *Compute output variables for HTF analysis*. For each ϑ, let $y_0(\vartheta)$ be the mean of $\tilde{y}(\vartheta)$. Then compute the deviations $\tilde{y}^{(1)}(\vartheta) = \tilde{y}(\vartheta) - y_0(\vartheta)$ and $\tilde{d}^{(1)}(\vartheta) = \tilde{d}(\vartheta) - 1$.

4. *Compute transient and phase-derivative HTFs.* To account for shifts in phase that affect all response variables, both a transient and phase-derivative HTF are computed. We compute the *transient HTF* from $\tilde{u}(\vartheta)$ to $\tilde{y}^{(1)}(\vartheta)$, denoted $\widetilde{H}_y$, and the *phase-derivative HTF* from $\tilde{u}(\vartheta)$ to $\tilde{d}^{(1)}(\vartheta)$, denoted $\widetilde{H}_d$, as follows. Let $z(\vartheta)$ be either $\tilde{y}^{(1)}(\vartheta)$ or $\tilde{d}^{(1)}(\vartheta)$. Compute the power spectral density (PSD) $p_{\tilde{u}\tilde{u}}(f_1)$ and the double-frequency cross-spectral density (CSD) $p_{\tilde{u}z}(f_1, f_2)$ (Bendat & Piersol 2000). The double-frequency CSD describes the relationship between the input signal $\tilde{u}(\vartheta)$ at input frequency f_1 and the output signal $z(\vartheta)$ at output frequency f_2. The PSD and CSD are computed using Welch's method with 40-cycle Hanning windows (aligned to start at an integer value of ϑ) and 50% overlap. The *k*-th mode of the HTF H_z from $\tilde{u}(\vartheta)$ to $z(\vartheta)$ is computed as $H_{z,k}(f_1) = p_{\tilde{u}z}(f_1, f_1 + kf_0)/p_{\tilde{u}\tilde{u}}(f_1)$. Note that H_z is a function of both the mode index *k* and the input frequency f_1.

5. *Compute transient and phase IRFs*. For an LTP mapping from $\tilde{u}(\vartheta)$ to $z(\vartheta)$, its HTF H_z can be converted to its phase-dependent IRF h_z using a Fourier series constructed from an inverse Fourier transform of each mode of the HTF. The IRF h_z is a function of response phase ϑ_r and

stimulus phase ϑ_s and can be used to represent the LTP mapping from $\tilde{u}(\vartheta)$ to $z(\vartheta)$ as

$$z(\vartheta_r) = \int_{-\infty}^{\vartheta_r} h_z(\vartheta_r, \vartheta_s)\, \tilde{u}(\vartheta_s) d\vartheta_s.$$

Using this procedure, compute the *transient IRF* $\tilde{h}_y$ and *phase-derivative IRF* $\tilde{h}_d$ from $\tilde{H}_y$ and $\tilde{H}_d$, respectively. Then compute the *phase IRF* by integrating the phase-derivative IRF:

$$h_\theta(\vartheta_r, \vartheta_s) = \int_{\vartheta_s}^{\vartheta_r} \tilde{h}_d(\tau, \vartheta_s) d\tau.$$

6. Compute IRFs. The IRFs $\tilde{h}_y$ and h_θ can be combined to obtain the IRF from *u*(*t*) to *y*(*t*) that is a function of response time t_r and stimulus time t_s. Here t_r and t_s are expressed in normalized time: time divided by the mean gait period and aligned so that stimulus time t_s equals true stimulus phase.

Steps 1-4 were computed on a trial by trial basis with averages of PSDs and CSDs taken across trials for each subject for completion of the HTF analysis and to compute the full PD-IRFs in step 6. Full PD-IRFs are shown in Figures 24 and 25, with vertical slices in Figures 26 and 27 showing the impulse response function at specific stimulus phases. Full PD-IRFs defined above are now termed PD-IRFs in the following text.

The PD-IRF for mechanical perturbations is a response to an impulse in motor position while the PD-IRF for visual perturbations is a response to an impulse in visual scene velocity, which is equivalent to the response to a step in

visual-scene position. A positive impulse response referred to as a positive response here indicates that the response variable's response is in the same direction as the perturbation and a negative impulse response referred to as a negative response here indicates that the response variable's response is in the same direction as the perturbation

Statistics

Statistical tests of the PD-IRFs of all response variables were performed at each stimulus phase. For illustration, confidence intervals computed based upon the sample mean using the Matlab function "normfit" are plotted in Figures 26 and 27. Permutation tests (1,000, Manly 1997) based on the t-statistic (null hypothesis mean=0) at all normalized response times up to five cycles post stimulus onset were tested simultaneously and family-wise error rate (FWER) was controlled at each stimulus phase for each response variable. EMGs had a more transient response nature and were tested up to two cycles post stimulus onset. The tmax method (Blair & Karnisky 1993) was used to adjust the p-value for each value at values of normalized response time within each stimulus phase (alpha = .05). These tests were performed in functions written by Groppe (Groppe et al. 2011). These tests are non-parametric and suited for this study as FWER control is strong compared to other methods (e.g. cluster-based permutation testing, false discovery rate) allowing determination of reliable effects in the PD-IRFS (Groppe et al. 2011).

Results

Phase-dependent impulse response functions (PD-IRFs) presented in Figure 24 show the stimulus phase by normalized response time mapping of both mechanical and visual perturbations to trunk orientation. A positive impulse response referred to as a positive response here indicates that the response variable's response is in the same direction as the perturbation and a negative impulse response referred to as a negative response here indicates that the response variable's response is in the same direction as the perturbation. For both perturbations, initial trunk orientation responses were observed in the same direction of the perturbation at all stimulus phases, as indicated by the diagonal red band observed in both Figure 24A and 24B which notes positive responses across phases. Put simply, the trunk deviates forward from vertical as rotating scene motion speeds up or the motor moves forward. This positive response is also due to the trunk orientation deviating backward from vertical as scene motion slows down or the motor moves backwards.

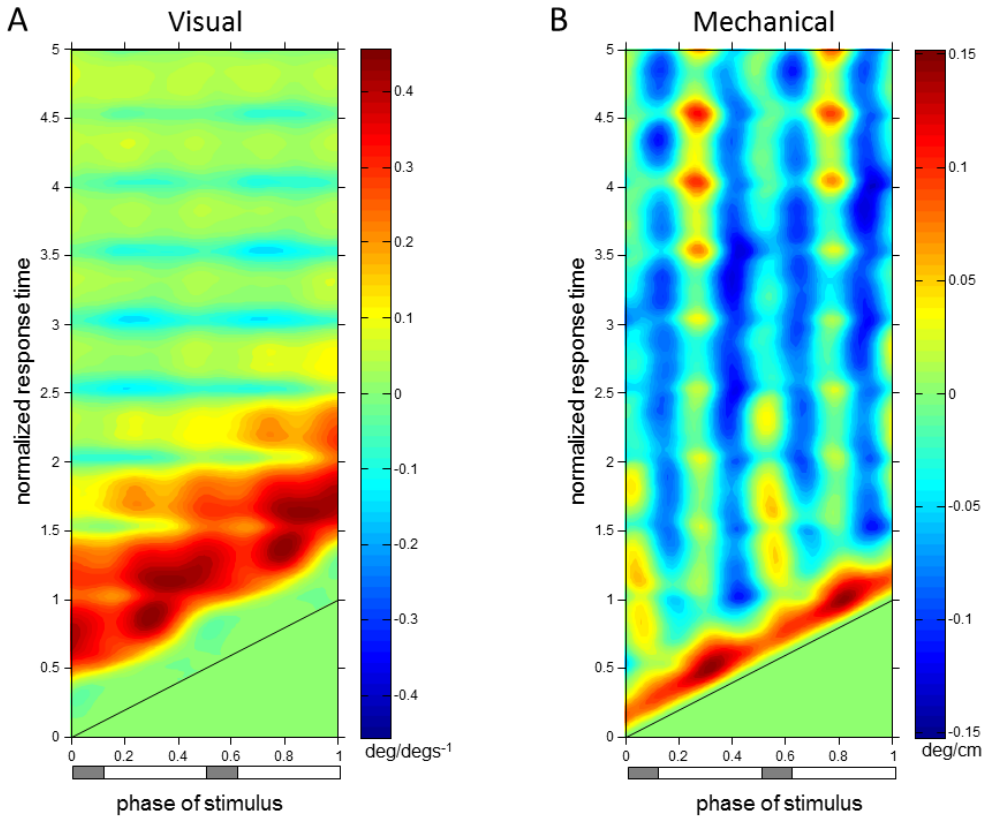

Figure 24. Trunk orientation PD-IRFs. PD-IRFs from visual scene velocity (A) and motor displacement (B) to trunk orientation. Intensity of colors indicate magnitude and direction at the plotted combination of stimulus phase and normalized response time. The diagonal black line is where stimulus phase is equal to the normalized response time, which indicates stimulus onset. The horizontal bar below indicates either double limb or single limb support phases in gray and white, respectively.

The red band in both figures is approximately parallel to the black line noting stimulus onset, indicating that onset of the response occurs with similar time delay across all phases in which the stimulus occurs. On average across stimulus phases, peaks of the initial response to vision observed in Figure 24A occur at .68 ± .06 (mean ± s.d.) cycles (normalized response time) after stimulus onset. As indicated by the black diagonal line in Figure 24, stimulus onset shifts based on stimulus phase, which means that these peak responses are occurring on average .68 y-axis units in Figure 24A from the black diagonal line at each stimulus phase with small variability across stimulus phases. These initial peaks

observed as darker red regions in Figure 24A have an average peak response value of .40 ± .05 deg/degs^{-1}, indicating a consistent response across stimulus phases. Figure 24B shows that initial peaks in trunk orientation responses to the motor displacement occur with comparatively shorter latency than responses to vision, with average peak responses occurring at .17 ± .01 cycles (normalized response time) after stimulus onset. These initial peaks in Figure 24B have average peak response value of .11± .02 deg/cm. Interestingly, vertical blue bands indicating a negative response to mechanical perturbations are observed at 4 stimulus phase ranges in Figure 24B. However, these negative responses are significant ($p<.05$, see *Methods*) only when stimuli are presented at .38-.46 and .88-.96 ("phase of stimulus") of the gait cycle. The properties of the trunk orientation response in these specific phases are further investigated with respect to other response variables in Figures 26 and 27 below.

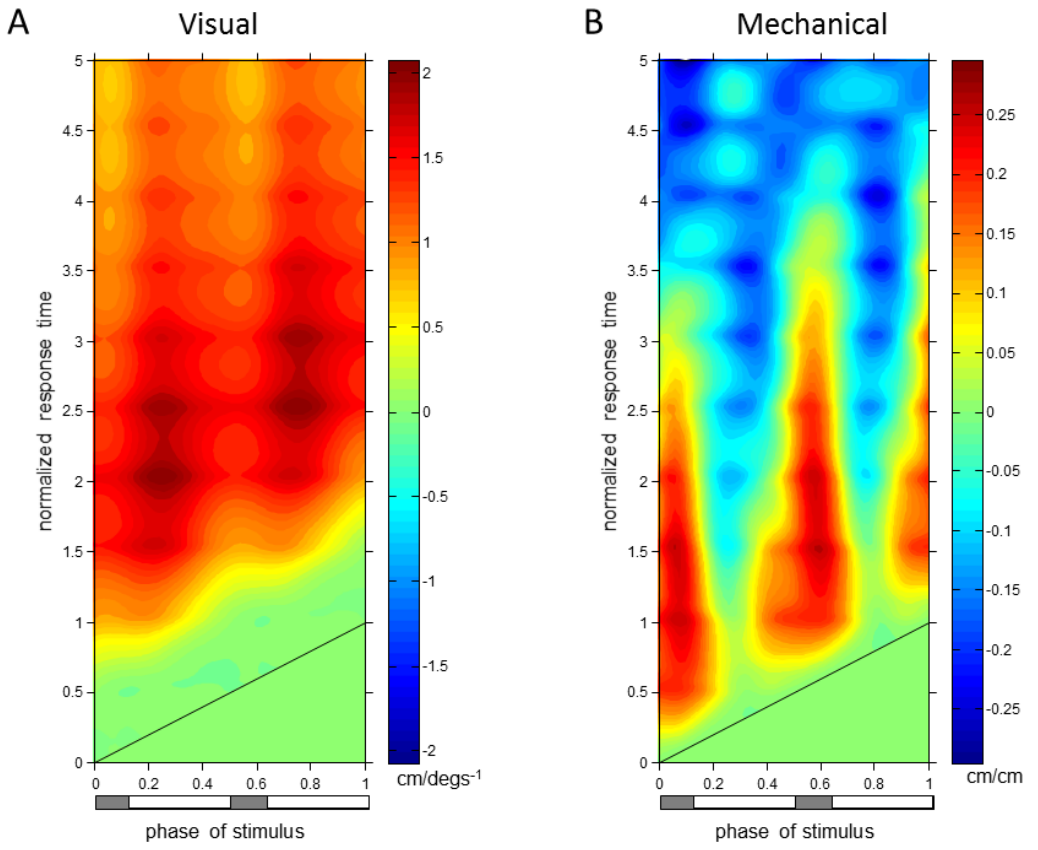

Figure 25. L1 displacement PD-IRFs. PD-IRFs from visual scene velocity (A) and motor displacement (B) to trunk displacement. Intensity of colors indicate magnitude and direction at the plotted combination of stimulus phase and normalized response time. The diagonal black line is where stimulus phase is equal to the normalized response time, which indicates stimulus onset. The horizontal bar below indicates either double limb or single limb support phases in gray and white, respectively.

Initial, positive responses were also observed in L1 displacement responses to both visual and mechanical perturbations. As observed in Figure 25A, positive responses to visual scene velocity occurred at all stimulus phases with similar time delay and persistence through the 4th gait cycle of normalized response time. On average across stimulus phases, peaks of the response to vision observed in Figure 25A occur at 1.89 ± .14 s.d. cycles (normalized response time) after stimulus onset. These initial peaks observed as darker red regions in Figure 25A have an average peak response value of 1.80 ± .17 deg/degs^{-1}. Initial, positive responses to motor position, on the other hand, were

not consistently observed across stimulus phases as seen in Figure 25B. When tested at each stimulus phase, significant responses were observed before and after heel strike at 0-.22, .40-.68 and .96-1 ranges of stimulus phase. Since phase is a circular variable, these values correspond to two ranges of stimulus phase which differ by roughly half a cycle: .40-.68 and .96 -1.22 Within these ranges, mean peak of the positive response occurred at .87 ± .30 cycles (normalized response time) after stimulus onset and had average peak response value of .21 ± .05 cm/cm. Although negative responses were observed as blue intensities in Figure 25B early at some phases and later at all stimulus phases, these were not significant responses when tested at each stimulus phase.

Figures 24 and 25 in combination with the report of significant responses found above, it is clear that the occurrence of responses to the mechanical perturbation depended on the phase of gait cycle when the stimulus occurred while responses to visual scene motion occurred regardless of stimulus phase. We now focus on specific phases of the gait cycle where simultaneous effects on trunk orientation and body displacement were observed to both stimuli. Common stimulus phases eliciting significant responses in the PD-IRFs in both Figures 24 and 25 were found at 40-.68 and .96 -1.22 ranges of stimulus phase, which is within late stance and early swing phase of each limb, marking a phase of single limb support transitioning into double support and back into single limb support.

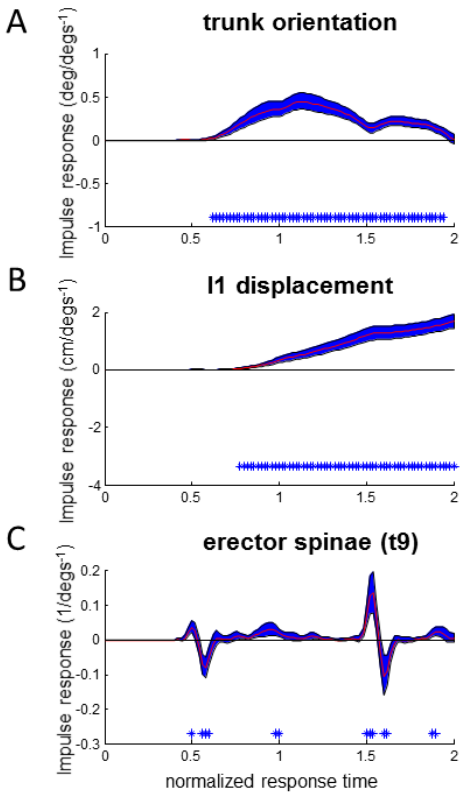

Figure 26. Responses to visual perturbation at 40% stimulus phase. Impulse response functions of trunk orientation (A), L1 AP displacement (B) and normalized erector spinae activations (C) to visual scene velocity. Shaded blue error bars represent confidence intervals at increment of normalized response time. Asterisks at base of subplots indicate significant difference from zero at increment of normalized response time, corrected for the multiple comparisons made within the stimulus phase ($p<.05$).

Vertical “slices” of the .40 stimulus phase of the PD-IRFs in Figures 24 and 25 are plotted in Figures 26 and 27 with accompanying thoracic erector spinae sEMG (EST) responses to investigate simultaneous responses of trunk orientation and L1 displacement to each perturbation. As noted in Figure 26A and 27B with asterisks, significant trunk orientation responses to the visual perturbation occurred prior to L1 displacement responses at this stimulus phase. Positive trunk orientation responses begin at .62 normalized response time (.22f normalized response time after the stimulus occurring at .40) while L1

displacement responses began at .78 normalized response time. In Figure 26C, a small positive response at .50 followed by a larger negative response at .56 is observed in the EST muscle, which is a trunk extensor. This negative response indicates a decrease in EST activation when virtual scene motion increases velocity or an increase in EST activation when virtual scene motion decreases velocity. This occurs prior to a positive response of trunk orientation, with trunk flexion occurring when scene motion increases velocity or extension occurring when scene motion decreases in velocity. Thus, the EST either decreases its activation prior to trunk flexion when scene motion increases velocity or the EST increases its activation prior to trunk extension when scene motion decreases velocity. Trunk orientation responses were initiated prior to L1 displacement responses at the majority (43/50 observed) of stimulus phases. The pattern of significant EST response followed by trunk orientation responses and then L1 displacement occurred at 20 of 50 stimulus phases, with the specific stimulus phases eliciting this pattern at .30-.44, .58-.68, .80, .84 and .92-.98 of the gait cycle. In all, the combination of responses illustrated in Figure 26 suggests that the EST muscle typically facilitates the response of trunk orientation to changes in visual scene motion.

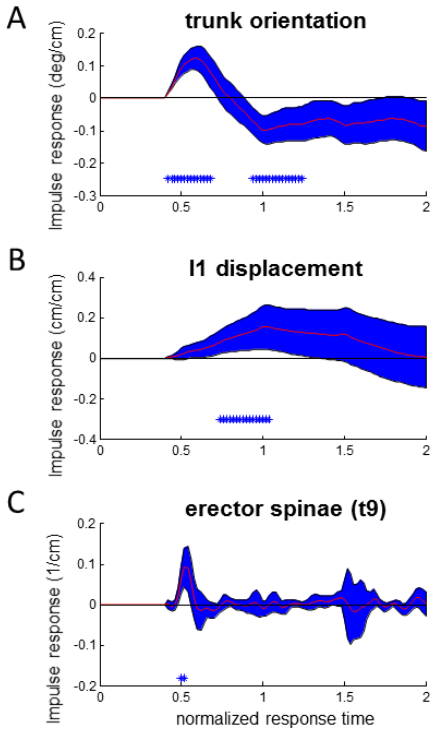

Figure 27. Responses to mechanical perturbation at 40% stimulus phase. Impulse response functions of trunk orientation (A), L1 AP displacement (B) and normalized erector spinae activations (C) to motor position. Shaded blue error bars represent confidence intervals at increment of normalized response time. Asterisks at base of subplots indicate significant difference from zero at increment of normalized response time, corrected for the multiple comparisons made within the stimulus phase ($p<.05$).

Responses of the trunk to the mechanical perturbation also show perturbation induced deviations in trunk orientation occurring prior to deviations in L1 displacement. Noted with asterisks at the stimulus phase of .40 shown in Figure 27, significant responses of trunk orientation are initiated at .42 normalized response time while responses in L1 displacement are first observed at .74 normalized response time. As the motor perturbation will first cause responses observed in kinematics which reflect passive responses of the body to increased or decreased pull of the motor-spring apparatus, sEMG responses to

the mechanical perturbation are a critical indicator that an active, neural driven response to the mechanical perturbation has occurred. Significant, positive responses of EST were first observed at .50 normalized response time at the .40 stimulus phase observed in Figure 27C. This occurs prior to start of the downward trend of the response of the trunk beginning at .60 normalized response time. The positive response of the trunk extensor indicates an increased or decreased EST activation when the motor is moved forward or backwards, respectively. A forward motion of the motor decreases the force of pulling at the trunk while a backward motion of the motor effectively increases the pulling force at the trunk. Thus, the positive response of EST, a trunk extensor, indicates a contribution of the EST activation to initiate trunk extension after an increased motor position has initiated trunk flexion or a decreased activation of EST for trunk flexion after a decreased motor position has initiated trunk extension. Significant EST responses to motor position were also observed at .22-.26, .40-.46, .74-.80 and .90-.92 stimulus phases, and were always observed after an initial positive response in trunk orientation and prior to the decrease from peak of the initial trunk orientation response. In sum, the EST response observed in Figure 27, in addition to that observed at other stimulus phases, indicates an active response which resists the mechanical effects of changing the motor position.

Discussion

Modifications of both sagittal plane trunk orientation and L1 A-P displacement due to changes in visual scene motion and motor position were

observed in this study. Responses of the trunk musculature occurred in conjunction with responses of trunk orientation kinematics to each perturbation, and reflect an active, neural-driven response for control of trunk orientation occurring prior to modifications enacted for whole-body displacement. These findings suggest that control for the subtask of trunk orientation is prioritized in time over control of the subtask of positional maintenance.

Subtask prioritization

Responses in the trunk resulting from both perturbations showed the initiation of an active response for sagittal plane trunk orientation control prior to onset of responses of L1 displacement, which is an indicator of A-P whole body motion on the treadmill. Decreased responses in EST to changing visual scene motion were observed prior to increased responses in trunk orientation. With the sign convention used here, this result indicates that EST responses facilitated the observed trunk orientation responses to vision. For the mechanical perturbation, an EST response occurs just prior to the trunk orientation's decrease from peak response. In late swing phase of either leg, this decrease in trunk orientation response eventually overshoots and becomes a negative response. The combination of these results suggests both an active resistance to the mechanical perturbation and use of visual scene motion information for maintenance of orientation upright occurs before active use of vision for positional maintenance on the treadmill.

The notion that one function, or subtask, of locomotion can be prioritized over another is certainly not a new idea. An early example observed in cats

found that animals will alter their strategy for responding to electrical stimuli placed at the dorsum of their paw in a phase-dependent manner (Forssberg 1975). So-called 'reflex reversals" whereby stimuli used during an animal's support phase increase extensor activation and delay a flexor withdrawal show that the animal prioritizes the subtask of upright stability at the expense of completing the withdrawal task. More recently, this prioritization of subtask has been observed in human walking obstacle avoidance and accommodation literature. The lowering strategy for obstacle avoidance has been shown to decrease step length of the perturbed limb on the treadmill with increased speed needed in ensuing recovery steps (Forner-Cordero 2003). In sum, subjects sacrifice maintenance of speed on the treadmill in order to avoid the obstacle, indicating subtask prioritization.

The prioritization of subtask in such studies and suggested here is in terms of time. Both the trunk toppling over the moving legs and being too forward or backward on the treadmill would have dire consequences for walking. However, trunk orientation responses are initiated prior to whole body displacement responses to both perturbations, suggesting that maintaining orientation upright, or postural control within locomotion, is the primary concern of the nervous system during treadmill walking.

A phase-dependence for mechanical perturbations?

As vision is a purely sensory perturbation it is clear that responses which occur to visual scene motion are active responses, and these responses were

observed at all phases of stimulus. Responses in muscular activations to the mechanical perturbation, however, show that active responses by the nervous system occurred in a phase-dependent manner.

These phase-dependent active responses to the mechanical perturbation suggest that the nervous system uses sensation at a critical, destabilizing phase in a reactive manner. Winter and colleagues have shown that the proximal musculature (erector spinae and others) activates prior to heel strike to counteract a destabilizing flexion of the head, arms and trunk (HAT) segment due to posterior hip acceleration occurring at heel strike (Winter et al. 1990; Winter 1995). The moment of force produced by CNS with combined activations of proximal musculature has been deemed the “balancing moment” while the destabilizing force has been deemed the “unbalancing moment” (Winter 1995). Tang and colleagues have noted that these results by Winter and colleagues were found during unperturbed walking, and suggested they reflect a phase-dependent proactive control when walking is not perturbed (Tang et al. 1998). Using perturbations at the support surface they found that proximal muscles of the trunk (rectus abdominus and erector spinae) are not sufficiently modulated during reactions to such stimuli, and do not play a role in active balance responses. Here we observe a counteracting erector spinae response to a mechanical perturbation which is applied at the trunk, providing a reactive, active balance response. Interestingly, common stimulus phases of both the responses in the erector spinae and the eventual “overshoot” responses in trunk orientation are observed at terminal swing phases in either foot of .40-.46 and .90-.92, and

these are phases in which Winter's "balancing moment" at the hip is ramping up to its peak to counteract the peak "imbalancing moment" of heel strike. Thus, the reactive response observed here occurs simultaneous with the proactive ramping up of muscular activations for the "balancing moment", and we can speculate the nervous system's control strategy is to diminish any (internal or external) destabilizing mechanical threats to upright trunk orientation at these critical phases of the gait cycle. In sum, both the site (lower or limb) of application and gait cycle phase will dictate if the nervous system needs to correct for deviations to a mechanical perturbation during walking.

Clearly, an active control in the mechanical perturbation must involve sensation of change in trunk orientation at some phase prior to initiating the phase-dependent active response. Phase-dependent stimulation of sensory afferents through perturbations such as vibration of trunk muscles could likely inform about the role of trunk muscle afferents for these phase-dependent modifications for trunk orientation. Vibration of erector spinae has been successfully performed during walking and has shown that continuous vibration can elicit deviations in walking trajectory (Courtine et al 2007; Schmid et al 2005). As phase-dependence in somatosensory inputs of the lower limbs has been well-documented (Duysens et al 1990; Sinkjaer et al 1996), it is surprising that trunk vibration dependent on gait cycle phase was not tested in those studies (Courtine et al 2007; Schmid et al 2005) and has not yet, to our knowledge, been tested in other studies. The question of whether or not somatosensory information regarding trunk motion is available to the nervous system on a phase-dependent

basis is an open one. Future studies could inform if phase-dependence of somatosensory input alone is the cause of the phase-dependence observed in this study.

Alternatively, somatosensory input may inform that trunk motion has been altered at all phases, yet this input is only used at specific, necessary phases. For example, the ES activations occurring at early stance observed here act to counteract the potentially increased “unbalancing moment” at the trunk due to the mechanical perturbation, and prevent too large flexion of the trunk after heel strike. Such a process would involve sensation occurring in preparation of destabilizing phases of trunk motion. In sum, it could be speculated that observation of active trunk responses to the mechanical perturbation is facilitated by a phase-dependent use of somatosensory input, and takes place because the phase of perturbation where the mechanical perturbation occurs is a known preparatory phase for balance adjustments.

Implications for locomotive control and future directions

Here we used simultaneous virtual scene motion and distributed pulling at the back of the trunk to probe control of treadmill walking. Using the control theoretic view of movement shown in Figure 28, visual scene motion in an immersive virtual environment perturbs input to the neural feedback portion of the control loop and a motor attached to the upper trunk through a spring is a mechanical perturbation that perturbs input to the musculoskeletal plant. A mechanistic extension of the experimental setup used here to study the

interaction of locomotive subtasks would be to work within a control theoretic framework with the long term goal of using the joint input-output (JIO) approach of system identification (Katayama 2005; van der Kooij 2005) to identify how the nervous system controls locomotion.

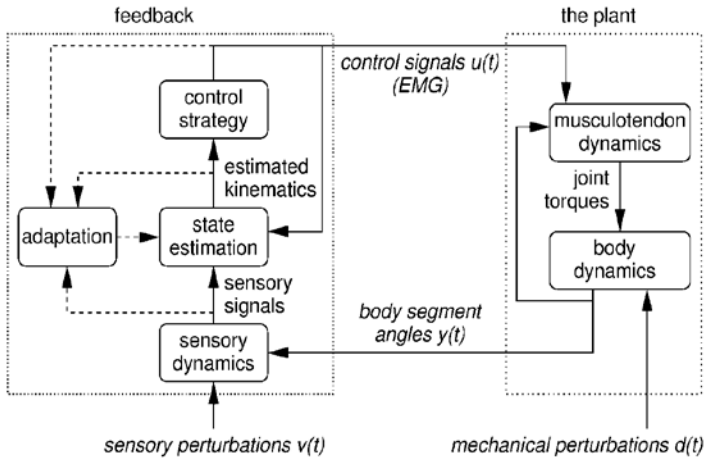

Figure 28. Control theoretic view of motor behavior. In this model, motor behavior consists of two components: plant and feedback. The plant is composed of joint torques produced by musculotendon dynamics and ensuing body dynamics, with muscle activity as precursor. Feedback consists of those sensory signals arising from sensory systems, which update the neural controller based on orientation and movements of the body. Positions and velocities are estimated (state estimation), and appropriate motor commands (control strategy) are specified in the feedback portion of the control loop. (Taken from Logan et al. 2010 with permission).

The JIO approach, coupled with modeling of biomechanical and neural components, has recently been used for identifying the control policy for standing posture (Kiemel et al. 2011). Working within the theoretical framework shown in Figure 28, mechanical and sensory perturbations have been successfully applied to non-parametrically identify both the musculoskeletal plant (Kiemel et al. 2008) and the sensorimotor feedback (Kiemel et al. 2011) portions of the control loop

during standing postural control. This identification relied on careful sensory and mechanical probes, and resulted in identifying minimization of muscle activation as the control strategy for standing postural control (Kiemel et al. 2011).

As an Initial step towards use of the JIO approach to understand walking control, the experimental implementation of sensory and mechanical probes used here could provide insight into different mappings of the neural control loop presented in Figure 28. For a sensory perturbation, the musculoskeletal plant maps EMG responses to kinematic responses. For a mechanical perturbation, sensorimotor feedback maps kinematic responses to EMG responses. The mappings rely on observing both kinematic and EMG responses to sensory and mechanical perturbations. There is the potential that multiple mappings making use of multiple sensory and mechanical perturbations could allow non-parametric identification of the musculoskeletal plant and neural feedback for walking, and this would require considerable advances in experimental methods from those used in this experiment.

Prior to full identification with use of the JIO, one can learn about a system with careful manipulation of experimental conditions. For example, if a mechanical perturbation produces the same kinematic responses but different EMG responses in an experiment with two conditions, it is indicated that properties of the neural feedback is changed between the two conditions. As we have emphasized trunk orientation control in this experiment, it is expected that an experiment with conditions which require varying needed corrections of trunk orientation such as use of a backboard or not would elicit changes in ES, and

potentially other muscles, contributing to the trunk orientation subtask. We expect that simultaneous mechanical and visual perturbations used during experimental conditions which subjects do and do not perform a specific function will inform about how that specific function is controlled during walking. Such experiments offer a novel way to distill out how control differs between subtasks, and even offers great promise for distinguishing differences in locomotive control between those with neural deficits and healthy controls.

Appendix

Technical Note: harmonic transfer functions and phase-dependent impulse response functions

The following technical note is composed of ideas and equations generated by Dr. Tim Kiemel. This material and additional proofs will soon be contained within a manuscript submitted for publication (Kiemel et al, *in prep*), as the application of harmonic transfer functions (HTFs) to human walking and ensuing impulse response functions (IRFs) is novel in its own right.

Approach

One approach to understanding how input-output relationships are altered based upon phase of the locomotive cycle is to apply a perturbation multiple times for each perturbation phase and then average the responses to estimate an impulse response function (IRF). Indeed, this approach was used for the experiment presented in chapter 3 of this dissertation to capture responses at 6 stimulus phases when assuming spatiotemporal symmetry of the left and right legs. To add many more stimulus phases would require prohibitively long experimental sessions to obtain a quality input-output characterization at each phase. To avoid this problem and characterize input-output relationships at many stimulus phases, experiments in chapters 4-6 used continuous broad-band stimuli, allowing the estimation of HTFs that identify input-output mappings from sensory or mechanical inputs to response variable outputs with limit cycle

properties. These relationships are then converted to the time domain via an inverse Fourier transform to obtain phase-dependent Impulse response functions (PD-IRFs) which depend on the gait cycle phase at which the stimulus occurred (stimulus phase) and the time at which the response is measured (response time, normalized by mean cycle period).

HTFs

The approach in 3 experiments (chapters 4-6) of this dissertation was to first determine input-output mappings from sensory or mechanical inputs to outputs of kinematics and muscle activity (EMGs) in the frequency domain. This work expands previous work (e.g., Peterka & Benolken 1995; Kiemel et al 2008) which probed standing postural control as a linear time invariant (LTI) system and characterized input-output relationships with frequency response functions (FRFs). Here, we use a control theoretic framework that has been informative for understanding the control of standing posture (van der Kooij et al. 2005; Kiemel et al 2008 and others) and apply it to the time-varying behavior of treadmill walking. We view walking as the behavior of a dynamical system with a limit cycle that is subject to both intrinsic perturbations and external perturbations applied by the experimenter. For small perturbations, the behavior of a limit-cycle system is similar to that of a linear time periodic (LTP) system, but with one important difference; a limit-cycle system has a phase variable that can be affected by perturbations, whereas such phase resetting cannot occur in an LTP

system. Below we show how LTP analysis methods can be applied to a limit-cycle system by letting phase take the place of time.

Figure 29 shows how a LTP system's input-output mapping can be expressed as the sum of an inifinite number of FRFs …,H_{-2}, H_{-1}, H_0, H_1, H_2, …, with a different frequency shift for each FRF yielding an infinite-dimensional operator termed the harmonic transfer function (HTF). This figure was taken from the dissertation of Möllerstedt (1998, with permission), who used HTFs for power system stability analysis of high speed rail lines (Möllerstedt and Bernhardsson 2000). We will refer to H_k as the k-th mode of the HTF.

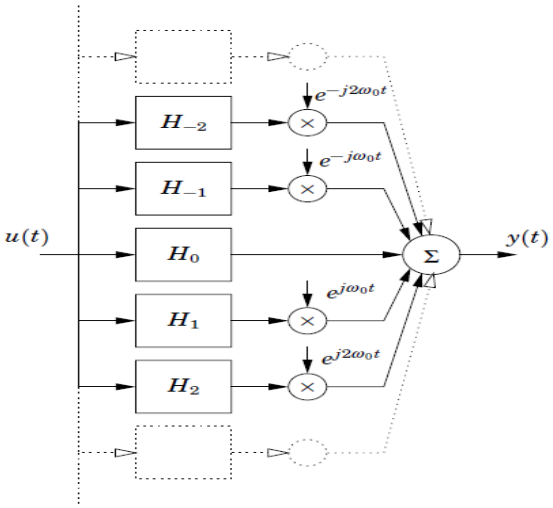

Figure 29. HTF illustration. Many LTI systems can make up the input output relationship of a LTP system to be represented by a HTF (Taken from Möllerstedt, 1998, with permission).

If we ignore the effects of phase-resetting, HTF theory predicts that for walking with gait frequency f_0, a sensory or mechanical input at frequency f will produce outputs at all output frequencies $|f + kf_0|$, where k is an integer. For example, for a gait frequency of 1 Hz, a 0.2 Hz sensory perturbation will produce outputs at 0.2 Hz, 1.2 Hz, 2.2 Hz, etc., and also at |0.2 – 1| Hz = 0.8 Hz, |0.2 – 2|

= 1.8 Hz, etc. For each *k*, the mapping from input frequency *f* to output frequency $|f + kf_0|$ is described by the *k*-th mode of the HTF.

Transient effects and phase effects

If there is phase resetting, then input at any frequency *f* produces output at and near $f + kf_0$. In this case, a single HTF does not fully characterize the input-output mapping. To find the input-output mapping for small perturbations of the limit cycle, HTFs for *phase resetting* and *transient responses* are combined. To explain what we mean by these terms, consider a limit-cycle system in which a small perturbation *u(t)* causes small changes in *y(t),* the system's output. Linearizing around the limit cycle, the system can be approximated by

$$\dot{\theta} = \omega_0 + g_\theta(\theta)u(t),$$

$$\dot{r} = A(\theta)r + g_r(\theta)u(t),$$

with scalar output $y = y_0(\theta) + b(\theta)r$.

Effects of perturbation *u(t)* on absolute phase θ result in a change in location along the limit cycle (phase resetting) while effects of *u(t)* on the deviation vector *r* result in deviations away from the limit cycle (transient responses). When we analyze data, we do not have access to the true phase θ, so we instead use an approximate phase and define phase resetting and transient responses in terms of this approximate phase. A key feature of our analysis is that for small perturbations, the PD-IRF we compute does not, to first order, depend on the particular phase approximation that we use.

Computation of phase and transient HTFs and the phase-dependent IRF.

The above ideas motivate our analysis of walking data. We now describe the steps we perform to carry out our analysis. The goal of the analysis is to describe the effect of *u*(*t*), a small sensory or mechanical perturbation, on *y*(*t*), a kinematic or EMG response variable.

1. *Approximate phase*. First we compute heel-strike times t_k $(k = 1,\ldots,K)$ for a reference leg. Then we compute $\bar{T}$, the mean of the stride times $t_{k+1} - t_k$ $(k = 1,\ldots,K-1)$, and compute the estimated gait frequency as $f_0 = 1/\bar{T}$. Next we define a discontinuous approximation of phase as $\theta_{\mathrm{d}}(t) = k + f_0(t - t_k)$ for $t_k \leq t < t_{k+1}$. To obtain a continuously-differentiable approximation of phase, $\theta(t)$, we apply a second-order low-pass filter to $\theta_{\mathrm{d}}(t)$:

$$\ddot{\theta}(t) + 2d(\dot{\theta}(t) - f_0) + d^2\theta(t) = d^2\theta_{\mathrm{d}}(t).$$

Note that in the absence of perturbations, approximate phase $\theta(t)$ matches the usual definition of the phase of the gait cycle.

2. *Replace time with approximate phase*. Let *p* be the inverse of *θ*: $p(\theta(t)) = t$ and $\theta(p(\vartheta)) = \vartheta$. Let approximate phase ϑ take the place of time $t = p(\vartheta)$ as the independent variable and compute $\tilde{u}(\vartheta) = u(p(\vartheta))$, $\tilde{y}(\vartheta) = y(p(\vartheta))$, and $\tilde{d}(\vartheta) = \dot{\theta}\big(p(\vartheta)\big)/f_0$. (We use the symbol ϑ to distinguish approximate phase as an independent variable from approximate phase as a function of time.)

3. *Compute output variables for HTF analysis*. For each ϑ, let $y_0(\vartheta)$ be the mean of $\tilde{y}(\vartheta)$. Then compute the deviations $\tilde{y}^{(1)}(\vartheta) = \tilde{y}(\vartheta) - y_0(\vartheta)$ and $\tilde{d}^{(1)}(\vartheta) = \tilde{d}(\vartheta) - 1$.

4. *Compute transient and phase-derivative HTFs*. We compute the *transient HTF* from $\tilde{u}(\vartheta)$ to $\tilde{y}^{(1)}(\vartheta)$, denoted $\widetilde{H}_y$, and the *phase-derivative HTF* from $\tilde{u}(\vartheta)$ to $\tilde{d}^{(1)}(\vartheta)$, denoted $\widetilde{H}_d$, as follows. Let $z(\vartheta)$ be either $\tilde{y}^{(1)}(\vartheta)$ or $\tilde{d}^{(1)}(\vartheta)$. Compute the power spectral density (PSD) $p_{\tilde{u}\tilde{u}}(f_1)$ and the double-frequency cross-spectral density (CSD) $p_{\tilde{u}z}(f_1, f_2)$ (Bendat & Piersol 2000). The double-frequency CSD describes the relationship between the input signal $\tilde{u}(\vartheta)$ at input frequency f_1 and the output signal $z(\vartheta)$ at output frequency f_2. The PSD and CSD are computed using Welch's method with 40-cycle Hanning windows (aligned to start at an integer value of ϑ) and 50% overlap. The *k*-th mode of the HTF H_z from $\tilde{u}(\vartheta)$ to $z(\vartheta)$ is computed as $H_{z,k}(f_1) = p_{\tilde{u}z}(f_1, f_1 + kf_0)/p_{\tilde{u}\tilde{u}}(f_1)$. Note that H_z is a function of both the mode index *k* and the input frequency f_1.

5. *Compute transient and phase IRFs*. For an LTP mapping from $\tilde{u}(\vartheta)$ to $z(\vartheta)$, its HTF H_z can be converted to its phase-dependent IRF h_z using inverse Fourier transforms. First take the inverse Fourier transform of each mode of the HTF,

$$h_{z,k}(\tau) = \int_{-\infty}^{\infty} H_{z,k}(f_1) e^{2\pi i f_1 \tau} \, df_1,$$

and then use the result to construct a Fourier series:

$$h_z(\vartheta_\mathrm{r}, \vartheta_\mathrm{s}) = \sum_{k=-\infty}^{\infty} h_{z,k}(\vartheta_\mathrm{r} - \vartheta_\mathrm{s}) e^{2\pi i k \vartheta_\mathrm{r}}.$$

The IRF h_z is a function of response phase ϑ_r and stimulus phase ϑ_s and can be used to represent the LTP mapping from $\tilde{u}(\vartheta)$ to $z(\vartheta)$ as

$$z(\vartheta_\mathrm{r}) = \int_{-\infty}^{\vartheta_\mathrm{r}} h_z(\vartheta_\mathrm{r}, \vartheta_\mathrm{s})\, \tilde{u}(\vartheta_\mathrm{s}) d\vartheta_\mathrm{s}.$$

Using this procedure, compute the *transient IRF* $\tilde{h}_y$ and *phase-derivative IRF* $\tilde{h}_d$ from $\tilde{H}_y$ and $\tilde{H}_d$, respectively. Then compute the *phase IRF* by integrating the phase-derivative IRF:

$$h_\theta(\vartheta_\mathrm{r}, \vartheta_\mathrm{s}) = \int_{\vartheta_\mathrm{s}}^{\vartheta_\mathrm{r}} \tilde{h}_d(\tau, \vartheta_\mathrm{s}) d\tau.$$

6. *Compute IRF*. Up to now, IRFs have been functions of response phase ϑ_r and stimulus phase ϑ_s. The IRFs $\tilde{h}_y$ and h_θ can be combined to obtain the IRF from *u*(*t*) to *y*(*t*) that is a function of response time t_r and stimulus time t_s:

$$h_y(t_\mathrm{r}, t_\mathrm{s}) = \tilde{h}_y(t_\mathrm{r}, t_\mathrm{s}) + y_0'(t_\mathrm{r}) h_\theta(t_\mathrm{r}, t_\mathrm{s}).$$

Here t_r and t_s are expressed in normalized time: time divided by the mean gait period and aligned so that stimulus time t_s equals true stimulus phase.

Example of a phase-dependent impulse response function

An example of the transient IRF and phase component IRF is observed in Figure 30A and 30B, respectively. The sum of these IRFs is presented in Figure 30C, which is the IRF that is referred to as the phase-dependent impulse response function (PD-IRF) and is the input-output mapping that is reported in several chapters of this dissertation. The specific data presented in Figure 30 are taken from foot segment angle responses to visual scene velocity presented in Chapter 5 in the no metronome condition.

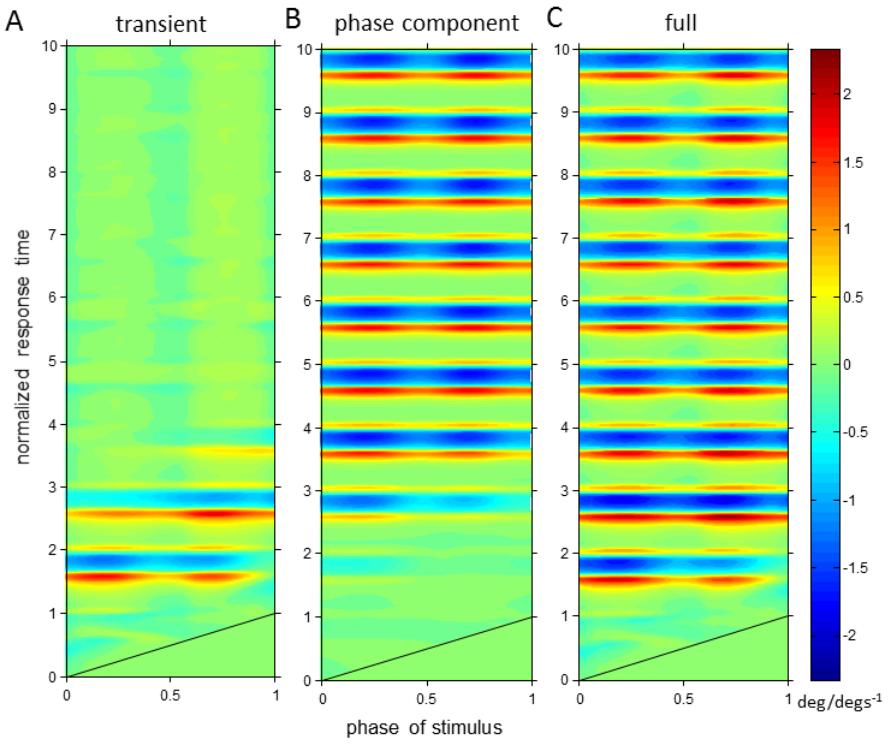

Figure 30. PD-IRF of foot segment angle from visual scene velocity. Transient PD-IRF (A) and phase component PD-IRF (B) which make up the full PD-IRF (C). These IRFs are computed as response of trunk orientation from visual scene velocity. These data are taken from the experiment presented in Chapter 5.

References

Ahn J, Hogan N Walking Is Not Like Reaching: Evidence from Periodic Mechanical Perturbations. *PLoS One* 7: e31767, 2012.

Ahn J, Hogan N. A simple state-determined model reproduces entrainment and phase-locking of human walking. *PLoS One* 7:e47963, 2012.

Anson E, Agada P, Kiemel T, Ivanenko Y, Lacquaniti F, Jeka J. Visual control of trunk translation and orientation during locomotion. *Exp Brain Res* 232:1941-51, 2014.

Aoi S, Ogihara N, Sugimoto Y, Tsuchiya K. Simulating Adaptive Human Bipedal Locomotion Based on Phase Resetting Using Foot-Contact Information. *Advanced Robotics* 22: 1697–1713, 2008.

Aoi S, Ogihara N, Funato T, Sugimoto Y, Tsuchiya K. Evaluating functional roles of phase resetting in generation of adaptive human bipedal walking with a physiologically based model of the spinal pattern generator. *Biol Cybern* 102: 373-87, 2010.

Bauby CE, Kuo AD. Active control of lateral balance in human walking. *J Biomech* 33: 1433–1440, 2000.

Bendat JS, Piersol AG. Random data: analysis and measurement procedures. Wiley, New York, 2000.

Benjamini Y, Hochberg Y. Controlling the false discovery rate: a practical and powerful approach to multiple testing. *J Roy Stat Soc B* 57: 289–300, 1995.

Benjamini Y, Yekutieli D. The Control of the False Discovery Rate in Multiple Testing under Dependency *Ann Stat* 29: 1165-1188, 2001.

Bent LR, Inglis JT, McFadyen BJ. When is vestibular information important during walking? *J Neurophysiol* 92: 1269-1275, 2004.

Bent LR, McFadyen BJ, Inglis JT. Vestibular contributions during human locomotor tasks. *Exerc Sport Sci Rev* 33: 107-113, 2005.

Berard J, Fung J, Lamontagne A. Impact of aging on visual reweighting during locomotion. *Clin Neurophysiol* 123:1422-8, 2012.

Bertram JE, Ruina A. Multiple walking speed-frequency relations are predicted by constrained optimization. *J Theor Biol* 209:445-53, 2001.

Blair RC, Karniski W. An alternative method for significance testing of waveform difference potentials. *Psychophysiology* 30:518-24, 1993.

Blouin JS, Dakin CJ, vandenDoel K, Chua R, McFadyen BJ, Inglis JT. Extracting phase-dependent human vestibular reflexes during locomotion using both time and frequency correlation approaches. *J Appl Physiol* 111:1484-1490, 2011.

Borghese NA, Bianchi L, Lacquaniti F. Kinematic determinants of human locomotion. *J Physiol* 494 (Pt 3):863-879, 1996.

Bruggeman H, Zosh W, Warren WH. Optic flow drives human visuo-locomotor adaptation. *Curr Biol* 17:2035-2040, 2007.

Capaday C, Stein RB. Amplitude modulation of the soleus H-reflex in the human during walking and standing. *J Neurosci* 6: 1308-1313, 1986.

Capaday C, Lavoie BA, Barbeau H, Schneider C, Bonnard M. Studies on the corticospinal control of human walking. I. Responses to focal transcranial magnetic stimulation of the motor cortex. *J Neurophysiol* 81:129-39, 1989.

Capellini G, Ivanenko YP, Poppele RE, Lacquaniti F. Motor patterns in human walking and running. *J Neurophysiol* 95: 3426-3437, 2006.

Cappellini G, Ivanenko YP, Dominici N, Poppele RE, Lacquaniti F. Motor patterns during walking on a slippery walkway. *J Neurophysiol* 103:746-60, 2010a.

Cappellini G, Ivanenko YP, Dominici N, Poppele RE, Lacquaniti F. Migration of motor pool activity in the spinal cord reflects body mechanics in human locomotion. *J Neurophysiol* 104:3064-3073, 2010b.

Chvatal SA, Ting LH. Voluntary and reactive recruitment of locomotor muscle synergies during perturbed walking. *J Neurosci* 32:12237-50, 2012.

Chvatal SA, Ting LH. Common muscle synergies of balance and walking. *Front Comp Neuro* 7:1-14, 2014.

Collins SH, Wisse M, Ruina A. A Three-Dimensional Passive-Dynamic Walking Robot with Two Legs and Knees. *Int J Robot Res* 20: 607–615, 2001.

Cordero AF, Koopman HJ, van der Helm FC. Mechanical model of the recovery from stumbling. *Biol Cybern* 91:212-20, 2004.

Cordo PJ, Nashner LM. Properties of postural adjustments associated with rapid arm movements. *J Neurophysiol* 47: 287-302, 1982.

Courtine G, De Nunzio AM, Schmid M, Beretta MV, Schieppati M. Stance- and locomotion-dependent processing of vibration-induced proprioceptive inflow from multiple muscles in humans. *J Neurophysiol* 97:772-9, 2007.

Cromwell RL, Pidcoe PE, Griffin L A, Sotillo T, Ganninger D, Feagin M. Adaptations in horizontal head stabilization in response to altered vision and gaze during natural walking. *J Vestib Res* 14: 367-373, 2004.

Danion F, Bonnard M, Pailhous J. Intentional online control of propulsive forces in human gait. *Exp Brain Res* 116:525-38, 1997.

Delval A, Krystkowiak P, Delliaux M, Blatt JL, Derambure P, Destée A, Defebvre L. Effect of external cueing on gait in Huntington's disease. *Mov Disord* 23:1446-52, 2008.

Despande N, Patla AE. Visual-vestibular interaction during locomotion: Effects of aging and blurring vision. *Exp Brain Res* 176: 43-53, 2007.

Dietz V, Faist M, Pierrot-Deseilligny E. Amplitude modulation of the quadriceps H-reflex in the human during the early stance phase of gait. *Exp Brain Res* 79: 221-4, 1990.

Dingwell JB, Cusumano JP. Nonlinear time series analysis of normal and pathological human walking. *Chaos* 10:848-863, 2000.

Dingwell JB, John J, Cusumano JP. Do humans optimally exploit redundancy to control step variability in walking? *PLoS Comput Biol* 6, 2010.

Drew T. Functional organization within the medullary reticular formation of the intact unanesthetized cat. III. Microstimulation during locomotion. *J Neurophysiol* 66:919-38, 1991.

Drew T, Jiang W, Kably B, Lavoie S. Role of the motor cortex in the control of visually triggered gait modifications. *Can J Physiol Pharmacol* 74: 426–442, 1996.

Duysens J, Trippel M, Horstmann GA, Dietz V. Gating and reversal of reflexes in ankle muscles during human walking. *Exp Brain Res* 82: 351-358, 1990.

Duysens J, Clarac F, Cruse H. Load-regulating mechanisms in gait and posture: comparative aspects. *Physiol Rev* 80: 83-133, 2000.

Eng JJ, Winter DA, Patla AE. Strategies for recovery from a trip in early and late swing during human walking. *Exp Brain Res* 102: 339-349, 1994.

de l'Etoile SK. The effect of rhythmic auditory stimulation on the gait parameters of patients with incomplete spinal cord injury: an exploratory pilot study. *Int J Rehabil Res* 31:155-7, 2008.

Faisal AA, Selen LP, Wolpert DM. Noise in the nervous system. *Nat Rev Neurosci* 9:292-303, 2008.

Forner-Cordero A, Koopman, B, van der Helm FCT. Multiple-step strategies to recover from stumbling perturbations. *Gait Posture* 18:47–59, 2003.

Forner-Cordero A, Ackermann M, de Lima Freitas M. A method to simulate motor control strategies to recover from perturbations: application to a stumble recovery during gait. Conf Proc IEEE Eng Med Biol Soc. 2011:7829-32, 2011.

Forssberg H, Grillner S, Rossignol S. Phase dependent reflex reversal during walking in chronic spinal cats. *Brain Res* 85: 103-107, 1975.

Forssberg H. Stumbling corrective reaction: a phase-dependent compensatory reaction during locomotion. *J Neurophysiol* 42: 936–953, 1979.

Forssberg H. Spinal locomotor functions and descending control. In: *Brain Stem Control of Spinal Mechanisms,* edited by Sjölund B, Björklund A. Amsterdam: Elsevier, 1982.

Friel KM, Drew T, Martin JH. Differential activity-dependent development of corticospinal control of movement and final limb position during visually-guided locomotion. *J* Neurophysiol 97: 3396–3406, 2007.

François M, Morice AHP, Bootsma RJ, Montagne G. Visual control of walking velocity. *Neurosci Res* 70: 214-219, 2011.

Grasso R, Prévost P, Ivanenko YP, Berthoz A. Eye-head coordination for the steering of locomotion in humans: an anticipatory synergy. *Neurosci Lett* 253: 115-118, 1998.

Graziano MS, Cooke DF. Parieto-frontal interactions, personal space, and defensive behavior. *Neuropsychologia* 44:2621-35, 2006.

Gibson JJ. Visually controlled locomotion and visual orientation in animals. *Br J Psychol* 49:182-194, 1958.

Groppe DM, Urbach TP, Kutas M. Mass univariate analysis of event-related brain potentials/fields I: A critical tutorial review. *Psychophysiology*, 48: 1711-1725, 2011.

Guerin P, Bardy BG. Optical modulation of locomotion and energy expenditure at preferred transition speed. *Exp Brain Res* 189: 393-402, 2008.

Hall P. Theoretical comparison of bootstrap confidence intervals. *Ann Stat* 16: 927-953, 1988.

Hausdorff JM, Purdon PL, Peng CK, Ladin Z, Wei JY, Goldberger AL. Fractal dynamics of human gait: stability of long-range correlations in stride interval fluctuations. *J Appl Physiol* 80:1448–1457, 1996.

Haridas c, Zehr EP, Misiaszek JE. Adaptation of cutaneous stumble correction when tripping is part of the locomotor environment. *J Neurophysiol* 99: 2789–2797, 2008.

Hicheur H, Vieilledent S, Berthoz A. Head motion in humans alternating between straight and curved walking path: combination of stabilizing and anticipatory orienting mechanisms. *Neurosci Lett* 383:87-92, 2005.

Hollands MA, Marple-Horvat DE. Visually guided stepping under conditions of step cycle-related denial of visual information. *Exp Brain Res* 109: 343-356, 1996.

Hollands MA, Patla AE, Vickers, JN. "Look where you're going!": gaze behaviour associated with maintaining and changing the direction of locomotion. *Exp Brain Res* 143:221-230, 2002.

Hollands MA, Ziavra NV, Bronstein AM. A new paradigm to investigate the roles of head and eye movements in the coordination of whole-body movements. *Exp Brain Res* 154:261-266, 2004.

Iles JF, Baderin R, Tanner R, Simon A. Human standing and walking: comparison of the effects of stimulation on the vestibular system. *Exp Brain Res* 178:151-166, 2007.

Ivanenko YP, Poppele RE, Lacquaniti F. Five basic muscle activation patterns account for muscle activity during human locomotion. *J Physiol* 556: 267-82, 2004.

Katayama T. Subspace methods for system identification. London: Springer, 2005.

Kay BA, Warren WH, Jr. A Dynamical Model of the Coupling between Posture and Gait. In: Timing of Behavior: Neural, Psychological, and Computational Perspectives (Rosenbaum DA, Collyer CE, eds), pp 293-322. Cambridge, Mass.: MIT Press, 1998.

Kay BA, Warren WH, Jr. Coupling of posture and gait: mode locking and parametric excitation. *Biol Cybern* 85:89-106, 2001.

Kiemel T, Elahi AJ, Jeka JJ. Identification of the plant for upright stance in humans: multiple movement patterns from a single neural strategy. *J Neurophysiol*. 100: 3394-3406, 2008.

Kiemel T, Logan D, Ivanenko YP, Lacquaniti F, Jeka JJ. A Comparison of the Effects of Visual-Scene Motion on walking and Standing and the Role of Stability. *Sixteenth US National Congress of Theoretical and Applied Mechanics*. State College, PA, 2010.

Kiemel T, Zhang Y, Jeka JJ. Identification of neural feedback for upright stance in humans: stabilization rather than sway minimization. *J Neurosci*. 31:15144-53, 2011.

Kiemel T, Zhang Y, Jeka JJ. Visual flow is interpreted relative to multisegment postural control. *J Mot Behav* 43:237-246, 2011.

Kiemel T, Logan D, Jeka JJ. Identifying input-output mappings for weakly perturbed biological oscillators. *In preparation.*

Kim SJ, Kwak EE, Park ES, Lee DS, Kim KJ, Song JE, Cho SR. Changes in gait patterns with rhythmic auditory stimulation in adults with cerebral palsy. *NeuroRehabilitation*. 29:233-41, 2011.

Kim SJ, Kwak EE, Park ES, Cho SR. Differential effects of rhythmic auditory stimulation and neurodevelopmental treatment on gait patterns in adults with cerebral palsy: a randomized controlled trial. *Clin Rehabil* 26:904-14, 2012.

Klenk, D. Phase resetting of human walking. Master of Science thesis, Dept. of Mech. Eng., MIT, Cambridge, MA, 2011.

Konczak J. Effects of optic flow on the kinematics of human gait: a comparison of young and older adults. *J Mot Behav* 26: 225-236, 1994.

Kobayashi M, Nomura T, Sato S. Phase-dependent response during human locomotion to impulsive perturbation and its interpretation based on neural mechanism. *Jpn J Med Electron Biol Eng* 38:20–32, 2000.

Lamontagne A, Fung J, McFadyen BJ, Faubert J. Modulation of walking speed by changing optic flow in persons with stroke. *J Neuroeng Rehabil* 4:22, 2007.

Latt MD, Menz HB, Fung VS, Lord SR. Walking speed, cadence and step length are selected to optimize the stability of head and pelvis accelerations. *Exp Brain Res* 184:201-9, 2007.

Lim I, van Wegen E, de Goede C, Deutekom M, Nieuwboer A, Willems A, Jones D, Rochester L, Kwakkel G. Effects of external rhythmical cueing on gait in patients with Parkinson's disease: a systematic review. *Clin Rehabil* 19: 695–713, 2005.

Logan D, Kiemel T, Dominici N, Cappellini G, Ivanenko Y, Lacquaniti F, Jeka JJ. The many roles of vision during walking. *Exp Brain Res* 206: 337-350, 2010.

Logan, D, Kiemel, T, Cappellini, G, Sylos-Labini, F, Ivanenko, YP, Lacquaniti, F, Jeka, JJ. Human Locomotion: Active compensation for a linear trunk on nonlinear legs. *Forty-first meeting of the Society for Neuroscience*, Washington, DC, 2011.

Logan D, Ivanenko YP, Kiemel T, Cappellini G, Sylos-Labini F, Lacquaniti F, Jeka JJ. Function dictates the phase dependence of vision during human locomotion. *J Neurophysiol* 112:165-80, 2014a.

Logan D, Kiemel T, Jeka JJ Asymmetric sensory reweighting in human upright stance. *PLoS One*. 9:e100418, 2014b

Maclellan MJ, Ivanenko YP, Cappellini G, Sylos Labini F, Lacquaniti F. Features of hand-foot crawling behavior in human adults. *J Neurophysiol* 107:114-25, 2012.

Mahboobin A, Loughlin PJ, Redfern MS, Sparto PJ. Sensory re-weighting in human postural control during moving-scene perturbations. *Exp Brain Res* 167:260-7, 2005.

Manly BFJ. Randomization, Bootstrap, and Monte Carlo Methods in Biology. 2nd ed. Chapman and Hall, London, 1997.

Marigold DS, Weerdesteyn V, Patla AE, Duysens J. Keep looking ahead? Re-direction of visual fixation does not always occur during an unpredictable obstacle avoidance task. *Exp Brain Res* 176: 32-42, 2007.

Marigold DS, Patla AE. Gaze fixation patterns for negotiating complex ground terrain. *Neuroscience* 144: 302-313, 2007.

Marigold DS. Role of peripheral visual cues in online visual guidance of locomotion. *Exerc Sport Sci Rev* 36:145-51, 2008.

Mazzaro N, Grey MJ, Sinkjær T. Contribution of afferent feedback to the soleus muscle activity during human locomotion *J Neurophysiol* 93: 167-177, 2005.

McGeer T. Passive dynamic walking. *Int J Robot Res* 9: 62–82, 1990.

McFadyen BJ, Bouyer L, Bent LR, Inglis JT. Visual-vestibular influences on locomotor adjustments for stepping over an obstacle. *Exp Brain Res* 179:235-43, 2007.

McGowan CP, Neptune RR, Clark DJ, Kautz SA. Modular control of human walking: adaptations to altered mechanical demands. *J Biomech* 43: 412–419, 2010.

Möllerstedt E. An aggregated approach to harmonic modelling of loads in power distribution network. Lic. Tech. thesis, Dept. Automatic Control, Lund Inst. Technology, Lund, Sweden, 1998.

Möllerstedt E, Bernhardsson B. Out of control because of harmonics: an analysis of the harmonic response of an inverter locomotive. *IEEE Contr Syst Mag* 20: 70-81,2000.

Mulavara AP, Bloomberg JJ. Identifying head-trunk and lower limb contributions to gaze stabilization during locomotion. *J Vestib Res* 12:255-269, 2002.

Musienko P, van den Brand R, Märzendorfer O, Roy RR, Gerasimenko Y, Edgerton VR, Courtine G. Controlling specific locomotor behaviors through multidimensional monoaminergic modulation of spinal circuitries. *J Neurosci* 31: 9264-9278, 2011.

Nakanishi J, Morimoto J, Endo G, Cheng G, Schaal S, Kawato M. Learning from demonstration and adaptation of biped locomotion. *Robotics and Autonomous Systems* 47:79–91, 2004.

Nashner LM. Balance adjustments of humans perturbed while walking. *J Neurophysiol* 44: 650-664, 1980.

Nashner LM, Forssberg H. Phase-dependent organization of postural adjustments associated with arm movements during walking. *J Neurophysiol* 55: 1382-94, 1986.

Neptune RR, Clark DJ, Kautz SA. Modular control of human walking: a simulation study. *J Biomech* 429: 1282–1287, 2009.

Nomura T, Kawa K, Suzuki Y, Nakanishi M, Yamasaki T. Dynamic stability and phase resetting during biped gait. *Chaos* 19:026103, 2009.

Nieuwenhuijzen PH, Schillings AM, Van Galen GP, Duysens J. Modulation of the startle response during human gait. *J Neurophysiol* 84:65-74, 2000.

Oie KS, Kiemel T, Jeka JJ. Multisensory fusion: simultaneous re-weighting of vision and touch for the control of human posture. *Brain Res Cogn Brain Res* 14: 164-176, 2002.

O'Connor SM, Xu HZ, Kuo AD. Energetic cost of walking with increased step variability. *Gait Posture* 36: 102–10, 2012.

O'Connor SM, Kuo AD. Direction-dependent control of balance during walking and standing. *J Neurophysiol.* 102:1411-9, 2009.

Oliveira AS, Gizzi L, Kersting UG, Farina D. Modular organization of balance control following perturbations during walking. *J Neurophysiol* 108:1895-906, 2012.

Patla AE. Visual control of human locomotion. In: *Adaptability of Human Gait,* edited by Patla AE. New York: Elsevier, 1991.

Patla AE, Prentice SD, Robinson C, Neufeld. Visual control of locomotion: strategies for changing direction and going over obstacles. *J Exp Psychol Hum Percept Perform* 17: 603-634, 1991.

Patla AE, Vickers JN. Where and when do we look as we approach and step over an obstacle in the travel path? *Neuroreport* 8:3661-3665, 1997.

Patla AE, Vickers JN. How far ahead do we look when required to step on specific locations in the travel path during locomotion? *Exp Brain Res* 148: 133-138, 2003.

Peterka RJ, Benolken MS. Role of somatosensory and vestibular cues in attenuating visually induced human postural sway. *Exp Brain Res* 105: 101-110, 1995.

Prokop T, Schubert M, Berger W. Visual influence on human locomotion. Modulation to changes in optic flow. *Exp Brain Res* 114: 63-70, 1997.

Queralt A, Weerdesteyn V, van Duijnhoven HJ, Castellote JM, Valls-Solé J, Duysens J. The effects of an auditory startle on obstacle avoidance during walking. *J Physiol* 586:4453-63, 2008.

Reynolds RF, Day BL. Visual guidance of the human foot during a step. *J Physiol* 569: 677-684, 2005.

Roerdink M, Lamoth CJ, Kwakkel G, van Wieringen PC, Beek PJ. Gait coordination after stroke: benefits of acoustically paced treadmill walking. Phys Ther 87:1009-22, 2007.

Rossignol S, Dubuc R, Gossard JP. Dynamic sensorimotor interactions in locomotion. *Physiol Rev* 86: 89-154, 2006.

Sarre G, Berard, J, Fung J, Lamontagne A. Steering behaviour can be modulated by different optic flows during walking. *Neurosci Lett* 436: 96-101, 2008.

Sandberg H, Möllerstedt E, Bernhardsson B. Frequency-Domain Analysis of Linear Time-Periodic Systems. *IEEE T Automat Contr* 50:1971-1983, 2005.

Schmid M, De Nunzio AM, Schieppati M. Trunk muscle proprioceptive input assists steering of locomotion *Neurosci Lett* 2005 384:127-32, 2005.

Schultz BB. Levene's test for relative variation. *Syst Zool* 34: 449-456, 1985.

Sherk H, Fowler GA. Neural analysis of visual information during locomotion. *Prog Brain Res* 134: 247-64, 2001.

Sillar KT, Roberts A. A neuronal mechanism for sensory gating during locomotion in a vertebrate. *Nature* 331: 262-265, 1988.

Simmons PJ, Rind FC, Santer RD. Escapes with and without preparation: the neuroethology of visual startle in locusts *J Insect Physiol* 56:876-83, 2010.

Sinkjær T, Andersen JB, Larsen B. Soleus stretch reflex modulation during gait in humans. *J Neurophysiol* 76: 1112–1120, 1996.

Tang PF, Woollacott MH, Chong RK. Control of reactive balance adjustments in perturbed human walking: roles of proximal and distal postural muscle activity. *Exp Brain Res* 119:141-52, 1998.

Terrier P, Turner V, Schutz Y. GPS analysis of human locomotion: Further evidence for long-range correlations in stride-to-stride fluctuations of gait parameters. *Hum Mov Sci* 24:97-115, 2005.

Terrier P, Dériaz O. Persistent and anti-persistent pattern in stride-to-stride variability of treadmill walking: influence of rhythmic auditory cueing. *Hum Mov Sci* 31:1585-97, 2012.

Terrier P. Step-to-step variability in treadmill walking: influence of rhythmic auditory cueing. *PLoS One* 7, 2012.

Terrier P, Dériaz O. Non-linear dynamics of human locomotion: effects of rhythmic auditory cueing on local dynamic stability. Front Physiol, 4:230, 2013.

Thaut MH, McIntosh GC, Rice RR, Miller RA, Rathbun J, Brault JM. Rhythmic auditory stimulation in gait training for Parkinson's disease patients. *Mov Disord* 11: 193-200, 1996.

Thaut MH, McIntosh GC, Rice RR. Rhythmic facilitation of gait training in hemiparetic stroke rehabilitation. *J Neurol Sci* 151:207-212, 1997.

Thaut MH, Miltner R, Lange HW, Hurt CP, Hoemberg V. Velocity modulation and rhythmic synchronization of gait in Huntington's disease. *Mov Disord* 14:808-19, 1999.

Vallis LA, Patla AE. Expected and unexpected head yaw movements result in different modifications of gait and whole body coordination strategies. *Exp Brain Res* 157:94-110, 2004.

Varraine E, Bonnard M, Pailhous J. Interaction between different sensory cues in the control of human gait. *Exp Brain Res* 142:374-384, 2002.

Von Wilzenben HD. Methods in the treatment of post encephalic Parkinson's. New York: Grune and Stratten, 1942.

Wall MB, Smith AT. The representation of egomotion in the human brain. *Curr Biol* 18: 191-194, 2008.

Warren WH, Kay BA, Yilmaz EH. Visual control of posture during walking: functional specificity*. J Exp Psychol Hum Percept Perform* 22: 818-838, 1996.

Warren WH Jr, Kay BA, Zosh WD, Duchon AP, Sahuc S Optic flow is used to control human walking*. Nat Neurosci* 4:213–216, 2001.

Wuehr M, Schniepp R, Pradhan C, Ilmberger J, Strupp M, Brandt T, Jahn K. Differential effects of
absent visual feedback control on gait variability during different locomotio n speeds. *Exp Brain Res* 224:287-94, 2013.

Wereley NM. Analysis and control of linear periodically time varying systems. PhD dissertation, Dept. of Aeronautics and Astronautics, MIT, Cambridge, MA, 1991.

Winter DA, Yack HJ. EMG profiles during walking: stride-to-stride and inter-subject variability. *Electroencephalogr Clin Neurophysiol* 67: 402-411, 1987.

Winter DA. Biomechanics of normal and pathological gait: Implications for understanding human locomotor control. *J Motor Behav* 21: 337-355, 1989.

Winter DA, Ruder GK, MacKinnon CD. Control of balance of upper body during gait. In: Winters JM, Woo S-LY (eds) Multiple muscle systems: biomechanics and movement organization. London: Springer, pp 534-41, 1990.

Winter DA. The Biomechanics and Motor Control of Human Gait: Normal, Elderly, and Pathological. Waterloo, Ontario: Waterloo Biomechanics Press, 1991.

Winter, DA. Human balance and posture control during standing and walking. *Gait Posture* 3:193-214, 1995.

Yamasaki T, Nomura T, Sato S. Possible functional roles of phase resetting during walking. *Biol Cybern* 88:468–496, 2003.

Yang JF, Stein RB, James KB. Contribution of peripheral afferents to the activation of the soleus muscle during walking in humans. *Exp Brain Res* 87: 679–687, 1991.

Zehr EP, Stein RB. What functions do reflexes serve during human locomotion? *Prog Neurobiol* 58: 185-205, 1999.

Zijlstra W, Rutgers AW, Van Weerden T W. Voluntary and involuntary adaptation of gait in Parkinson's disease. *Gait Posture* 7: 53-63, 1998.

Zoubir A, Boashash B. The bootstrap and its application in signal processing. *IEEE Signal Processing Magazine* 15: 56-76, 1998.